FEDERAL UNIVERSITY OF SANTA MARIA
CENTER OF TECHNOLOGY
ELECTRICAL ENGINEERING GRADUATE PROGRAM

João Manoel Lenz

MULTI-OBJECTIVE DESIGN TOOL FOR OPTIMIZING CAPACITOR SELECTION IN POWER CONVERTERS BASED ON THE MISSION PROFILE.

Doctoral Dissertation

Santa Maria, RS
2019

João Manoel Lenz

Multi-Objective Optimization Design Tool for Capacitors in Power Converters Based on the Mission Profile

Doctoral Dissertation presented to the Doctorate Course of the Electrical Engineering Graduate Program, in the Energy Processing research area, of the Federal University of Santa Maria (UFSM, RS), as a partial requirement to obtain the degree of **Doctor in Electrical Engineering.**

Advisor: Prof. Dr. José Renes Pinheiro

Santa Maria, RS
2019

João Manoel Lenz

MULTI-OBJECTIVE DESIGN TOOL FOR OPTIMIZING CAPACITOR SELECTION IN POWER CONVERTERS BASED ON THE MISSION PROFILE.

Doctoral Dissertation presented to the Electrical Engineering Graduate Program, in the Power Electronics research area, of the Federal University of Santa Maria (UFSM, RS), as a partial requirement to obtain the degree of **Doctor in Electrical Engineering.**

Approved in September 13, 2019

José Renes Pinheiro, Dr. (UFSM)
(Chair / Advisor)

Huai Wang, PhD. (Aalborg University)

Fabrício Hoff Dupont, Dr. (UNOCHAPECÓ)

Mário Lúcio da Silva Martins, Dr. (UFSM)

Hamiltom Confortin Sartori, Dr. (UFSM)

Santa Maria, RS
2019

PREFACE

This dissertation is a summary of the Doctoral project entitled "Multi-objective Design Tool for Optimizing Capacitor Selection in Power Converters Based on the Mission Profile", and it marks the closure of my pursuit towards a doctorate. This project was developed thanks to the Power Electronics and Control Group (GEPOC) by the Electrical Engineering Graduate Program (PPGEE), Federal University of Santa Maria (UFSM), Brazil. Also, this work has been possible thanks to the financial support of both the Coordination for the Improvement of Higher Education Personnel (CAPES) and the National Council for Scientific and Technological Development (CNPq).

This project was supervised by Prof. José Renes Pinheiro from the Electrical Engineering Graduate Program of Federal University of Santa Maria (UFSM). First and foremost, I would like to give my deepest thanks to Prof. Renes for setting the road in which this work traveled, for all the long talks and uninterruptable support. I sincerely thank Prof. Huai Wang for receiving me at Aalborg University and his invaluable guidance and suggestions for this project. Also, I appreciate the help and collaboration given throughout this work by Prof. Hamiltom Sartori from UFSM and Prof. Dao Zhou from AAU.

I express my great acknowledgments to the Center of Reliable Power Electronics (CORPE) from the Energy Technology Department, at Aalborg University, wherein a considerable part of this work was done. I appreciate the hospitality and support of the Energy Technology Department's Staff and Professors. Once again, I thank the Brazilian National Council for Scientific and Technological Development for investing in this research and providing financial support so I could go to Denmark to greatly improve this work.

I would also like to express my gratitude to the Examining Committee of this doctoral dissertation, for their evaluating and providing great insights and suggestions that improved this project since the Qualifying Exam, and which will improve future works derived from it.

Finally, my most sincere and special thanks to my parents and family, for their unwearying love and support. I also give my warm regards to my friends and colleagues from Brazil and from Denmark, especially Camila, Lóren, Tiago, Thomas, Caio, Thieli, Gustavo, André, William, Henrique, Rodrigo, Gleisson, Allan, Pedro, Gabrielle, and Pudim.

João M. Lenz

*"**Do**. Or **do not**. There is no **try**."*
Yoda

ABSTRACT

Multi-objective Design Tool for Optimizing Capacitor Selection in Power Converters Based on the Mission Profile

AUTHOR: João Manoel Lenz
ADVISOR: José Renes Pinheiro

Long-term effective and reliable power electronics systems are one of the next big challenges in the energy sector. Power converter's efficiency and reliability are key elements for expanding renewable sources installed capacity and should be taken into account in annual power processing estimation and in its design phases. Thus, in order to maximize energy yield, reduce costs, and increase revenues by power generation, a power converter must be designed according to the specific system characteristics and its energy profile. Considering photovoltaics (PV) systems as a case study, the instantaneous power delivered is dependent on several factors, such as solar irradiance, ambient temperature, module orientation and mounting type, solar cell performance, among others. This Doctoral dissertation aims to contribute to this topic by proposing a comprehensive and novel multi-objective design methodology for designing capacitors in power converters, based on the energy and environmental mission profile in which they will operate. To achieve this goal, a mission profile characterization method was developed in order to enable the designer with a set of information about the long-term behavior of a PV power plant. Also, in order to enable the long-term analysis of power converter performance, an electro-thermal and lifetime modeling of energy buffer capacitors are done in the function of varying conditions of both ambient levels and energy processing. Results for a single-stage PV inverter are presented and discussed with the following objectives: 1) to understand how different mission profiles affect the performance of power converters and 2) how to use this knowledge in order to properly design the capacitors on a long-term view. A multi-step design tool is developed to reach this goal, where cost, volume, and reliability of multiple capacitor bank designs can be quickly evaluated by the designer. To further demonstrate the usefulness of this proposed design tool, analyses and results of a second case study are also presented, where the DC-link capacitors of a double-conversion uninterruptable power supply are designed.

Keywords: Multiobjective power converter design, mission profile, power electronics reliability, capacitor lifetime modeling

RESUMO

Ferramenta de Projeto Multiobjetivo para Otimizar a Seleção de Capacitores em Conversores de Potência Baseado no Perfil de Missão

AUTOR: João Manoel Lenz
ORIENTADOR: José Renes Pinheiro

Sistemas de eletrônica de potência eficientes e confiáveis a longo prazo são um dos próximos grandes desafios no setor de energia. A eficiência e a confiabilidade do conversor de potência são elementos-chave para expandir a capacidade instalada de fontes de energia renováveis e devem ser levadas em consideração na estimativa de processamento anual de energia e em suas fases de projeto. Assim, para maximizar o rendimento energético, reduzir custos e aumentar o lucro por geração de energia, um conversor de potência deve ser projetado de acordo com as características específicas do sistema e de seu perfil energético. Tomando como estudo de caso sistemas fotovoltaicos, a potência instantânea fornecida depende de vários fatores, como irradiância solar, temperatura ambiente, orientação e tipo de montagem do painel, eficiência das células solares, entre outros. Esta tese de doutorado visa contribuir com este tópico propondo uma nova e abrangente metodologia de projeto multiobjetivo para a seleção de capacitores em conversores de potência, com base no perfil de missão energética e ambiental em que o sistema irá operar. Para atingir esse objetivo, um método de caracterização do perfil da missão foi desenvolvido para permitir ao projetista um conjunto de informações sobre o comportamento de longo prazo de uma usina fotovoltaica. Além disso, para realizar uma análise de longo prazo do desempenho do conversor de energia, é feita uma modelagem eletro-térmica e de vida útil dos capacitores que atuam como *buffer* de energia, em função das condições variáveis das condições ambientais e do processamento de energia. Os resultados de um inversor fotovoltaico de estágio único são apresentados e discutidos com os seguintes objetivos: 1) entender como os diferentes perfis de missão afetam o desempenho dos conversores de potência e 2) como usar esse conhecimento para projetar adequadamente os capacitores com uma visão de longo prazo. Uma ferramenta de projeto de várias etapas é desenvolvida para atingir esse objetivo, onde o custo, o volume e a confiabilidade de vários projetos de banco de capacitores podem ser avaliados rapidamente pelo designer. Para demonstrar ainda mais a utilidade desta ferramenta de projeto proposta, também são apresentados análises e resultados de um segundo estudo de caso, onde os mesmos passos são utilizados para projetar os capacitores do DC-link de uma fonte ininterrupta de potência de dupla conversão.

Keywords: Multiobjective power converter design, mission profile, power electronics reliability, capacitor lifetime modeling.

FIGURE LIST

TABLE LIST

LIST OF ABBREVIATIONS AND ACRONYMS

1x – PV panel on 1-axis mechanical tracker
2x – PV panel on 2-axis mechanical tracker
BOS - Balance of System
BSRN - Baseline of Solar Radiation Network
CEC - California Energy Commission
DFR - Design for Reliability
ECS - Energy Conversion Systems
Fixed – PV panel on horizontal mounting
Horiz – PV panel on fixed tilt angle mounting
IEC - International Electrotechnical Commission
IZA - Izaña
LCOE - Levelized Cost of Electricity
LIN - Lindenberg
LUT – Look-Up Table
MIL-HDBK-217 – Military Handbook 217 - Reliability Prediction of Electronic Equipment
MP - Mission Profile
MPP - Maximum Power Point
MPPT - Maximum Power Point Tracker
MTBF – Mean Time Between Failure
MTTF - Mean Time to Failure
NOCT - Normal Operating Cell Temperature
PoF - Physics of Failure
PV - Photovoltaic
RES - Renewable Energy Sources
ROI - Return of Investment
ROM – Relevant Operation Maps
SSSP – Single-stage single-phase power converter
STC - Standard Test Conditions
TAY - Typical Average Year

LIST OF SYMBOLS

a_D – Diode ideality factor

C_{DC} – Capacitance of DC-link capacitor bank

ESR – Equivalent Series Resistance

FF – Fill Factor

f_G – Grid voltage

f_h – Harmonic frequency

f_{SW} – Switching frequency

G_{NOCT} – NOCT irradiance

G^{PV} – irradiance on the module surface

G^{PV} – Total irradiance incidence on PV surface

$G^{PV}{}_{diffuse}$ – Diffuse irradiance incidence

$G^{PV}{}_{direct}$ – Direct irradiance incidence

I_{cell} – PV cell output current

i_{DC} – Instantaneous current through the DC-link

$I_{PV}{}^{MPP}$ – Current @ maximum power point

I_S – Diode's reverse saturation current

$I_{SC}{}^{STC}$ – Short-circuit current

I_λ – Photocurrent

L – Lifetime in hours

LC – Life consumption

$max\Delta T_{CAP}$ – Maximum core temperature elevation

$nCAPS$ – Number of capacitors in parallel connection

P_{AC} – Instantaneous power injected into the grid

P_{CPR} – Consumed Power Ratio

P_{DC} – Converter instantaneous power level

P_{loss} – Capacitor power losses

$P_{MPP}{}^{STC}$ – Maximum power

P_R – Converter rated power

R_S – Series resistance

R_{SH} – Shunt resistance

R_{th_ca} – Case-to-ambient thermal resistance

R_{th_cc} – Core-to-case thermal resistance

$T_{a,NOCT}$ – Ambient temperature at NOCT
T_{abc} – Ambiance temperature
T_{amb} – Ambient temperature,
T_{CAP} – Capacitor core temperature
T_{cell} – Average between instantaneous and previous temperature
T_{NOCT} – Normal operating cell temperature
V_{CAP} – Capacitor instantaneous voltage
V_{DC} – DC-link average voltage
v_{DC} – Instantaneous voltage across the DC-link
V_{OC}^{STC} – Open circuit voltage
V_{PV}^{MPP} – Voltage @ maximum power point
α – Sun elevation angle
β – PV panel tilt angle relative to ground
γ – PV panel azimuth angle
ΔV_{DC} – DC-link ripple voltage
η_{inv} – Inverter efficiency
θ_i – Incidence angle between Sun and PV module,
μ_I – Short-circuit temperature coefficient
μ_P – Power temperature coefficient
μ_V – Open voltage temperature coefficient
τ_{CAP} – Capacitor thermal time constant

TABLE OF CONTENTS

1 INTRODUCTION

The twenty-first century began amidst a major paradigm shift regarding power generation and energy consumption. Non-pollutant and sustainable processes became a popular demand and a subject for new government policies, affecting not only the industry but also the energy sector. In November of 2016, the Paris Agreement went into effect as a turning point action-plan to reduce global warming and greenhouse gas emissions. The core of this agreement lies in energy processing (IEA, 2016), and it gives focus to increase renewable sources in the power sector and expands the debate over how the electricity market is designed.

Renewable energy has a key role on finding a solution to reduce human-caused climate change, especially considering the perspective of a 30% to 50% rise in global energy demand by 2050 (REN21, 2016). Several reports alert, however, that the needed growth in electric power production should be independent of fossil fuels in order to mitigate CO_2 emissions, pollution, global warming, and other environmental problems. The estimated energy supply investment necessary in the 66% 2°C Scenario (OECD/IEA et al., 2017) is shown in Figure 1; although the needed average annual investment is fairly constant, it shifts away from fossil fuel sources.

Figure 1 – Perspectives for Energy Transition.

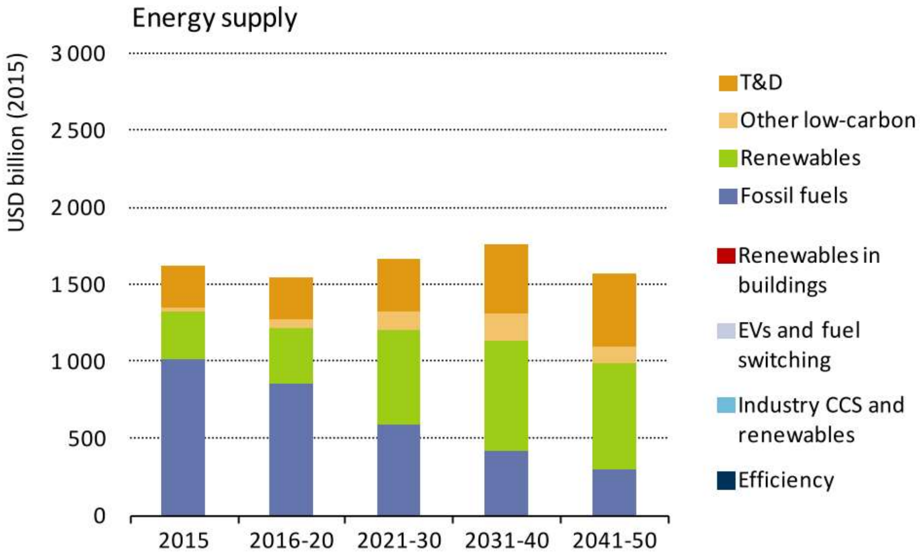

Source: IEA/IRENA

According to (OECD/IEA et al., 2017), two main action fronts are required to achieve this difficult goal:

a) **Political changes:** unparalleled effort to pass green policy measures in all countries, including the phase-out of fossil fuel subsidies, global implementation, and rise of carbon tax, and energy market reforms;

b) **Renewable energy:** massive insertion and investments of alternative power sources in order to achieve the needed transition of the energy sector; the share of primary energy supplied by renewables needs to increase from 15% in 2015 to 65% by 2050.

The addition of renewable energy sources (RES) by itself, however, is only part of the solution. Improvements to energy and material efficiency are also key components towards a low-carbon transition. It is expected that by 2050 renewables and energy efficiency would meet the vast majority of emission reduction needs according to the International Renewable Energy Agency (IRENA, 2016). The global emissions abatement by technology relative to the 66% 2°C Scenario of the Paris Agreement is represented in Figure 2.

Figure 2 – Global emissions abatement by technology.

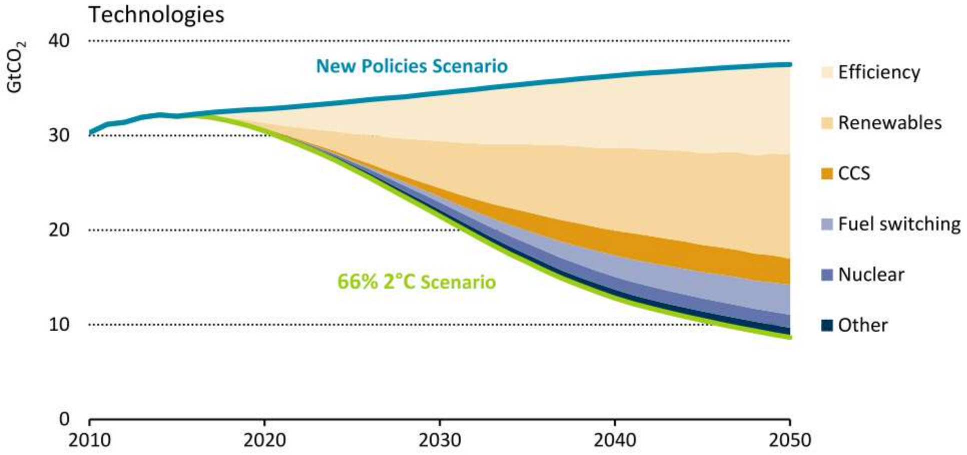

Source: IEA/IRENA, 2016

Efficiency improvement across all end-uses was appointed as the *motor of change* in the 2016's International Energy Agency report, where the need for improving electric energy conversion systems was highlighted. By 2040, an estimated US$ 23 to 35 trillion investment is required for improving efficiency across the energy, industry, and transport sectors.

Thus, research and development on the auxiliary systems required for power conditioning – used to assure safety and standards compliance – will also play a major role in the Paris Agreement fulfillment. The betterment of RES efficiency is a multi-disciplinary task that comprises manufacture and technology advances, utilization rate maximization, smart-grids full deployment and better energy management, and design and performance improvement of power converter systems.

There is a direct relationship between improving energy efficiency and increasing the cost-competitiveness of renewables. The ideology of sustainable energy sources will only succeed if the necessary technological advances are made for it to be economically viable in the face of traditional fossil fuels. Hence the efforts by industry through technology research and development, as well as by governments through subsidies, to reduce the levelized cost of electricity (LCOE) of renewables. The LCOE is the net unit-cost of electricity over the lifetime of a specific power plant and it represents the minimum average price at which electricity must be sold in order to reach break-even.

$$LCOE = \frac{\text{sum of lifetime costs}}{\text{sum of lifetime electricity generated}} \tag{1}$$

Main factors to LCOE calculation include capital costs, fuel costs, fixed and variable operation and maintenance (O&M) costs, financing costs, and return projection (U. S. ENERGY INFORMATION AGENCY, 2017). Although it has inherent uncertainties and regional variations, the LCOE projections are useful both as an indicator of the average cost per unit of electricity and as a comparison method for different generation technologies.

LCOEs of the more consolidated technologies – such as biomass, geothermal, and hydropower – have been in the range of fossil fuel prices for a long time and are broadly stable since 2010 (IRENA, 2015), with regional exceptions. Solar and wind-powered source prices have been consistently falling for more than a decade and 2016 was the landmark year where solar PV weighted average LCOE matched that of fossil fuel, depicted in Figure 3.

The importance of scientific research and development on RES and on energy processing is highlighted in this context; reducing the LCOE of renewables is both an industry concern as a social one. Thus, the Doctoral dissertation presented here aims to make a new contribution in the field of power electronics and energy processing for photovoltaic systems, by proposing a design methodology to enhance the performance and reliability of power converters.

Figure 3 – Rethink Energy 2017

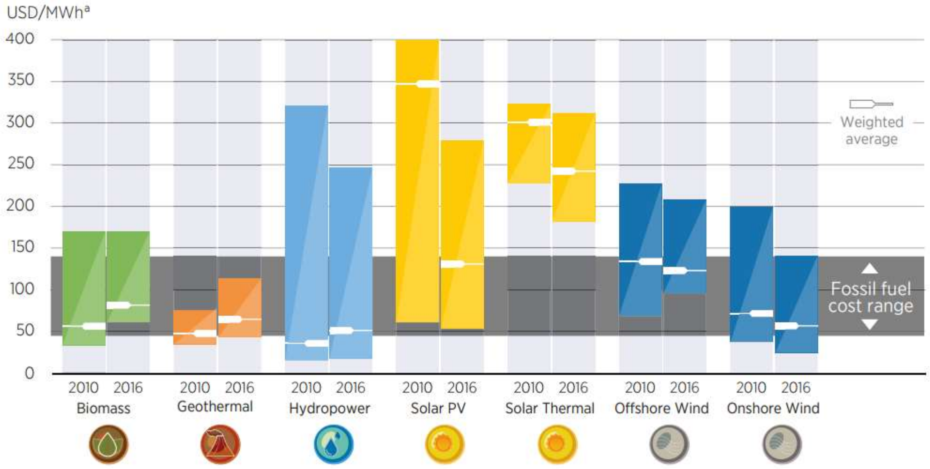

Note: a) MWh: megawatt-hour
b) All costs are in 2016 USD. Weighted Average Cost of Capital is 7.5% for OECD and China and 10% for Rest of World

Source: IEA/IRENA

1.1 ENERGY PROCESSING

The continuous increase of RES penetration into the grid imposed a new set of challenges such as power fluctuation, harmonic content mitigation, stability and safety regulations, among others. Power electronics is one of the fields most capable of resolving a wide variety of issues since it is a required interface between the RES and the mains.

For instance, maximum power point trackers (MPPT) – which are a necessity in the wind and solar application due to their intermittent characteristic - are employed through power converter control (CHAVES et al., 2016; ZHAO et al., 2015; ZINE et al., 2014) to ensure that the maximum available energy is being harvested. Harmonics resultant of switching frequency is reduced nowadays mainly through proper *L*- and *LCL*-filter design (CHANNEGOWDA; JOHN, 2010; ELSAHARTY; ASHOUR, 2014); while low order harmonics are usually mitigated by the use of advanced modulation and control techniques (CIOBOTARU et al., 2005). Additionally, transformerless inverters are a trend in medium and high power applications since higher global efficiencies can be achieved when the isolation transformer is removed (Hung et al., 2010); the ground current in these topologies is, however, a major concern and its minimization is mandatory.

Optimization techniques are also a modern solution to achieve high performance and reliable power converters for RES; optimizing one or multiple parameters in the design stage can lead to an enhanced performance of power converters in the considered scenario. Nevertheless, optimization requires an additional group of information when compared to traditional design techniques. The knowledge of specific ambient conditions and energy profile in which the converter will operate are needed since the designer can only optimize a system inside a specific set of constraints.

The use of optimization methodologies in the design and operation of RES power converters are a smart solution to achieve higher efficiency, longer lifetime, and better performance. In addition, a wide range of parameters and objectives may be approached through these techniques, from the optimum control of reactive power circulation to improve thermal behavior in wind power converters (ZHOU et al., 2014), to the optimal design of transformerless PV inverter in terms of component reliability increase (SARIDAKIS et al., 2013).

The increase of overall efficiency in energy processing systems is a global priority, as previously described, especially in renewable sources. However, only photovoltaic energy will be used as a study case in this Doctoral dissertation since solar energy still is dominant in residential and commercial applications. Nevertheless, the methodology and considerations proposed in this document may be expanded, within its limitations, to others applications, topologies, and/or energy systems.

1.2 PHOTOVOLTAIC OUTLOOK

Since 2000, the cumulative installed solar PV power capacity increased 29% year-on-year; an addition of over 450% in total global PV capacity was registered from 2010 to 2015 (EUROPE, 2017). Projections of the most probable scenario foresee an increase of 97 GW of installed PV capacity by 2020, as shown in Figure 4. Although this positive view of the market, the cost of financing is still a crucial criterion for investment decisions by both utility-scale and homeowners. Modules and balance of system (BOS) correspond to 50% of a solar power plant cost (SPE 2017) being the inverter responsible for a considerable amount of this total; O&M services and insurances correspond to another big share of PV costs.

The cost of energy of PV systems is highly dependent on the DC/DC converter and inverter (IRENA, 2013), not only due to installation costs but also for processing energy throughout the year in various ambient conditions. The overall efficiency of the power electronic systems dictates the amount of PV energy injected into the grid, hence affecting also self-consumption, feed-in revenues, and payback time. Thus, topology selection and converter design are critical to ensuring the success and viability of a PV plant.

Figure 4 – Global annual solar PV Market scenarios until 2020.

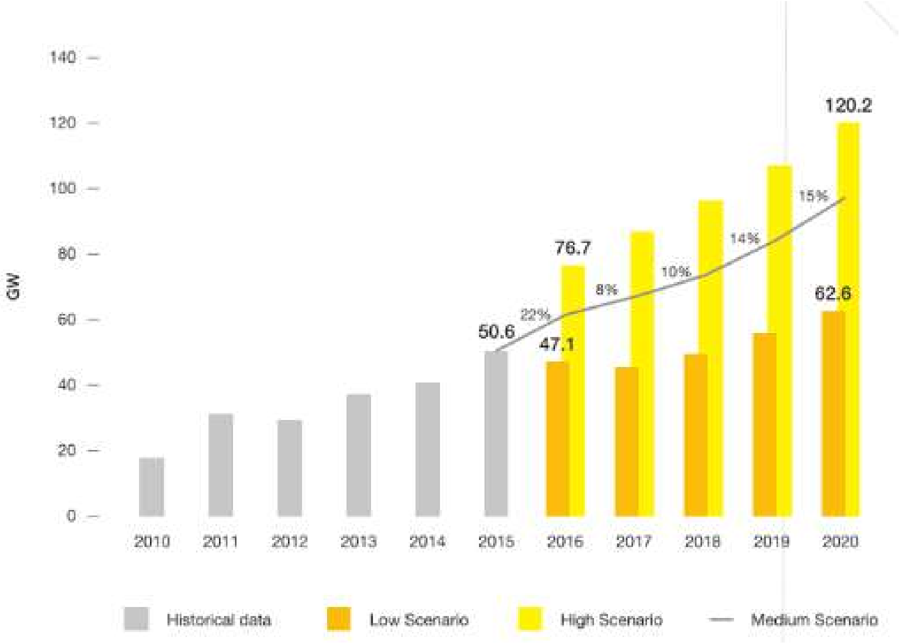

Source: EPIA 2016

Several configurations are currently used in order to harvest and transfer the PV power to the grid, as it is depicted in Figure 5. The association of series and paralleled PV panels in multiple strings is designed according to the expected power plant size, module technology, available location for the installation, among other factors. The coupling of DC-DC converters and DC-AC inverters is also a major designer decision and is usually made according to the PV panels output voltage and power rating.

Central inverters are normally employed in three-phase grid-tied PV plants with larger power ratings since they have the benefit to achieve relatively high efficiencies with lower costs. However, this configuration requires high voltage DC cables (KJAER, et al., 2005) and may suffer from low PV utilization due to power mismatch caused by shading and other differences in module operation. The string and multi-string configurations solve this issue by employing an individual DC-DC converter in each string, ensuring an adequate MPPT and increasing power production. However, DC-module converter and/or AC-module inverter are required in order to achieve the maximum energy-per-panel yield; these are a flexible solution for PV systems of low power ratings and also for module-level monitoring and diagnostics (YANG; BLAABJERG, 2015).

Figure 5 – Configurations used to harvest and transfer the PV power to the grid.

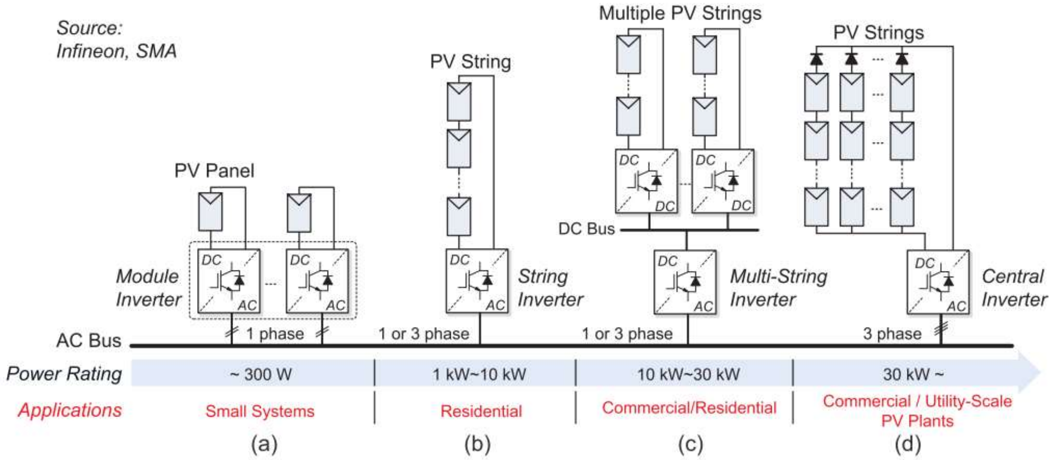

Source: Infineon, SMA

The module concept and string/multi-string inverters are the most used configuration in small single-phase PV systems, where the galvanic isolation is one of the most important safety measures due to ground leakage currents. Traditionally, an isolation transformer may be placed either at the grid-side or as a high-frequency transformer, as shown in Figure 6a and Figure 6b, respectively. The transformerless solution, shown in Figure 6c, tends to increase overall efficiency and power density due to the bulky transformer's removal, but control complexity and safety requirements are also increased in face of a common-mode voltage presence.

1.3 HIGH-PERFORMANCE PHOTOVOLTAIC SYSTEMS

Long-term effective and reliable systems are the next big challenge in the photovoltaic generation and cost competitiveness is still one of the constraining causes in the PV industry. Case studies frequently show that power converters are still the element most prone to failure in PV systems and therefore, the design of more reliable power converters is a necessity (RISTOW et al., 2008; ZHANG et al., 2012).

Figure 6 – Typical architectures for single-phase grid-tied PV systems: a) with low-frequency transformer, b) with HF frequency transformer, and c) transformerless.

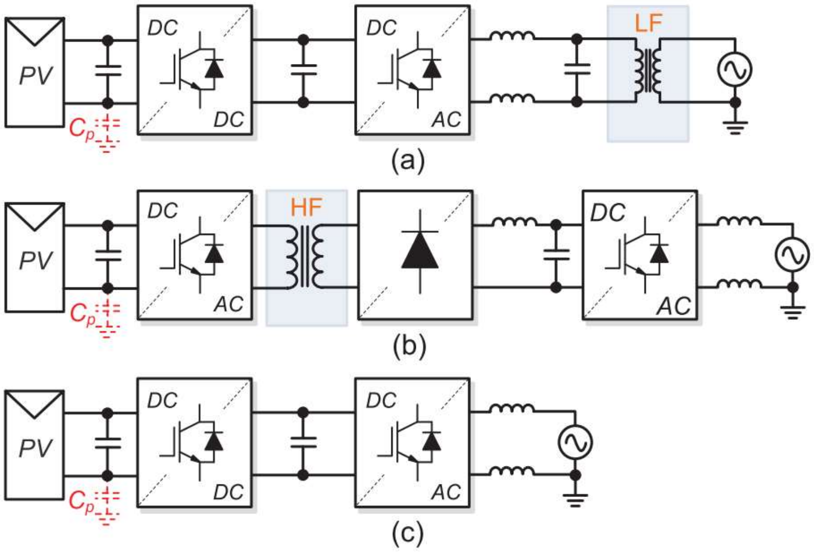

Source: Yang, Y., 2014

Power converters' efficiency and reliability are key elements for expanding PV installed capacity and should be taken into account in solar energy generation and in its design phases. Thus, in order to maximize energy yield, one must design and size a power converter according to the PV system characteristics and its generation profile. Instantaneous power delivered by PV power plants is dependent on several factors, such as solar irradiance, ambient temperature, module orientation and mounting type, solar cell performance, among others (RHODES et al., 2014; VERGURA, 2015). Previous knowledge of in situ characteristics becomes essential for a correct system design, since inaccuracies in calculating rated and maximum values of energy yield estimation may propagate through all design stages.

In this context, designing and manufacturing more reliable and more efficient power converters is crucial for enhancing a photovoltaic power plant cost-effectiveness. An accurate characterization of the PV mission profile should be the first step for any analysis involving reliability and pre-design, as knowing the available energy profile allows the understanding of the electrical and thermal behavior in which a power converter and its elements will operate.

A mission profile (MP) is a simplified representation of the relevant conditions that the system in focus will be exposed in its intended application (ZVEI, 2008). In photovoltaic systems, MP can be defined as a dataset of annual power generation, energy estimation, environmental, and graphical results; from these, designers are able to extract the minimum, average, and maximum current, voltage, and temperature values in which the PV system will operate and build a relevant operation map. A detailed MP serves to accomplish different analyses, such as defining the optimum orientation for a PV power plant, performing financial feasibility studies, adequately choosing and sizing PV modules and power converters, among other aspects, as summarized in Figure 7. Previously characterizing the PV mission profile enables a comprehensive pre-design phase and supplies the designer with a valuable set of knowledge that can lead to enhancing the overall performance of photovoltaic energy processing.

Figure 7 – Proposed characterization of the PV mission profile through multiple variables.

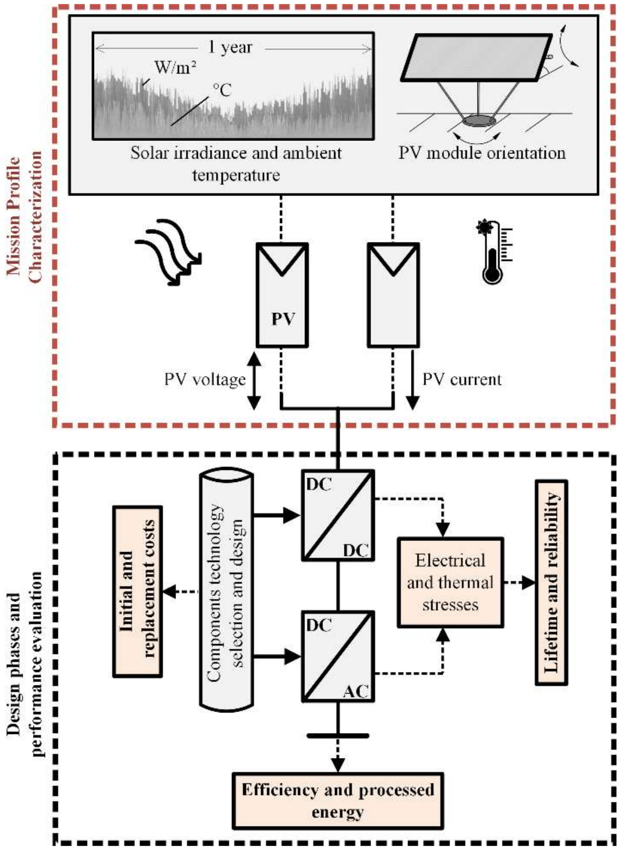

Source: Personal archive.

Array and PV inverter sizing methodologies also benefit from the PV MP definition, like the one proposed by (MONDOL et al., 2006); the authors presented a correlation between optimum sizing ratio and PV/inverter cost ratio as functions of insolation and inverter type. Multiple factors for different European locations were considered, such as orientation and inclination, tracking mechanism, insolation, total system output, among others. Typically, the sizing ratio to maximize the energy produced per system investment ranges from close to 1 to approximately 2 (PEIPPO; LUND, 1994) and different approaches have been proposed to find the ideal PV/inverter ratio. An analytical method for calculating the optimum inverter size in grid-connected PV plants was proposed by (DEMOULIAS, 2010) using two observations: that the DC power of a PV plant can be represented as a straight line and that the efficiency curve of any inverter can be accurately defined by deriving three parameters from datasheet information. In contrast, a method to find the optimum PV plant for a specific inverter was presented by (FARANDA et al., 2015) through the extraction of a general efficiency curve for different DC/AC converters.

1.3.1 Optimization Techniques for Converter Design

Modern design methodologies for PV DC/DC converters and inverters are focused on multi-criteria improvement, as an increase in energy efficiency, reduction of volume and/or cost, and increase in lifetime. Optimization techniques for choosing the appropriate components technology and operating point have been proposed in order to enhance power density (SARTORI et al., 2013; SCARPA et al., 2011). The trade-off between efficiency and power density was also studied by (KOLAR et al., 2009) in an optimized design for a PFC dual-boost converter, where maximum efficiency was analyzed at the rated power.

Even though photovoltaic generation is somewhat unpredictable on a very short term, it hardly operates at the system's rated power. As thoroughly discussed by (DUPONT et al., 2012; KLEIN et al., 2009), contribution to PV energy is higher at mid-range solar irradiance levels. For this reason, (BELTRAME et al., 2014) proposed an optimum design of a PV boost converter where the operating point, magnetic materials, and semiconductors were selected in a database to increase annual power processing. By matching the DC/DC converter's efficiency curve with local weighted average solar irradiation, the boost's performance is greater in the most frequent irradiance levels. However, the authors used only data from horizontal irradiance measurements from a single location and did not explore the impact of different locations and/or realistic PV power plants on the design parameters.

A methodology for the optimal design of transformerless grid-connected PV inverters targeting cost-effectiveness was proposed by (KOUTROULIS; BLAABJERG, 2013), where the inverter's switching frequency, output filter values, and heat sink type were optimally chosen according to the lowest LCOE. The optimization algorithm proposed by the authors relies on a set of inputs such as 1-hour average solar irradiance and ambient temperature, operational characteristics of the PV array, and technical and economical characteristics of multiple component types. Inverter maintenance costs are based relative to the number of predicted failures calculated by Mean Time To Failure (MTTF) methods.

1.3.2 Reliability and Lifetime of Photovoltaic Converters

Lifetime improvement of power electronics is becoming a demand in the PV industry, different approaches have been proposed in recent years to design more robust and reliable converters and inverters applied in photovoltaics. A reliability-oriented design guideline was proposed in (WANG et al., 2013) aiming to increase the long-term operation of a transformerless PV inverter, where an analysis was performed to select the input capacitor bank with minimum overall stress and maximum lifetime. According to a five-year study in a large PV power plant (MOORE and POST, 2008), PV inverters were the element responsible for most of the unscheduled maintenance and repair costs.

The effect of different MPs, due to climate variation in different global locations in the reliability of a PV push-pull was analyzed by (DE LEON-ALDACO et al., 2015), using local measures of irradiation, temperature, and humidity. Diodes and capacitors presented higher failure rates and more susceptibility to thermal stresses, where the diodes were significantly affected by the number of thermal cycles on the long-term operation. Although the authors used the outdated U.S. Military Handbook 217 methodology to calculate failure rates, their work demonstrates the possibilities and advantages of using mission profile and reliability as parameters to design and evaluate power converter performance.

1.4 MOTIVATION AND OBJECTIVES

The past decade was marked by an intense work of proposing and putting into effect several electrical standards regarding photovoltaics, both by the International Electrotechnical Commission (IEC) and legislative agents. Solving the complex issues of grid-connection, however, should not compromise the cost-competitiveness of photovoltaics; considering the reliability, power density, and overall efficiency in the design stage is one of the main steps needed for achieving high-performance power converter systems.

1.4.1 General View

The main objective of this doctoral dissertation is to propose a new methodology for multi-objective design of capacitors in power converters through an optimum component selection and sizing of the capacitor bank, as depicted in Figure 8. Capacitors are chosen as a focus due to being one of the most prone-to-failure components in power electronics. Reliability, cost, and volume are the main figures of merit to be evaluated and prioritized by the designer.

This design tool is mainly focused on time-variant energy processing systems, where the previous knowledge of available energy profile is essential in order to perform optimization techniques since a converter can only be optimally designed for a specific set of conditions. Thus, defining the specific mission profile in which the power converter will operate is the foundation for the proposed methodology. Two case studies are considered and analyzed: 1) photovoltaic systems are used as the main case study where, aside from the design tool, it also proposed a mission profile characterization methodology; 2) double-conversion uninterruptable power sources (UPS) are also analyzed in a second case study, since capacitors play a key role in these systems due to their energy storage capability. However, the design tool described here is easily applicable to other renewable or time-variant energy systems.

1.4.2 Specific Objectives

a) Develop a methodology to characterize the PV mission profile through long-term weather data for any location, PV technology, and mounting configuration. The PV MP definition must provide a comprehensive set of information regarding the PV system current and voltage levels, relevant operating regions;

b) Elaborate a lifetime analysis tool for power converter components in function of time-variant load and ambient conditions. This tool must be able to estimate lifetime and degradation for time and energy-variant operating conditions through electro-thermal modeling;

c) Create a figure of merit to be used in the pre-design and design stages of power converters. This should aid the designer to make compromise choices between cost and reliability;

d) Develop a methodology for multi-objective design of capacitors in power converters using reliability, cost, and volume as figures-of-merit.

Figure 8 – Diagram of the proposed methodology for power converter design based on the mission profile and lifetime analysis.

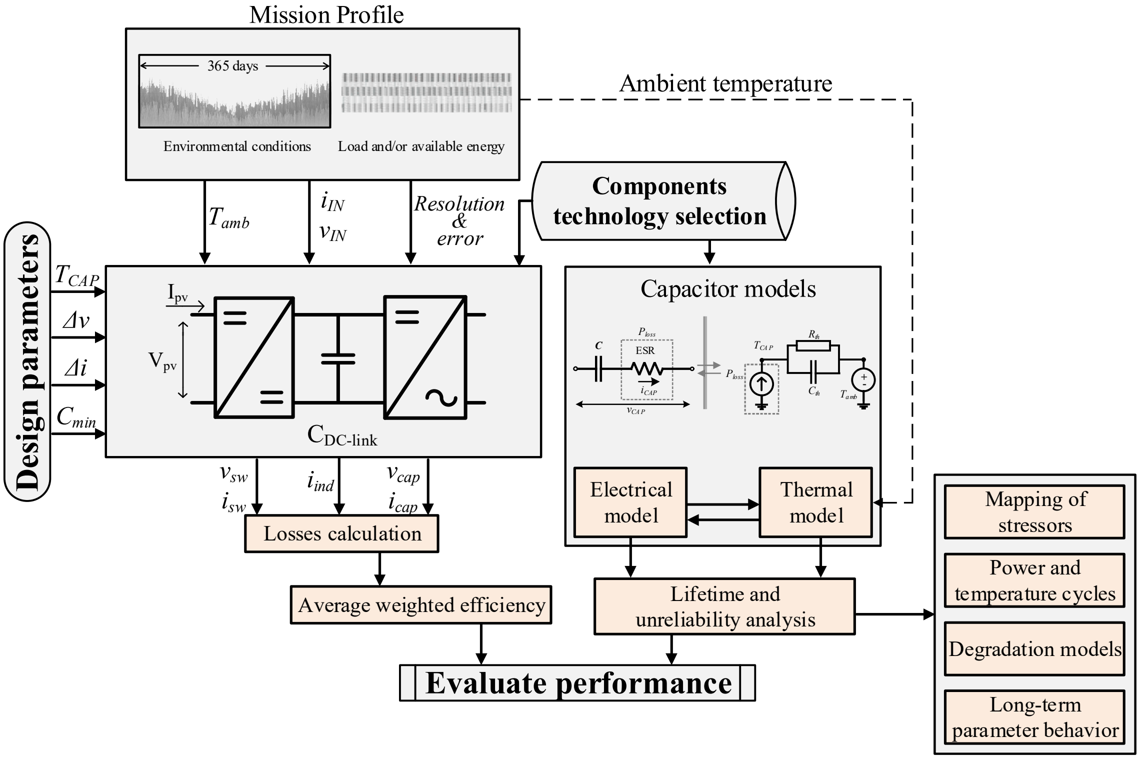

Source: Personal archive.

1.4.3 Dissertation Structure

Following the same foundations showed in the diagram of Figure 8 diagram, this Dissertation begins with a discussion on the importance of characterizing the power converter mission profile for reliability-oriented and optimum design of power converters. Since this work defined photovoltaic generation as the main case study, Chapter 2 brings a proposed methodology to accurately characterize the energy profile of PV systems. It is hoped that the models and results obtained in that chapter may serve as a guideline tool for designing high-performance PV power converters.

In Chapter 3, a comprehensive electro-thermal modeling of electrolytic capacitors is presented along with experimental results for validation at component and system levels. The proposed design tool focuses on capacitors since they are well-known to be one of the bottlenecks for reliability in power electronics. In Chapter 4, the current paradigm of reliability studies is discussed and why it is becoming a hot topic in energy conversion systems. Also, details on how the lifetime and reliability estimation of power converter capacitors in long-term operation are presented.

In Chapter 5, results and models from the previous chapters are combined and analyzed in two different scenarios: a 1) single-stage single-phase full-bridge PV inverter; 2) a single-phase double-conversion UPS unit. Although UPS systems are not discussed during most part of this dissertation, this case study is investigated to further exemplify the capabilities of the proposed tool. Results from these two scenarios are presented and a further discussion is issued regarding how this proposed methodology may aid power electronics designers to make better decisions.

Finally, final considerations are presented in Chapter 6, along with a reflection of the current limitations of this work and what is planned for future improvements in this research.

2 PV MISSION PROFILE CHARACTERIZATION

In Chapter 1, it was stated that one of this work's main objective is to develop a power converter design tool that enables the designer from a long-term perspective. Two pillars are essential to achieving this goal, being the first the inclusion of a reliability/lifetime metric as a design parameter, which is discussed in the next chapter. The second necessary foundation is a comprehensive understanding of the energy profile in which the power converter will operate.

A system is only optimized for a closed set of constraints and, analogously, a lifetime estimation is valid for a specific set of conditions. When talking about ECS, the definition of these constraints and conditions translates to accurately knowing the energy processing profile. In this manner, photovoltaic generation was chosen as a study case for this work and this chapter details a proposed methodology for characterizing a PV mission profile.

2.1 PV MODELING

In order to estimate correctly the energy processed annually by an inverter at a specific location, the solar cell was mathematically modeled to determine output power, current, and voltage of a PV panel for different conditions of irradiation and temperature. The well-accepted one-diode equivalent circuit for a PV cell shown in Figure 9 was used, where a current source emulates the current generated by the photoelectric phenomenon, and the diode represents the semiconductor's non-linear characteristics. Losses are represented both by shunt and series resistances, R_{SH} and R_S, where the former represents the effects of internal leakage current and the latter is ohmic losses from PV's metallic conductors.

Figure 9 – Solar cell parameters and the one-diode equivalent circuit.

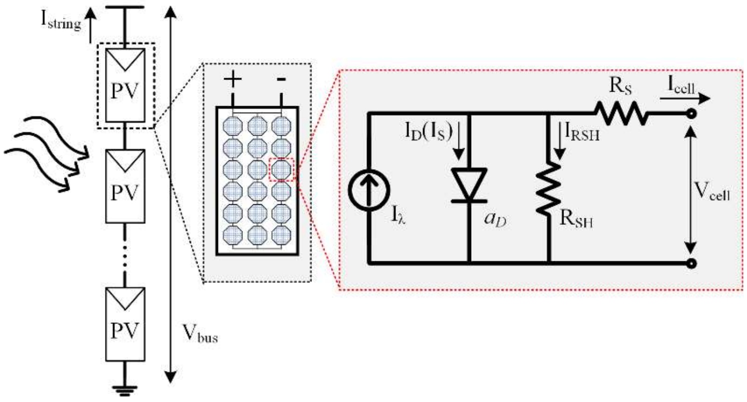

Source: personal archive

Analysis of Figure 9 gives that the PV cell output current (I_{cell}) is obtained by

$$I_{cell} = I_{\lambda} - I_{D} - I_{RSH} \tag{2}$$

where I_{λ} is the photocurrent, I_{RSH} is the current due to losses in parallel resistance, and I_D is the current flow in the cell's intrinsic *p-n* junction.

2.1.1 PV cell 1-diode model

A commercial module from Sun Earth® was used for modeling and validating the studied PV system, the model TPB 235 W with polycrystalline cells was chosen due to availability for experimental testing and for having an adequate amount of datasheet information – the following methodology can be reproduced for any panel manufacturer or module type. Main characteristics of the used panel are shown in Table 1, for standard test conditions (STC).

Table 1 – Sun Earth® TPB 165×165-60-P 235 W datasheet information.

Parameter	Value	Description
I_{SC}^{STC}	8.47 A	Short-circuit current
I_{PV}^{MPP}	8.05 A	Current @ maximum power point
V_{OC}^{STC}	36.7 V	Open circuit voltage
V_{PV}^{MPP}	29.2 V	Voltage @ maximum power point
P_{MPP}^{STC}	235 W	Maximum power
μ_P	-0.45%/°C	Power temperature coefficient
μ_V	-0.35%/°C	Open voltage temperature coefficient
μ_I	0.05%/°C	Short-circuit temperature coefficient

Source: personal archive

Modeling of the equivalent circuit, displayed in Figure 9, consisted of finding four key parameters: diode's reverse saturation current (I_S), shunt and series resistances, and diode's ideality factor (a_D). Since the panel output current is non-linearly dependent on the output voltage, V_{PV}, (2) can be rewritten as (2) and an iterative method is needed to solve this transcendental equation.

$$I_{cell} = I_{\lambda} - I_{S}\left(\exp^{\left(\frac{q(V_{cell}+R_S I_{cell})}{kT_{cell}a_D}\right)} - 1\right) - \frac{V_{cell} + R_S I_{cell}}{R_{SH}} \tag{3}$$

where V_{cell} and I_{cell} are the voltage and current, respectively, of a single photovoltaic cell, q and k are the electron charge ($q = 1.602 \times 10^{-19} C$) and the Boltzmann ($k = 1.38065 \times 10^{-23} J/K$) constants, and T_{cell} is the PV cell temperature, in Kelvin.

The methodology proposed by Villalva et al. (2009) was used for determining I_S, R_{SH}, and R_S, through the values exposed in Table 1. An initial guess of the shunt resistance was set and the iterative process of I_S, R_{SH}, and R_S was conducted until the maximum power point (MPP) at STC was calculated with an error less than 0.5%. According to Villalva et al. (2009), the dimensionless ideality factor can be parametrically adjusted, thus, a first estimation of a_D was set as the $I \times V$ curve fill factor (FF) inverse, as in (4). The calculated parameters for the described model are presented in Table 2.

$$a_D = FF^{-1} = \frac{V_{OC}^{STC} I_{SC}^{STC}}{V_{MPP}^{STC} I_{MPP}^{STC}} \tag{4}$$

where V_{OC}^{STC} is the open circuit voltage, I_{SC}^{STC} is the short-circuit current, and V_{MPP}^{STC} and I_{MPP}^{STC} are the MPP voltage and current, respectively. Assuming that $I_{\lambda} \approx I_{SC}$ and with the initial guess for a_D given by (4), I_S, R_{SH}, and R_S were calculated by solving (3) through and an iterative process (VILLALVA et al., 2009). Afterward, a parametrical adjustment on the ideality factor was done with the objective to minimize the V_{MPP}^{STC} error relative to the datasheet value.

Table 2 – Sun Earth® TPB 165×165-60-P 235 W modeled parameters.

Parameter	Value	Description
R_{SH}	648.76 Ω	Shunt resistance
R_S	0.145 Ω	Series resistance
I_{S0}	1.2783×10^{-7} A	Diode reverse saturation current
a_D	1.312	Diode ideality factor

Source: personal archive

2.1.2 Panel Operating Temperature

Photovoltaic efficiency decreases with the rise of operating temperature, as discussed in the literature (ACCETTA et al., 2012; COELHO et al., 2009; RAHMAN et al., 2014; SKOPLAKI; PALYVOS, 2009b); the well-accepted model described by (5) was chosen for estimating cell operating temperature (T_{cell}). Although simple, this model is considered accurate for calculating T_{cell} in function of incident irradiance and ambient temperature, for crystalline silicon PV cells (SKOPLAKI; PALYVOS, 2009a).

$$T_{cell} = T_{amb} + \left(T_{NOCT} - T_{a,NOCT}\right)\frac{G^{PV}}{G_{NOCT}} \tag{5}$$

where T_{amb}, T_{NOCT}, and $T_{a,NOCT}$ are the ambient temperature, normal operating cell temperature (NOCT), and ambient temperature at NOCT, respectively; G^{PV} and G_{NOCT} are the irradiance on the module surface and the NOCT irradiance. The main issue of (5) is that it considers only steady-state temperature. In order to account for thermal dynamics and avoid abrupt temperature variations due to irradiance change, actual T_{cell} as an average between instantaneous and previous temperature values was estimated.

2.2 PV SYSTEM VALIDATION

Each Sun Earth® model is composed of 60 (sixty) cells in a series connection, thus the PV panel output current was mathematically reproduced through (3) and the parameters of Table 2. The $I \times V$ characteristic curve in function of the cell operating temperature and incident solar radiation was modeled for varying environmental conditions. In order to validate the PV modeling and energy estimates, simulated results were compared with long-term experimental measurements from a real photovoltaic plant. This system is composed of twenty-eight Sun Earth® Polycrystalline TPB 235 W modules equally divided in two parallel strings; each string has fourteen modules in series connection with a total of 3.29 kW installed power. The power plant is on a rooftop using fixed mounting, with a tilt angle of 24° towards North, located at S 29°42'48.379" and W 53°43'2.5986".

A central inverter (SMC 6000TL from SMA) performed MPPT, DC bus regulation, and energy processing. An instrumentation system measured current and DC bus voltage; ambient and PV module temperatures, and in-plane irradiance; one-second measures were acquired and one-minute averages were stored. String current and DC bus data were compared with simulation results in order to validate the PV modeling. Estimated and measured current and voltage are depicted in Figure 10 where three days with different irradiance and temperature conditions are highlighted.

Discrepancies found from measured results can be explained, mainly, by the fact that the MPPT carried out by the inverter is non-ideal and the real system may not be operating exactly at the MPP. The MPPT also tends to operate less effectively at low irradiances, which may explain why the model is significantly overestimating in very-low-power conditions. In addition, possible mismatch and soiling of PV panels in each string were not included, which can cause difficulties for the central inverter to find the global maximum power point.

Figure 10 – I×V curve of modeled PV panel validated according to datasheet information and compared with experimental measurements for varying seasonal conditions of irradiance and temperature.

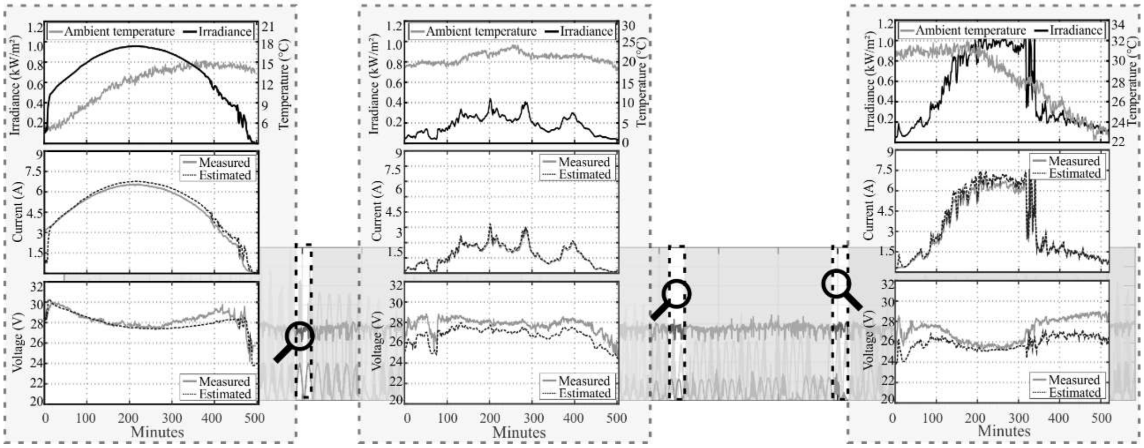

Source: personal archive

A scatter plot of the estimated power versus measured values is shown in Figure 11, where each point represents PV string power in one minute. Although simulation results seemed to overestimate the power produced by the PV string, there is an evident relationship between estimated and experimental values.

Furthermore, the PV operating temperature is another source of possible inconsistencies in the obtained results since both the PV module efficiency and output voltage are highly dependent on the solar cell temperature. Despite being widely used, this work is limited to the model of (5) to estimate the PV module temperature; this model does not take into consideration cooling caused by the wind, heat transfer or any other thermal dynamics. A more sensible and complex approach for estimating the PV operating temperature should improve the presented results, but it is out of this work’s scope.

Figure 11 – Comparison between simulated and experimental PV maximum power for various conditions of irradiance and temperature.

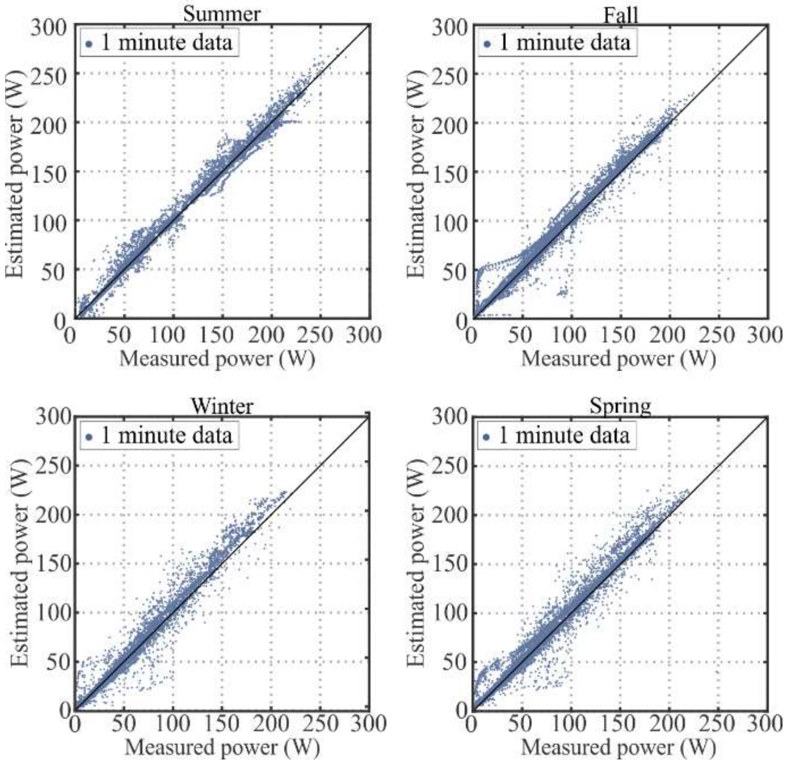

Source: personal archive

Although neglecting these aspects, the PV string generated energy measured was equal to 1.615 MWh, while estimated was equal to 1.654 MWh, resulting in an overall error of 2.42%. Mean Absolute Error (*MAE*) for power, voltage, and current estimates were calculated by (6) and normalized with respect to the mean measures of each variable.

$$MAE = \frac{\sum_{i=1}^{n} \left| y_i - x_i \right|}{np} \tag{6}$$

where *np* is the number of data analyzed, and *y* and *x* are the estimates and measurements. Normalized *MAE* of power, voltage, and current were equal to 0.0654, 0.0496, and 0.0465, respectively.

2.3 DATASETS

Solar energy maps and databases are useful for feasibility analysis and assessing PV energy in locations with none or small data availability, as in (HULD et al., 2012; KHAN; AHMAD, 2012); while forecasting techniques are valuable tools for operating plants and making short-term decisions, as presented by (CHEN et al., 2011; GULIN et al., 2017). However, in order to maximize energy harvesting, quality data and from long periods must be used in the design stages of photovoltaic systems and its power converters. Uncertainties in solar data can make the difference between profit and loss (PAULESCU et al., 2013), especially in large-scale PV plants with high financial investments.

In this work, data from three meteorological stations were used; these stations are under the responsibility of various climate/weather agencies and belong to the Baseline of Solar Radiation Network (BSRN). Further information on data quality and retrieval are available via (WRMC-BSRN, 2017).

2.3.1 Dataset and quality check

In order to investigate the impact of weather variability on photovoltaic energy, three locations with distinct climates were analyzed. Furthermore, these cities were chosen for having certified BSRN stations with a long period of available data and being fully equipped for radiometric measurements. These stations are localized at Petrolina (PTR), Brazil, Izaña mountain (IZA), Tenerife, Spain, and Lindenberg (LIN), Germany. Further information is described in Table 3.

Table 3 – Station information from the data used in this work.

Station	Latitude	Longitude	Elevation	Number of months with data
PTR	09°07’ S	40°32’ W	387 m	119
IZA	28°31’ N	16°50’ W	2373 m	87
LIN	52°21’ N	14°12’ E	125 m	80

Source: personal archive

Horizontal positioning is hardly employed in photovoltaic systems and clear sky is scarcely possible in normal weather conditions. Even though being unrealistic scenarios, global horizontal data and clear sky models are frequently used to design and analyze PV systems, as in (DAUT et al., 2011; DUPONT et al., 2012; SINTAMAREAN et al., 2014). To avoid inaccuracies, measured data of global horizontal, direct, and diffuse irradiances and ambient temperature was used.

Each of these four variables was recorded in a one-minute resolution along with a timestamp, totaling more than two million data points per year per location. A ten-year period dataset was collected from PTR and an eight-year period from LIN and IZA, which ensures a precise set of data.

Since stations that belong to the BSRN are required to undergo calibration and standard checks, data of each considered variable was submitted to a quality control process. A two-step procedure to examine data quality was realized through BSRN Toolbox (SCHMITHÜSEN et al., 2012) and the following quality checks were done:

a) Verify and flag if a sample is outside physically possible limits;

b) Verify and flag if a sample is physically possible but extremely rare;

The limits and quality control recommendations presented by (LONG; DUTTON, 2004) were used.

2.3.2 Typical average year

According to the previously described instructions, data samples that failed the physically impossible and extremely rare tests were discarded. In order to maintain the consistency of measurements, all samples in the same minute were excluded if one variable failed the quality test; *e.g.*, if a diffuse irradiance measurement was outside the physically possible limit, all other data in that same minute were discarded and considered as not a number.

For each analyzed city, a long-term dataset of four variables in one-minute measurements was formed. With such a large span of time and data, it was possible to obtain a representative annual profile of both solar irradiance and ambient temperature. Due to climate long-term variability and weather short-term randomness, the large dataset used in this work favors the analysis under the perspective of the average operating conditions at each location, in a period length relevant to the PV plant lifetime.

The Typical Average Year (TAY) was obtained by grouping and averaging the variables of interest according to the timestamp in which they were measured. Minute-by-minute measurements of irradiance (horizontal, direct, and diffuse) and ambient temperature were placed in separate arrays; in order to obtain equally sized arrays (525,600 minutes for each year), additional days of leap years were discarded. After this data handling, the Typical

Average Year was formed by taking the minute average of all samples within the same array position (same timestamp) across each year with available data. Thus, TAY of each location is a 4×525600 matrix, and its values are the representative average condition of each variable throughout the year.

2.3.3 Irradiation and temperature profile

In order to observe and illustrate the difference between profiles of all irradiances and temperature from each location, Figure 12 depicts the daily averages of all variables obtained from the calculated TAY. Available solar energy in the TAY in relation to irradiance level is depicted in Figure 13, alongside annual irradiance on the ground surface. The differences between the analyzed profiles permit to characterize how different ambient conditions affect PV generation and distinct elements of power processing units.

Figure 12 – TAY profile for solar irradiance from a) Petrolina, b) Izaña, and c) Lindenberg, and ambient temperature from d) Petrolina, e) Izaña, and f) Lindenberg.

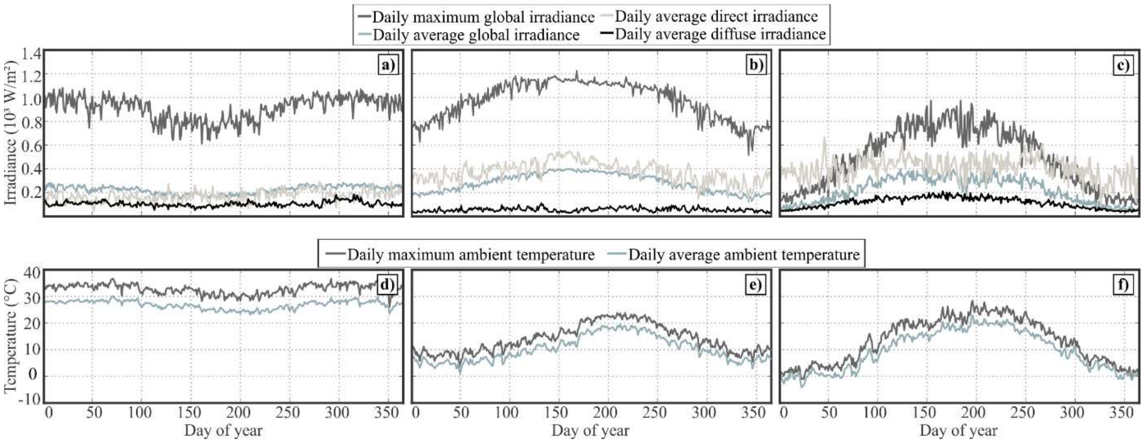

Source: personal archive

2.4 PV MOUNTING AND POSITIONING

Accurate estimation of photovoltaic energy production is not a trivial task since it relies on the precision of multiple models and datasets combined. In this preliminary work, available datasets of solar energy and a Sun path calculation algorithm were used as input; afterward, a mathematical model is used to determine PV panel orientation relative to the ground and the incidence angle between Sun and PV surface. Finally, a photovoltaic cell model to estimate output power throughout a one-year operation was used.

2.4.1 Surface irradiance incidence

Evaluation of annual irradiance incidence on a PV module with fixed mounting, or mechanical tracking, was done through a multiple-step algorithm, summarized as follows:

Figure 13 – Solar radiation at a) Petrolina, b) Izaña, and c) Lindenberg in different irradiance levels in the TAY.

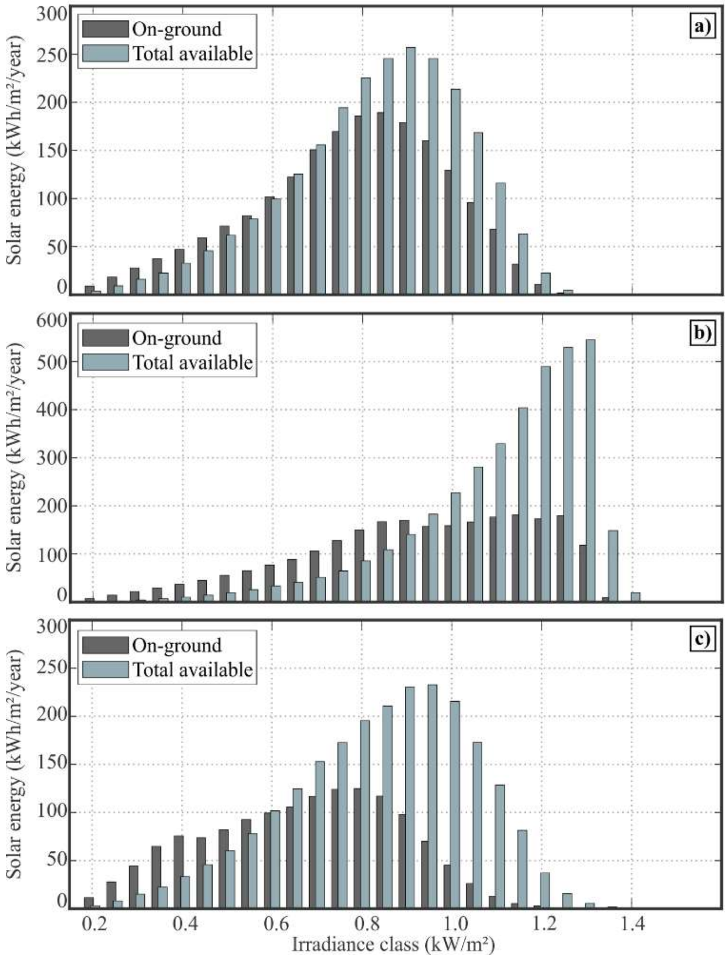

Source: personal archive

a) Calculate the Sun angular path for each location and for a whole year, in high-resolution, with reference to a coordinate system centered on the PV panel, with North-South, East-West, and Zenith axes;

b) Determine the module angular position vector, $\vec{N}$, in the same coordinate system, where:

- Mechanical tracking is simulated by making the PV panel azimuth (γ) continuously follow the Sun's azimuth (φ);

- Module's azimuth is oriented due South for northern hemisphere locations (IZA and LIN), and due North for PTR;

- An optimum tilt angle is used for fixed and 1-axis tracking configuration, and for a 1-axis tracking system following the Sun azimuth;

c) Calculate the incidence angle between Sun and module, minute by minute per 1-year for all mounting configurations, and estimate the total quantity of solar irradiance on the PV panel surface using the radiometric data.

Geometry needed for incidence angle determination is illustrated in Figure 14, wherein key elements are the Sun vector position and the surface normal vector. Mounting configuration determines the value of the tilt angle between ground and PV panel, β, and if the module's azimuth is fixed or variable.

Figure 14 – Geometry for calculating solar irradiance incident angle on an arbitrarily oriented surface.

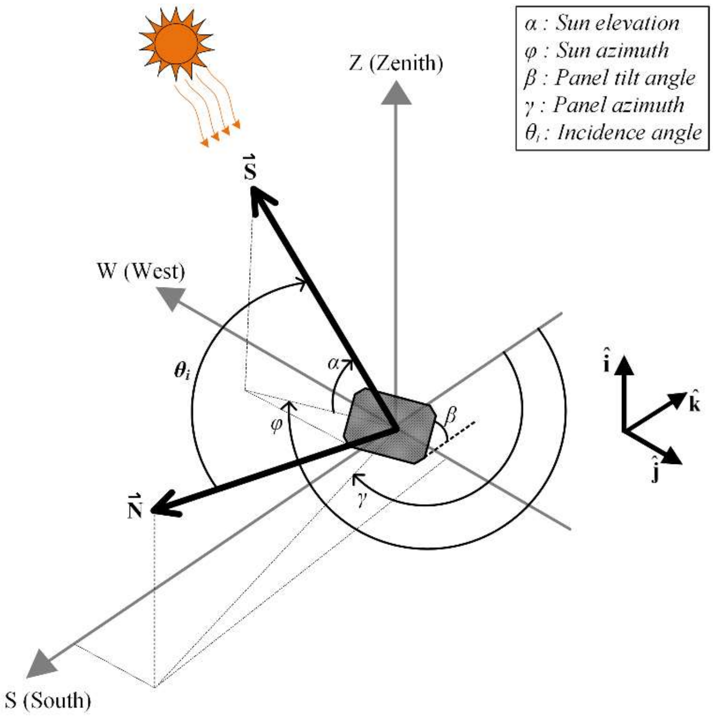

Source: personal archive

Calculation of Sun vector position, $\vec{\mathbf{S}}$, in relation to the observer is a well-discussed subject in literature and different methodologies can be used according to the precision needed. In this study, equations presented by (REDA; NREL, 2008) were used as a reference for developing an algorithm to calculate Sun's elevation and azimuth angles (α and φ, respectively) in function of time. The incidence angle between the PV surface and Sun was calculated as (7), while instantaneous irradiance was estimated according to (8) to (10).

$$\theta_i = \cos^{-1}(\vec{\mathbf{S}} \cdot \vec{\mathbf{N}}) \tag{7}$$

$$G_{direct}^{PV} = G_{direct} \cos(\theta_i) \tag{8}$$

$$G_{diffuse}^{PV} = G_{diffuse} \left(\frac{1+\cos(\beta)}{2} \right) \tag{9}$$

$$G^{PV} = G_{direct}^{PV} + G_{diffuse}^{PV} \tag{10}$$

where θ_i is the incidence angle between Sun and PV module, G_{direct} and $G_{diffuse}$ are the measured data of each irradiance type and G_{direct}^{PV}, $G_{diffuse}^{PV}$, and G^{PV} are the estimated, direct, diffuse, and total irradiance incidence over the panel surface. Reflected irradiance was not considered due its contribution to total solar irradiance is many times smaller than the direct and diffuse components, besides being more complex to model since reflection is dependent on the surroundings specific geographical characteristics. The main steps used for PV energy estimation and mission profiling are depicted in Figure 15.

Calculation of the position vectors, $\vec{\mathbf{S}}$ and $\vec{\mathbf{N}}$, is done through (11) and (12), where $\hat{\mathbf{i}}, \hat{\mathbf{j}}, \hat{\mathbf{k}}$ are unit vectors along the Zenith (z), East (e), and North (n) axes. The components of each position vector along the z, e, and n axes can be obtained through (11.1) and (12.1) by geometrically solving Figure 14.

$$\vec{\mathbf{S}} = S_z \hat{\mathbf{i}} + S_e \hat{\mathbf{j}} + S_n \hat{\mathbf{k}} \tag{11}$$

$$\begin{cases} S_z = \sin(\alpha) \\ S_e = \cos(\alpha)\sin(\varphi) \\ S_n = \cos(\alpha)\cos(\varphi) \end{cases} \tag{11.1}$$

$$\vec{\mathbf{N}} = N_z \hat{\mathbf{i}} + N_e \hat{\mathbf{j}} + N_n \hat{\mathbf{k}} \tag{12}$$

$$\begin{cases} N_z = \sin(\beta) \\ N_e = \cos(\beta)\sin(\gamma) \\ N_n = \cos(\beta)\cos(\gamma) \end{cases} \tag{12.1}$$

where S_z, S_e, S_n and N_z, N_e, N_n are the Zenith, East, and North components of the Sun position vector ($\vec{\mathbf{S}}$) and PV module normal ($\vec{\mathbf{N}}$), respectively.

Figure 15 – Steps of the proposed methodology for photovoltaic energy estimation.

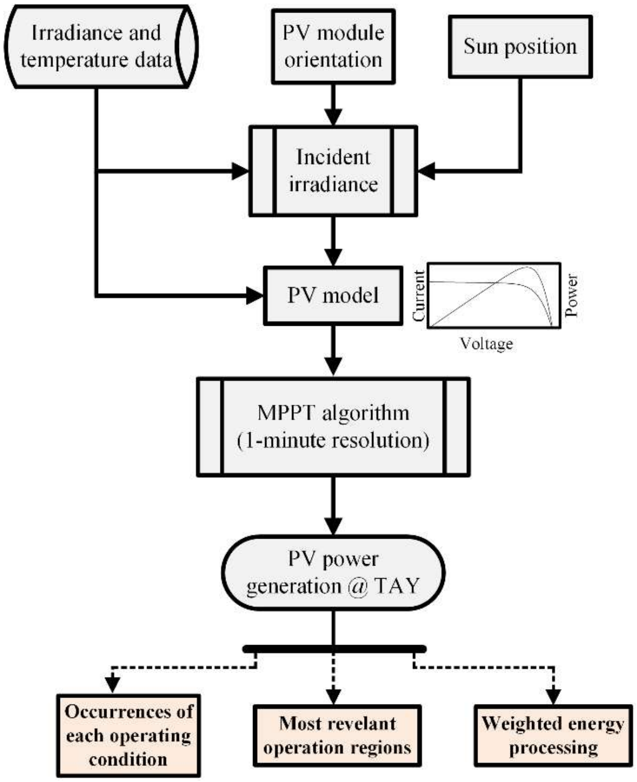

Source: personal archive

2.4.2 Incidence angle of moving surfaces

A mechanical tracker model for PV systems requires the Sun's annual angular path for the location of interest and its respective position vector ($\vec{S}$) in function of time, as described in Section 2.1. The movement of PV modules can be estimated through varying the panel's tilt angle (β) and/or azimuth (γ) in time. This will result in two time-varying position vectors, $\vec{S}$ and $\vec{N}$, which can be solved through (11) and (12), respectively.

Different types of tracker mechanisms (CLAVIJO, 2012; GRUPO CLAVIJO, 2012; MECA.SOLAR, 2014a, 2014b) and control strategies (Pesos.Solar.Products, 2015) are presented in the PV industry, varying from horizontal to polar mountings, from astronomical sun tracking to external radiation sensor-based. Since it is not the scope of this work, factors such as mechanical tracking efficiency, drive losses, control accuracy, and backtracking were not considered.

A single-axis tracker with tilted modules and a degree of freedom along the East/West axis is considered in the following sections, where tracking is accomplished by making the PV panel azimuth follow the Sun's. In dual-axis systems, both the panel's tilt and azimuth are movable and follow the Sun's respective angles, α e φ. A continuous tracking with null error is assumed in both scenarios.

2.5 CUSTOM OPTIMUM TILT ANGLE

The definition of the panel tilt angle with respect to the ground may have a significant impact on annual energy processing. The most common practice adopted by PV contractors is outdated equations for calculating the tilt angle as a constant factor of the local latitude. Such methods, as (LEWIS, 1987; REINDL et al., 1990), assume that climate and weather conditions are homogeneous for equal latitudes, which is far from true. An extensive study by (DEB et al., 2007) demonstrated that PV panel positioning has a deep impact not only in annual irradiation but also in overall system efficiency and financial savings for a grid-connected system.

Tilt angle calculation performed by (CHANG; YANG, 2012; YADAV; MALIK, 2015) was restricted by only 1-year of measured data, which might over or underestimate the availability of solar energy if such period was influenced by abnormal climatic conditions. However, (CHANG; YANG, 2012) used probability in order to reduce error and consider weather condition uncertainties. Urban topology was considered by (SIRAKI; PILLAY, 2012) in an investigation to determine how the shadowing from nearby obstacles affected the optimum tilt angle in different latitudes, whereas (FREITAS et al., 2015) used genetic algorithms to perform PV layout optimization to maximize energy yield.

By using a TAY considering several years of data, it was possible to find a β_{opt} that satisfied the average profile of solar irradiation for each city, which avoids designing a PV system based on non-typical data. The surface positioning model depicted in Figure 14 was used to find which tilt angle maximized the solar energy incidence for each mission profile.

For fixed mounting configuration, PV panel orientation was varied in order to determine the tilt angle and azimuth that resulted in maximum solar irradiation. Annual irradiance incidence in function of β and φ is depicted in Figure 16. Since obstacle shadowing was not included, true South resulted in the maximum solar incidence for IZA and LIN. At Petrolina, the azimuth orientation choice has a low impact for small tilt angles, since the city is located near the Equator line. Optimum orientation for each scenario is described in Table 4.

The tilt inclination for PV systems with 1-axis trackers is often disregarded and calculated with the same methods as in fixed mounting. Smaller tilt angle favors incidence during midday, where the Sun is at its highest position. Nevertheless, higher β favors morning and afternoon energy generation due to the Sun's smaller elevation. Thus, the optimum tilt angle for single-axis trackers is a trade-off and must be assessed for each specific application.

The relationship between tilt angle and annual solar incidence for single-axis trackers is shown in Figure 17. Optimum orientation angles for each mission profile are described in Table 5; energy generated by a single PV module in these conditions and energy gain compared to panels in a horizontal position is also presented.

Table 4 – Optimum orientation and total processed energy in the Typical Average Year.

Location	Mounting type	Optimum tilt angle -	Azimuth angle	Single module generation in TAY (kWh)	Gain relative to horizontal surface
Petrolina, Brazil	Fixed	6°	0°	371.77	1.27%
	1-axis tracking	32°	-	419.24	14.20%
	2-axis tracking	-	-	432.64	17.85%
Izaña, Spain	Fixed	21°	180°	537.36	6.77%
	1-axis tracking	46°	-	707.63	40.60%
	2-axis tracking	-	-	745.83	48.19%
Lindenberg, Germany	Fixed	36°	180°	336.62	17.66%
	1-axis tracking	53°	-	417.51	45.94%
	2-axis tracking	-	-	430.90	50.62%

Source: personal archive

Figure 16 – In-plane solar energy incidence of a fixed surface in function of tilt angle and azimuth orientation for a) Petrolina, b) Izaña, and c) Lindenberg.

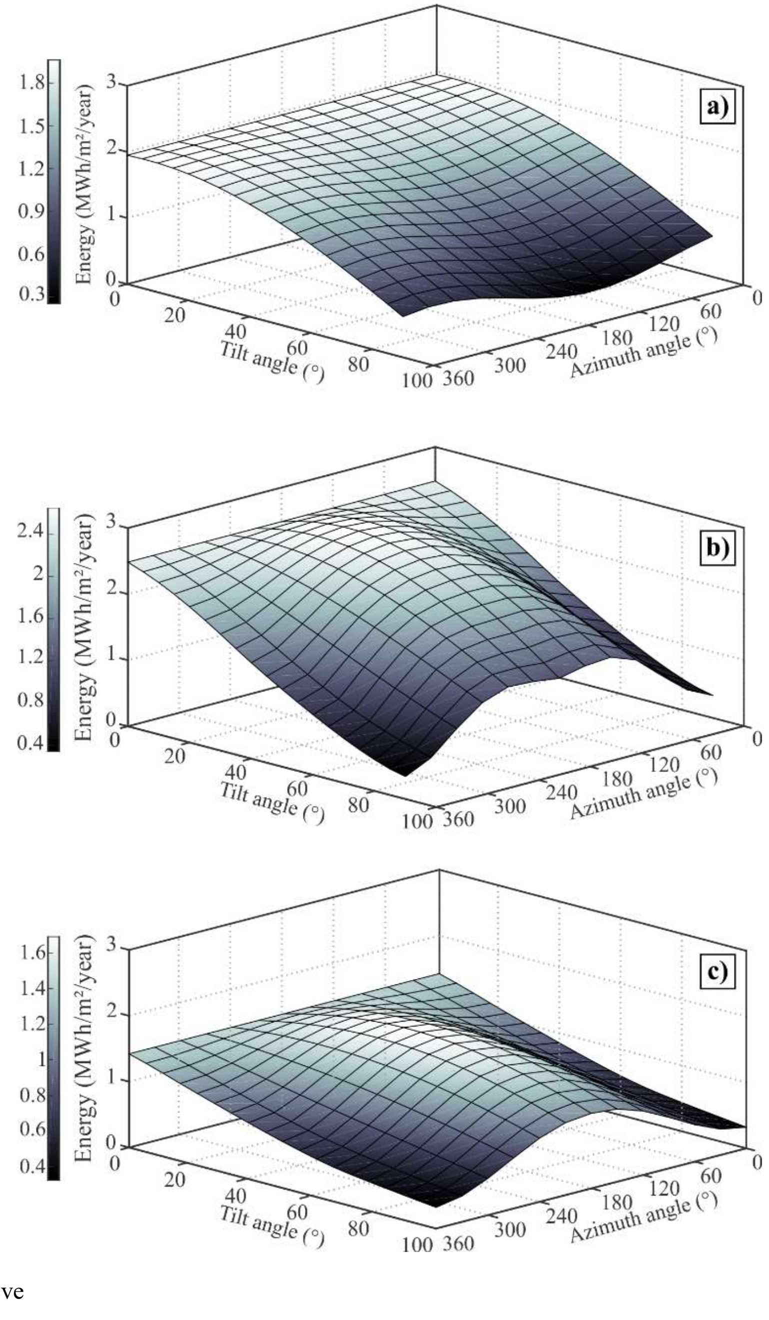

Source: personal archive

Figure 17 – Annual energy yield for varying tilt angles at Petrolina, Izaña, and Lindenberg, for 1-axis tracker.

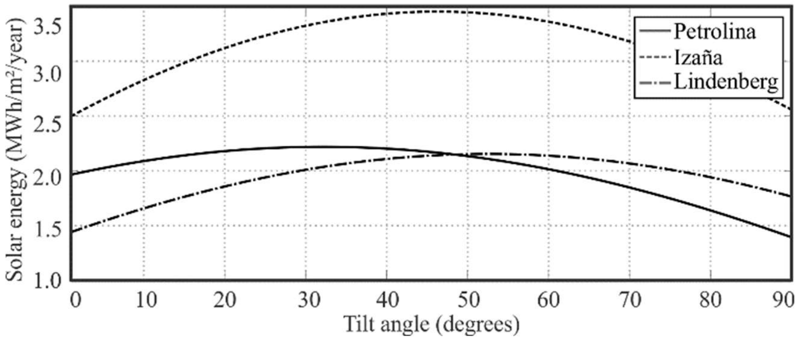

Source: personal archive

2.6 ANALYSIS OF PV MISSION PROFILE AND ENERGY GENERATION

As previously demonstrated, the somewhat random and variable nature of irradiation and temperature has a deep impact on photovoltaic energy generation. The previous characterization of local conditions allows a comprehensive detailing of the energetic behavior to expect from a PV power plant. In addition, it also favors the improvement of energy processing since power converters can be optimally designed or specified to meet the application's particularities.

2.6.1 Operating points behavior

The input current is a key parameter for designing a power converter since rated and maximum values are essential for component specification, losses calculation, and other subsequent design stages. In addition, current levels are also crucial for reliability analysis due to its impact on the thermal and stress behavior of all main converter components.

Therefore, previous knowledge of PV panel current behavior, absolute maximums, and average curves are essential for characterizing photovoltaic mission profiles. As summarized in Figure 15, the current and voltage profile is dependent on both irradiance incidence and panel temperature. Thus, PV operation in the TAY was estimated in a one-minute resolution, considering fixed mounting (horizontally and with fixed tilt) and use of mechanical trackers (1-axis and 2-axis), for each location described in Table 3.

One-year operating current and voltage pair are shown in Figure 18 where each pixel depicts a resolution of 100 mV by 100 mA, for the following scenarios:

PTR-2x: 2-axis tracker system in Petrolina, Figure 18a and Figure 18d;

IZA-fixed: Fixed tilt with an optimum angle in Izaña, Figure 18b and Figure 18e;

LIN-horiz: Horizontal position in Lindenberg, Figure 18c and Figure 18f.

Color scale in Figures 18a-c represents the frequency of operation, in hours, for each *I*×*V* pair, while the heat map in Figures 18d-f depicts the amount of processed PV energy, in kWh. For a better visualization, only *I*×*V* pairs that occurred for at least 2 minutes and contributed with at least 50 Wh are depicted. This type of graphical results may be called as Relevant Operation Maps (ROM) of a studied PV system.

Figure 18 – One-year current vs. voltage operating points for a single PV module relative to occurrence frequency, in hours, for a) Petrolina, b) Izaña, and c) Lindenberg; and relative to processed energy, d), e), and f), respectively.

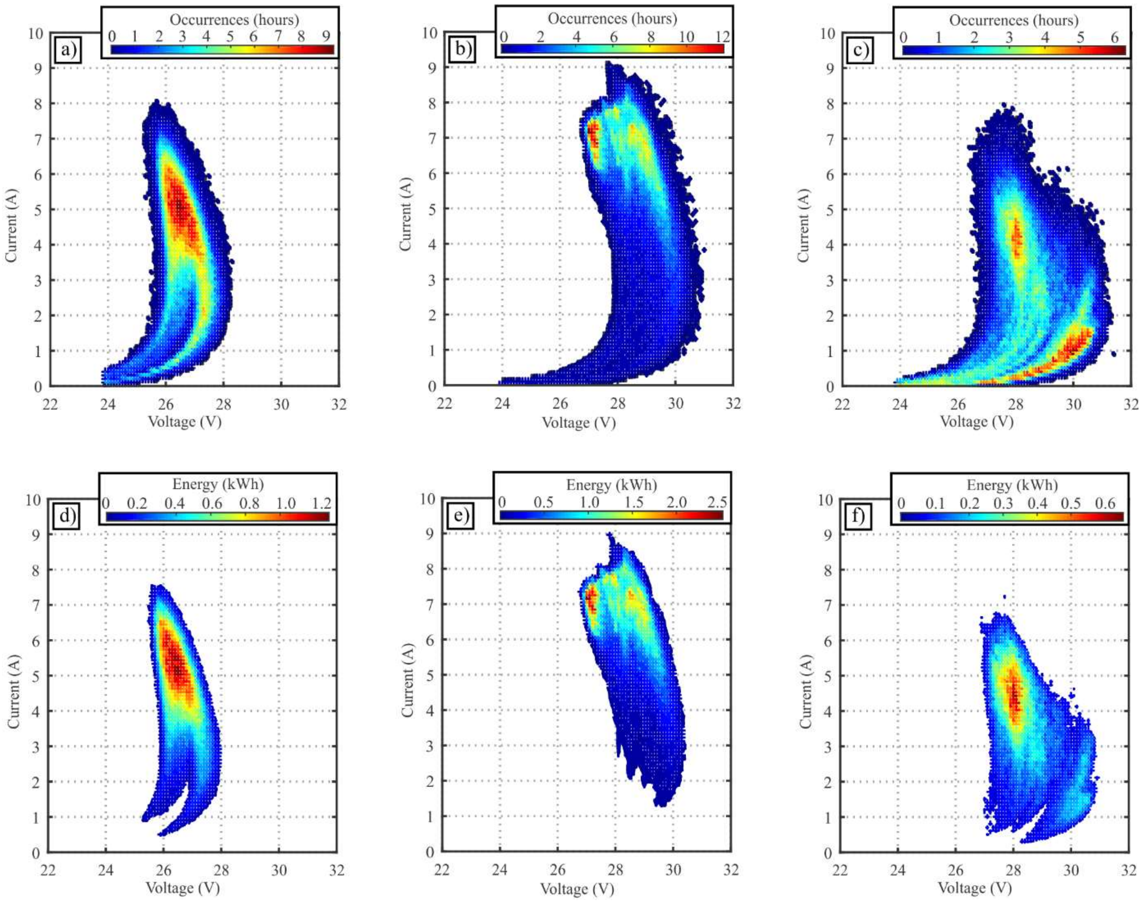

Source: personal archive

Due to its steadier and sunnier climate, Figure 18a indicates that a PV system in Petrolina operates most frequently in a well-defined region of PV current ranging from 4 to 6

A; this region of $I \times V$ operation is the same region responsible for most of the power processing in a one-year period. For having a warmer climate and higher average ambient temperatures, lower MPP voltages are more significant, which indicates that an inverter with maximum efficiency in rated DC level is not favorable for PTR-2x.

In contrast, MPP voltages are most frequently found at higher values on the other locations, due to lower ambient temperatures, especially in Lindenberg. Results indicate that for LIN-horiz, occurrences of operating $I \times V$ are distributed in two different regions, wherein the most frequent condition of PV operation is not the same that produces the most output of PV energy.

Izaña station is situated at a high altitude and frequently above cloud level, resulting in lower levels of diffuse irradiance (Figure 12b) and solar energy variability. This also explains the high energy gains due to the use of mechanical trackers (Table 4) since direct irradiance can be harvested more efficiently. In addition, the most frequent $I \times V$ region for IZA-fixed (Figure 18b) is significantly thinner than the other considered profiles and produced PV energy is highly concentrated in short ranges on the $I \times V$ map.

The relationship between the most frequent and the most relevant operating condition for energy processing is vital for optimum design of PV converters. Previous knowledge of a complete mission profile allows the designer to improve a converter's efficiency in the region where it will process more energy. Furthermore, long-term information of ambient conditions and occurrences of different operating conditions allow a DFR approach through a lifetime analysis of each power element in a PV system.

Analysis of Figure 18 clearly demonstrates that different mission profiles, i.e. different levels of solar irradiation and ambient temperature have a significant impact on PV generation. Therefore, converter performance throughout the year is directly dependent on such variations, once that PV output values dictate the power processing characteristics.

Furthermore, panels mounting and positioning affect power processing, since PV mechanical tracking results in higher irradiance, current, and power levels. Lower variability in voltage is a consequence of *p-n* junction behavior of photovoltaic cells, while greater current variation is due to the current source characteristic.

2.7 AMBIENT TEMPERATURE INFLUENCE

Through the methodology proposed and discussed so far, an analysis was carried out to evaluate how the mission profile and ambient temperature affect PV panel output and its produced energy. Using the TAY from each location and the profiles described in the previous section, the relationship between ambient temperature and annual processed energy is depicted in Figure 19.

Figure 19 – One-year energy processed by a single PV module relative to ambient temperature.

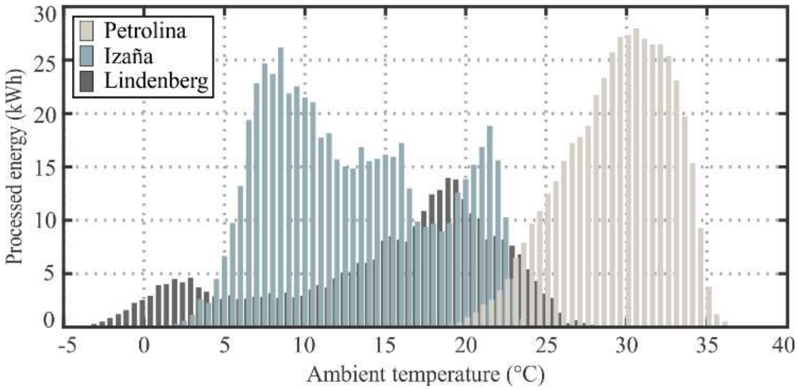

Source: personal archive

Lindenberg is located in a temperate climate zone, with well-defined seasons and high thermal amplitude. For this reason, PV energy processing occurs along a wide range of ambient temperatures, with small distinction in Figure 18. Meanwhile, at Petrolina, most of PV generation happens in a smaller range of higher temperatures, due to its tropical location closer to the Equator Line.

Despite the fact that it is located in a sub-tropical climate, Izaña's station high altitude favors great energy yield at low ambient temperatures, which is not a common feature in photovoltaic systems. This indicates that PV panels operate with higher conversion efficiency and power converters can process more energy with less thermal stress.

Ambient temperature is a crucial set of information and should be considered in the design phases of a PV power converter since its thermal behavior is dependent on the outside temperature. Steady-state and cyclical temperature is the main source of stress for power and electronic elements (ZVEI, 2008), increasing its failure rate. In order to enhance reliability, one must ensure that the selection and design of each component will sustain the mission profile's temperature dynamics.

2.7.1 Impact on energy processing

The mission profile oriented design of power electronics is capable of improving overall efficiency and reduce long-term costs, as this concept considers all main peculiarities that will rule energy processing. Recent works in this scope include considering semiconductor reliability in a PV inverter design (SINTAMAREAN et al., 2014) and an optimization technique for a PV boost converter focusing on weighted average efficiency increase (BELTRAME et al., 2014).

An accurate energy and mission profile is a key asset for developing high-performance photovoltaic power plants and converters. Conventional design of DC/DC converters aims to achieve higher efficiency at rated power. However, maximum powers are some of the least occurring events in PV applications due to weather variability. Techniques for design optimization aiming to improve annual energy processing, as in (BELTRAME et al., 2013), rely on previous knowledge of accurate energy and mission profiles.

In order to understand which PV operating points contribute the most to energy generation, an analysis of the PV power plant previously described was conducted from the point of view of power processing during a one-year operation. Output current was grouped in ranges of 500 mA, assuming an ideal MPPT, and the annual processed energy was obtained through summing PV power in one-minute samples. Figure 20 depicts energy yields in reason of operating MPP current for each location.

Because of its more variable climate, PV energy profile at Lindenberg with a fixed tilt mounting was distributed more evenly in the MPP current spectrum. This is consistent with the findings presented in Figure 18f, where the $I \times V$ operation regions more relevant for power processing are not concentrated. The use of mechanical trackers increases PV energy generation and concentrates the relevant MPP current on a thinner region. It is also noticeable that even though the 2-axis tracker configuration has a higher energy gain, the 1-axis tracker has a more defined region of relevant energy processing in mid-currents.

Due to its more constant weather condition, PV profile at Petrolina showed less variability among different PV mountings and smaller ranges of MPP current are responsible for most of the energy processing. Despite having very different irradiance and temperature profiles than Lindenberg, MPP current occurrences are somewhat similar.

The higher solar irradiance available at Izaña caused most energy processing in greater values and thinner ranges of MPP current. It is clear that mechanical trackers tend to decrease the range of currents significant to energy yield. Also, Figure 20shows that PV panel operation at rated and maximum currents (Table 1) are extremely rare, and only a 2-axis tracker system at IZA resulted in substantial energy contribution in this range.

Figure 20 – One-year energy processed by a single PV module relative to the operating current at MPP, for a) Petrolina, b) Izaña, and c) Lindenberg.

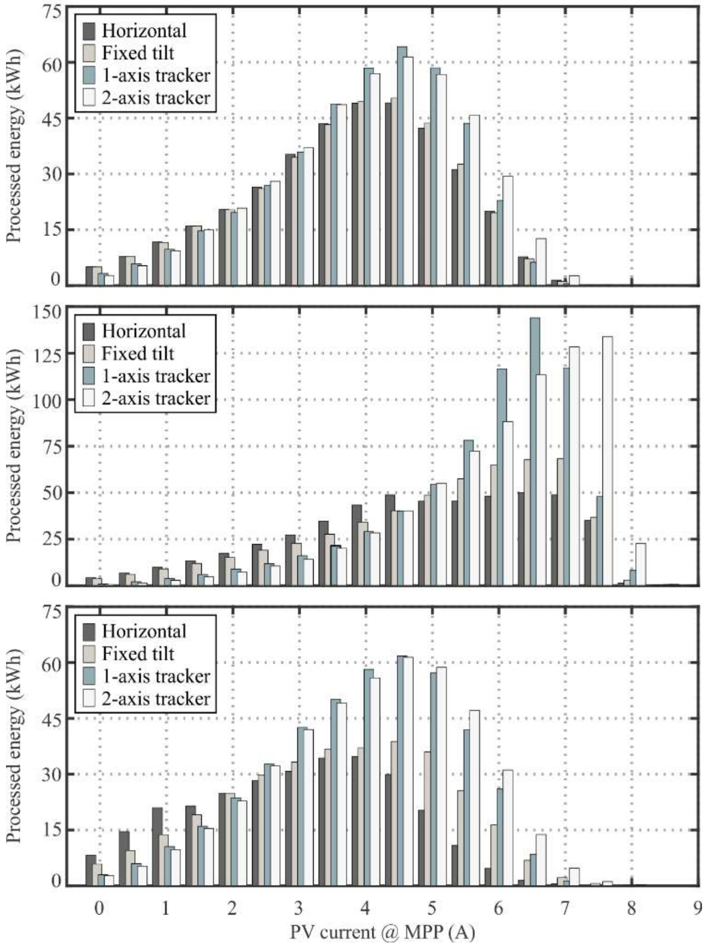

Source: personal archive

2.8 WEIGHTED PHOTOVOLTAIC ENERGY

The total generated energy of the experimental PV system, described in Section 3.2.3, was estimated as if it were operating under the mission profile conditions previously analyzed. The power processed by the SMC6000TL central inverter (SMA, 2016) was divided according to the load conditions of the California Energy Commission (CEC) for grid-tied inverters (Bower et al., 2004), where six power classes are considered (10%, 20%, 30%, 50%, 75, and 100% of rated output power). Figure 21 depicts the energy processed and active time of each power class in a one-year operation at PTR, IZA, and LIN for various mounting configurations.

Figure 21 – PV energy processed and active time in one-year operation relative to CEC power classes for a) Petrolina, b) Izaña, and c) Lindenberg.

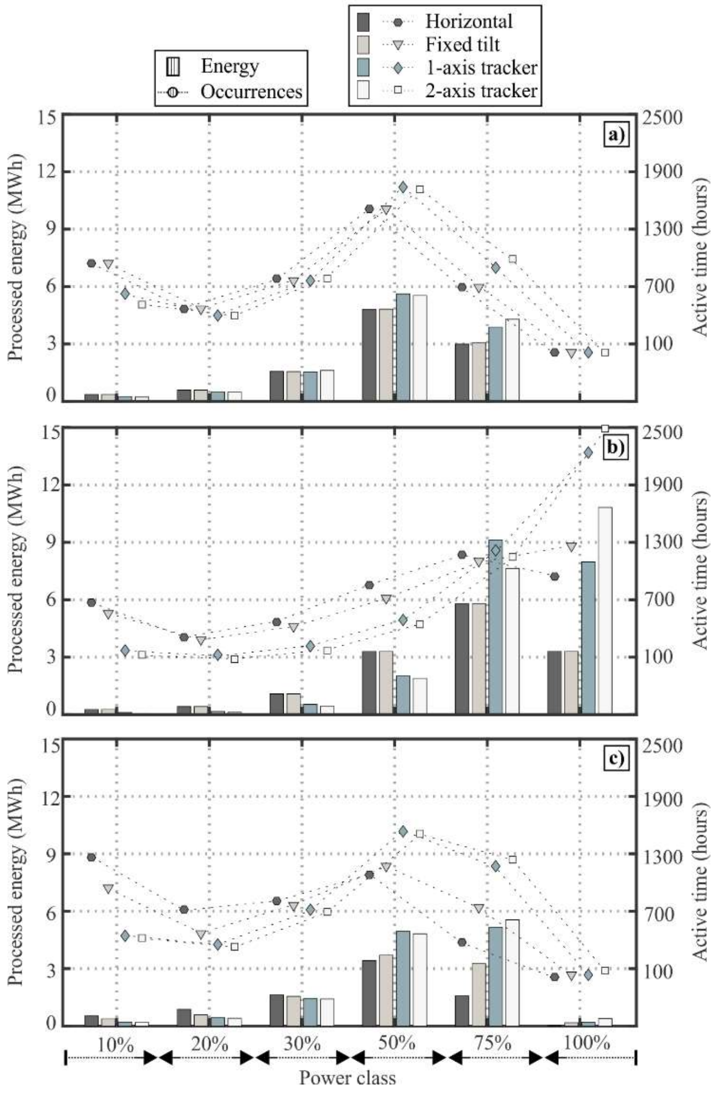

Source: personal archive

Photovoltaic power converters are usually sized with respect to the system's nominal condition, which is the module's maximum power in STC. However, PV panels hardly operate at maximum capacity due to thermal losses and irradiance variability, as can be seen in Figure 18 and Figure 20. Due to this over-dimensioning, Figure 21 shows that the 100% power class had the least contribution in energy processing in almost all studied scenarios.

Moreover, traditional converter design techniques favor only rated power levels, which are not the most relevant in PV systems. Thus, in order to maximize annual energy processing, one must design the PV power converter so that its efficiency curve is similar to the distribution of its PV mission profile, as in Figure 21. Design optimization can lead to higher efficiency in the power classes that contribute with most of the annual energy for a specific PV mission profile, which is analogous with matching array-to-inverter power ratio, as proposed by (RODRIGO et al., 2016).

Also, Figure 21 shows that power converters in PV plants with the use of mechanical trackers must be carefully designed, because the use of horizontal or fixed irradiance data may underestimate operation levels. Tracking alters not only critical and maximum values of energy and current but also the most relevant region for power processing. One should design a power converter that is more efficient and reliable in these regions according to the specific mission profile.

2.9 DISCUSSION

Designers should use a comprehensive approach to multiple areas of interest to model, design, and operate high-performance PV power plants. Power electronics elements play a fundamental role in this context since they are responsible for conditioning the solar energy in order to meet grid-quality standards and extract the maximum available power. Besides the technological challenges, power converters and inverters should be specified according to the local environment and specific PV system characteristics. Different design techniques can be used in order to enhance the overall performance of PV power converters. Nevertheless, one should first characterize an accurate mission profile to obtain a map of all the relevant conditions in which the power converter will operate.

Photovoltaic MP is composed of multiple analyses and results, and each one is relevant in different steps of the pre-design and design process. The definition of the PV system mounting type and orientation serves to evaluate what the average annual power production profile will be. In addition, the use of long-term meteorological data aids to find the optimum tilt angles which will maximize solar energy yield. This information is valuable for sizing the photovoltaic power plant and performing financial feasibility analysis. Furthermore, the estimation of average and maximum values of PV current and voltage, as presented in Figure 18 allows a proper choice and sizing of electronic and power elements in the DC/DC and/or DC/AC stages.

Moreover, previous knowledge of the most frequent $I \times V$ values and ambient temperatures, as shown in Figure 18 and Figure 19, enables the reliability-oriented design of power converters. With the mentioned analyses, the designer can perform lifetime estimations, select more appropriate topologies and/or component technologies, improve thermal performance and propose better heat-transfer solutions, and more. Lastly, estimation of the most relevant conditions in the power processing point-of-view, as presented in Figs. 18, 20-21, empowers the designer to know in advance which region of operation of the power converter is the most valuable. The weighted processed power (Figure 21) figure of merit provides needed information for executing the optimized design of power converters.

3 CAPACITOR ELECTRO-THERMAL MODELING

Among the several phases that exist during design process of a power converter, the component choice is certainly a critical one, which could drastically affect the system's performance. While the cheapest component may provide a subpar performance and lead to a premature failure, the most expensive one may be well beyond the requirements and yield in an over-engineered design. In addition, industry is more likely to make this selection within the list of components that are already available at their disposal or used in previous designs.

Although being of vital importance in power electronics, one could say that capacitors are not looked at with as much depth in the design process as the magnetics or power devices. Due to not having a major impact on power losses, capacitors are usually designed and selected just to be "big/small enough" in order to simply be used as an energy buffer. This fact can easily be verified when comparing the number of application guides and design methodologies available for capacitors and for power devices. Nevertheless, capacitors still account for a considerable share of cost and failure occurrences in power electronics.

3.1 ELECTROLYTIC CAPACITOR MODEL

To estimate the long-term electro-thermal stresses, a simplified equivalent circuit of the electrolytic capacitor composed by the capacitance (*C*) and its equivalent series resistance (*ESR*) is used, Figure 22a. The capacitor core temperature (T_{CAP}) is calculated using the thermal model shown in Figure 22b, where the power losses (P_{loss}) are dissipated in the thermal resistance (R_{th}) between the capacitor core and the ambient, C_{th} is the capacitor thermal capacitance, and T_{amb} the ambient temperature. T_{hs} is the inverter's estimated heat sink temperature and is considered the capacitor local ambient temperature, the model used for estimating this value is described further in the results section.

Figure 22 – Electrical and thermal models for electrolytic capacitors.

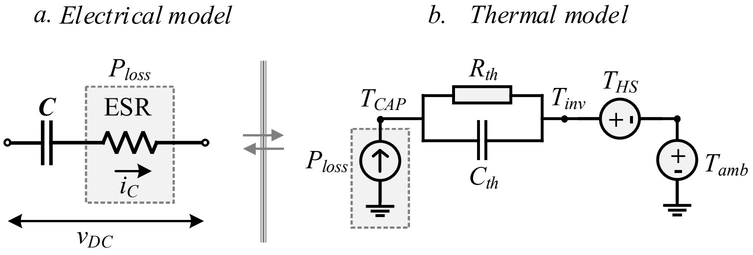

Source: personal archive

A Fast Fourier Transform (FFT) of the current through the DC-link capacitors is done in order to match the current harmonic spectrum to the *ESR* in function of frequency (Yang et al., 2015a). The *ESR* value in relationship to temperature and frequency is modeled either using the information provided by the manufacturer or experimentally. Therefore, the instantaneous losses are calculated through

$$P_{loss} = \sum_{h=1}^{N} I_h^2 \left(f_h \right) ESR_i \left(f_h, T_{cap} \right) \tag{13}$$

where N is the number of time-series points available of ripple current i_{cap}, I_h is the current contribution on the harmonic h.

The electrolytic capacitor's internal heating is a direct result of the power losses dissipated through its layers (electrolyte, anode and cathode foils, conductors, and insulation). Each of these layers has different thermal properties and their modeling could become quite complex (Freiburger, 2015), especially considering the geometry and coupling of heat propagation. However, a simplified thermal model that considers only the thermal resistances between core-to-case and case-to-ambient and the total thermal capacitance, as shown by the equivalent circuit of Figure 22, can still provide satisfactory results.

After the power losses are obtained, the increase of capacitor core temperature relative to the ambient (ΔT_{cap}) is calculated through

$$\Delta T_{CAP} = P_{loss} R_{th} \left[1 - \exp^{\frac{-t}{\tau_{CAP}}} \right]. \tag{14}$$

where τ_{CAP} is the capacitor's thermal time constant.

3.1.2 Capacitance variation

The capacitance C of Figure 22 is the equivalent AC series capacitance as measured from the circuit's input, and is generally dependent on the dielectric relative constant, surface area, and thickness. The capacitance decreases with frequency because of the impedance characteristics of the aluminum electrolyte capacitor, however, this decrease is usually smaller than 10% in low-frequencies.

In addition, the capacitance varies with temperature and its rate of change is dependent on the capacitor size and rated voltage. Nevertheless, this change is much less significant than of the *ESR's*, where *C* typically increases less than 5% from 25 °C to high-temperature limits (CDE, 2019; EPCOS AG, 2015).

Although these parametric variations of the capacitance may affect considerably the capacitor expected operation and circuit stability, it has little impact on power losses and heating. Thus, it is not considered in the following results of this proposed design tool, but will be a study subject for future works.

3.2 CAPACITOR ELECTRO-THERMAL CHARACTERIZATION

Two samples of the ESMR451VSN821MA50S capacitor from NCC are tested in order to obtain their *ESR* vs. temperature behavior. These capacitors were specially manufactured by NCC with a hole drilled through their vertical axis wherein a thermocouple was placed in order to measure their core temperature.

The two samples are heated to a temperature of 80 °C and their *ESR* is measured while cooling down to room temperature individually. The *ESR* is measured in six different frequency levels, in order to obtain a full *ESR* vs. frequency vs. temperature behavior. Although their core temperatures are decreasing during this procedure, they are assumed to be fairly constant within the measurements of each frequency level due to their high thermal capacitance. Figure 23 shows the average *ESR* values measured from both samples in function of frequency and for different temperatures.

In order to be used in the design tool, the previous results are fitted into a spline so the *ESR* can be determined for any value of temperature. Figure 24 shows the experimentally modeled behavior of the *ESR* in function of both frequency and temperature.

Figure 23 – Measured ESR for different frequency and temperature values.

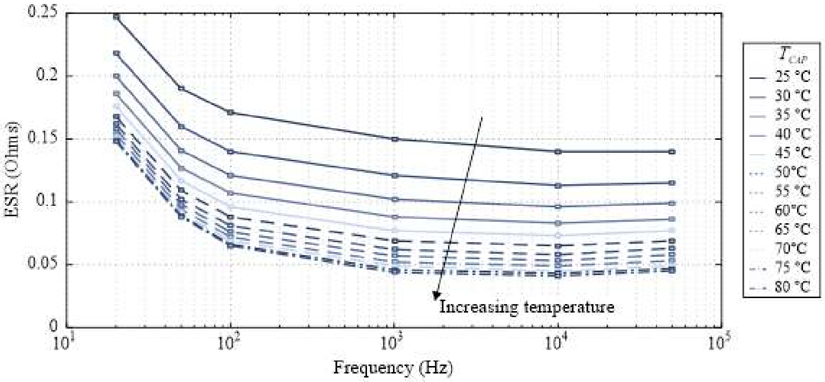

Source: personal archive

Figure 24 – Characterized model for ESR in function of temperature and frequency.

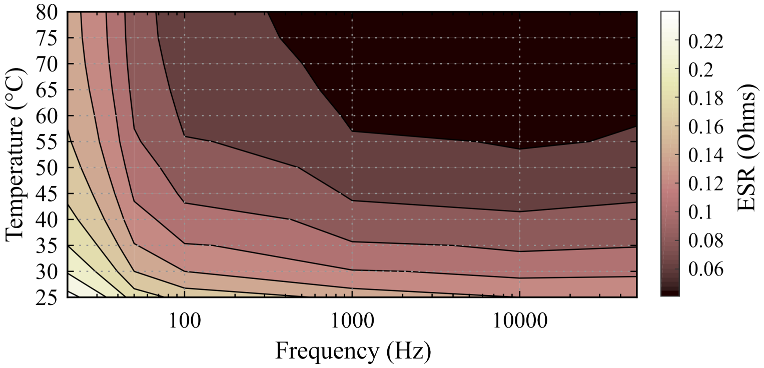

Source: personal archive

3.2.1 Thermal parameters characterization

The thermal characterization of these samples is done using a controllable ripple current tester Chroma 11801. With it, the capacitors under test are injected with a controlled ac current of a specific frequency and magnitude and are biased with a controlled dc voltage, as depicted in Figure 25. In addition, the capacitor's setup is placed inside a climatic chamber where the temperature is controlled at a desired value.

The value of τ_{CAP} is calculated before the capacitor's thermal resistance because τ_{CAP} is a transcendental function. While heating because of a ripple current, the capacitor power losses will decrease in time with the decrease of its *ESR*, even if the current's magnitude remains constant. Hence, due to both P_{loss} and T_{CAP} being constantly changing during the transitory of a thermal time response, τ_{CAP} is determined in a zero current test condition.

Figure 25 – Overview of capacitor test setup using a controllable ripple current source.

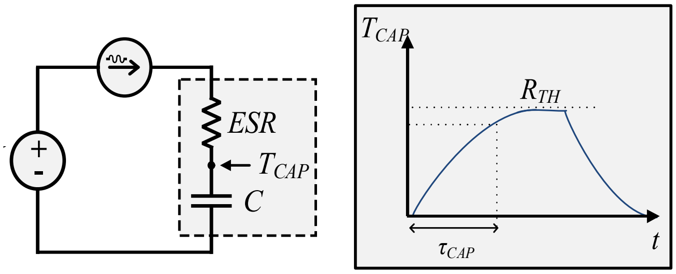

Source: personal archive

Initially, the thermal time constant is determined by heating the capacitor to a known temperature and measuring the time and τ_{CAP} through the cooling process. With these measurements, the τ_{CAP} of the thermal model of Figure 22 is then calculated. Two tests in different conditions are done in order to have consistent results, as follows:

- Cooling condition #1: T_{CAP} = 35 °C, T_{amb} = 27 °C
- Cooling condition #1: T_{CAP} = 75 °C, T_{amb} = 25 °C

Figure 26 shows the averaged measurements in time of both tests, where the obtained τ_{CAP} is equal to approximately 940 and 1020 seconds, for cooling conditions #1 and #2 respectively. Thus, an average τ_{CAP} equal to 980 seconds (16.33 minutes) is obtained for this capacitor.

Figure 26 – Measured capacitor core temperature in time during the cooling test.

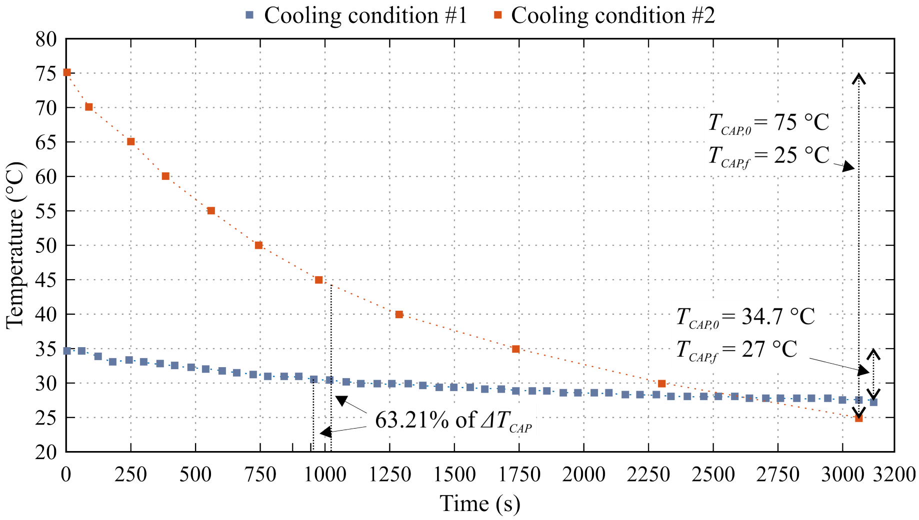

Source: personal archive

A second test is now performed in order to obtain the thermal resistances and, to further validate the electro-thermal modeling, the capacitors are evaluated at two different power loss and ambient conditions, described as follows:

- Heating condition #1: in an ambient temperature equal to 27 °C, the capacitors are subject to a current ripple of 3.2 A @ 120 Hz and DC voltage bias equal to 400 V. In addition to the T_{CAP}, the case temperature is also measured using an infrared thermometer – measurements were done at the same time and consistently at the same spot in the capacitor's side.
- Heating condition #2: with T_{amb} equal to 40 °C, the capacitors are subject to a current ripple of 4.65 A @ 1000 Hz and DC voltage bias equal to 400 V.

Figure 27 shows the experimental temperature measurements in time for both conditions and averaged between both capacitors.

Figure 27 – Measured capacitor temperature in time for different power loss and ambient temperature conditions.

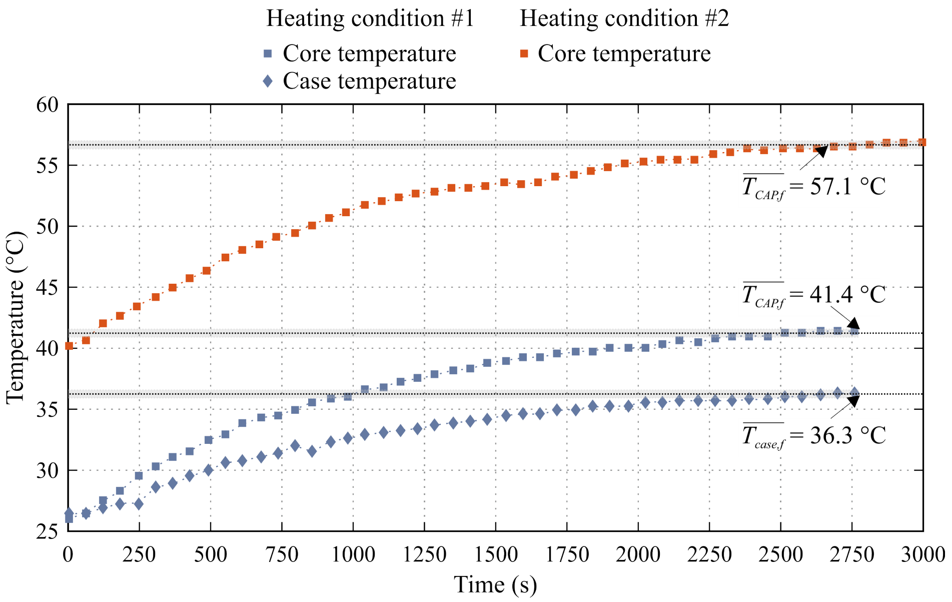

Source: personal archive

Using (13) and Figure 24, the power losses are estimated for heating conditions #1 and #2, respectively. Rewriting (14) in steady-state, the thermal resistances are then obtained through

$$R_{th} = \frac{\Delta T}{P_{loss}}, \tag{15}$$

$$R_{th} = R_{thcc} + R_{thca} \tag{16}$$

where R_{thcc} and R_{thca} are the thermal resistances between core-to-case and case-to-ambient, respectively.

3.2.2 Free convection vs. forced cooling

After R_{th} and τ_{CAP} were already determined and while performing other tests, some significant errors – greater than 4 °C, in some cases – were observed between model and measurements. After some thorough investigation, it was determined that another variable was not being included in the analysis so far: the heat transfer mechanism. In the tests previously conducted, the climatic chamber was inoperant for most of the time and, thusly, the capacitors were dissipating their heat through free convection.

However, to perform tests in higher ambient temperatures, the climatic chamber was constantly running with an air circulating system in order to maintain the desired value of T_{amb}. Although it was not possible to measure the airflow inside the chamber, it can be fairly assumed that it increases the heat transfer between capacitor and ambient – decreasing the value of R_{th}. As discussed in previous sections, the literature in capacitor electro-thermal modeling is not comprehensive, especially when compared to power devices, and no clear relationship or discussion between R_{th} and airflow has been found. Nevertheless, to include these conditions of free convection and forced cooling in the thermal model being developed so far, a second round of tests described by Figure 25 is done to obtain R_{th}, described as follows:

- Heating condition #3: in a controlled ambient temperature equal to 55 °C, the capacitors are subject to a current ripple of 3 A @ 1000 Hz and DC voltage bias equal to 400 V.
- Heating condition #4: same T_{amb} and V_{CAP}, with a current ripple of 3.38 A @ 1000 Hz and DC voltage bias equal to 400 V.
- Heating condition #5: same T_{amb} and V_{CAP}, with current ripple of 1.6 A @ 120 Hz and DC voltage bias equal to 400 V.

Figure 28 shows the temperature measurements in time for these conditions and averaged between both capacitors. The values of R_{th} are determined through (15, 16) and Table 5 gives a summary of the obtained thermal resistances for both free convection and forced cooling conditions.

Figure 28 – Measured capacitor temperature in time in the second test, for different power loss and ambient temperature conditions.

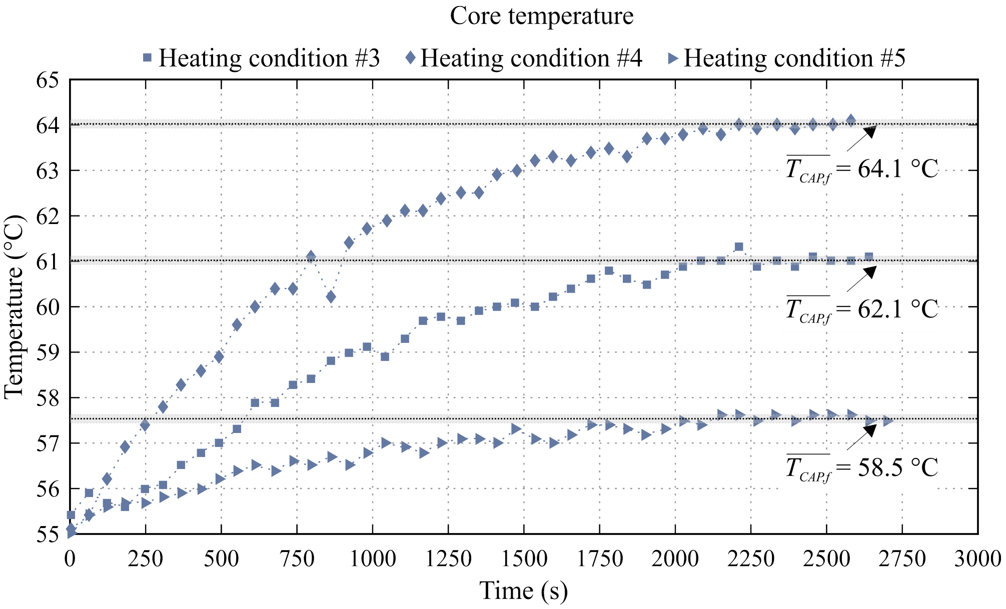

Source: personal archive

Table 5 – Obtained values of thermal resistance for the sample tested.

	Free convection	**Forced cooling**
R_{thcc}	3.37	3.37
R_{thca}	11.47	7.13
R_{th}	14.84	10.50

The obtained thermal impedance of the ESMR451VSN821MA50S capacitance is shown in Figure 29.

Figure 29 – Capacitor samples' thermal impedance.

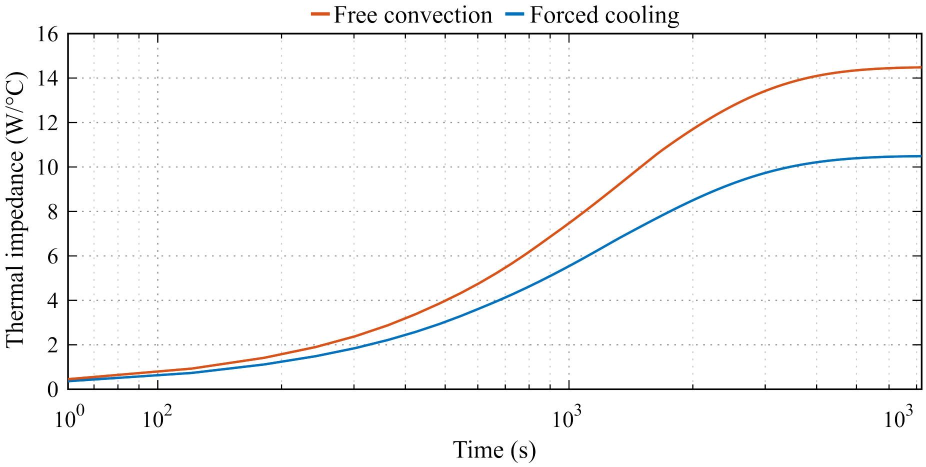

Source: personal archive

3.3 THERMAL MODEL VALIDATION

To validate the modeling done so far, a two-step thermal response test is done with the same procedures as previously described. With an ambient temperature equal to 40 °C, the capacitors are subject to a 400 V DC bias and ripple current of 4.65 A @ 1000 Hz. Initially, the climatic chamber is turned off in order to have free convection as the heat transfer mechanism; then, at an arbitrary moment, the climatic chamber is turned on but and still controlled to 40 °C. At this moment, a forced cooling condition is then ensued and the capacitor temperature drops due to the smaller thermal resistance. Since the ripple current is not altered, the power losses will increase in reason of the ESR change; eventually, an equilibrium between the heating caused by power loss increase and cooling caused by the forced cooling is achieved.

Figure 30 shows the comparison between the estimated temperature by the capacitor electro-thermal model and the actual core temperature measurements in time. It is highlighted that there is a drop of approximately 1.7 °C in T_{amb} from the beginning of the test until the first half in reason of the climatic chamber being turned off – even though it is hermetically sealed. Evidently, this inserts an error in the modeling but the estimated results are still considered to be satisfactory in represent the capacitor's electro-thermal dynamics.

3.3.1 Capacitor bank thermal model validation

A comprehensive capacitor electro-thermal modeling in function of power losses and ambient conditions has been presented in the previous section for a single component only.

Figure 30 – Validation of the electro-thermal modeling for the used capacitor, under different heat transfer mechanisms.

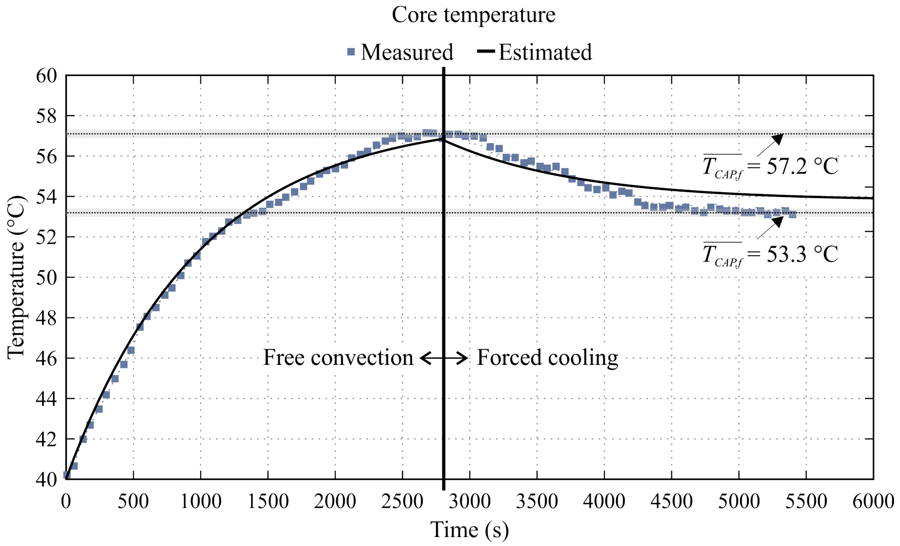

Source: personal archive

However, the proposed design tool in work aims to give the designer proper solutions for a whole capacitor bank for an arbitrary mission profile. Thus, the following sections will present the electro-thermal validation of multiple capacitors for different profiles of ripple current and ambient temperatures.

3.3.1.1 Steady-state thermal response

Considering that all capacitors inside a bank are equal – same part number, the total current through it is assumed to be equally divided among all components since the impedance difference among them may be disregarded. Then, the equivalent circuit of a bank with an arbitrary number of capacitors in parallel (N_{CAPS}) is described by Figure 31.

Figure 31 – Circuit diagram of a bank with capacitors connected in parallel.

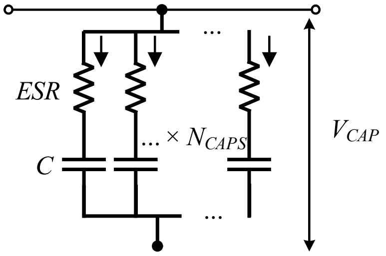

Source: personal archive

Four different capacitor banks composed of the same part number previously used are tested in order to validate their steady-state thermal response, with N_{CAPS} equal to 2, 3, 4, and 5. Using the maximum ripple current ripple of this part number as a reference, the capacitor banks are tested in four different levels of total current and at three different ambient temperatures, resulting in a total of 48 different tests, as follows:

- Tested capacitor bank sizes: $N_{CAPS} = 2, 3, 4, 5$;
- Total RMS ripple current: 1.6 A, 3.2 A, 4.8 A, and 6.4 A @ 120 Hz;
- Ambient temperatures: 40 °C, 55 °C, and 65 °C;
- Heat transfer mechanism: forced cooling.

For each test condition, all the capacitors start with T_{CAP} equal to the ambient temperature and with no stored energy. The ripple current and voltage bias are then applied and their core temperature is measured. The distance between each capacitor is approximately greater than 3 cm and hence any kind of thermal coupling is disregarded, however, this will be included in future works. Also, although several capacitors are used in this test, the core temperature is measured only from the two available samples with internal thermocouples.

After thermal steady-state is reached, T_{CAP} is measured and then compared with the estimated value using the model described previously. It is highlighted that the measurements of T_{CAP} are continually fluctuating even at steady-state; this is possibly caused by a continuous heat transfer between the capacitors and the circulating air, and also due to the imprecision of the measuring devices. For these reasons, three different measurements of T_{CAP} are considered for each test condition: a minimum, average, and maximum.

Figures 32-34 show the comparison between measured and estimated T_{CAP} for ambient temperatures of 40 °C, 55 °C, and 65 °C, respectively.

Figure 32 – Comparison between experimental and modeled steady-state temperature for capacitor banks in different power loss condition and at 40 °C of ambient temperature.

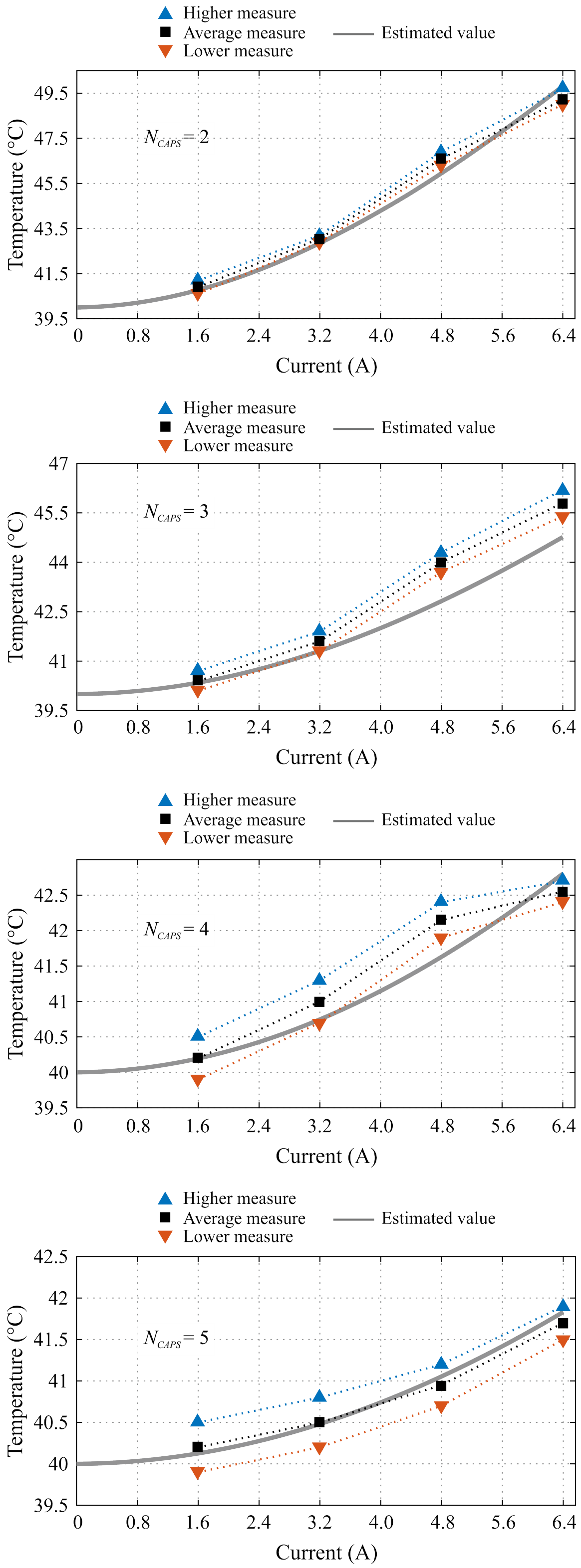

Source: personal archive

Figure 33 – Comparison between experimental and modeled steady-state temperature for capacitor banks in different power loss condition and at 55 °C of ambient temperature.

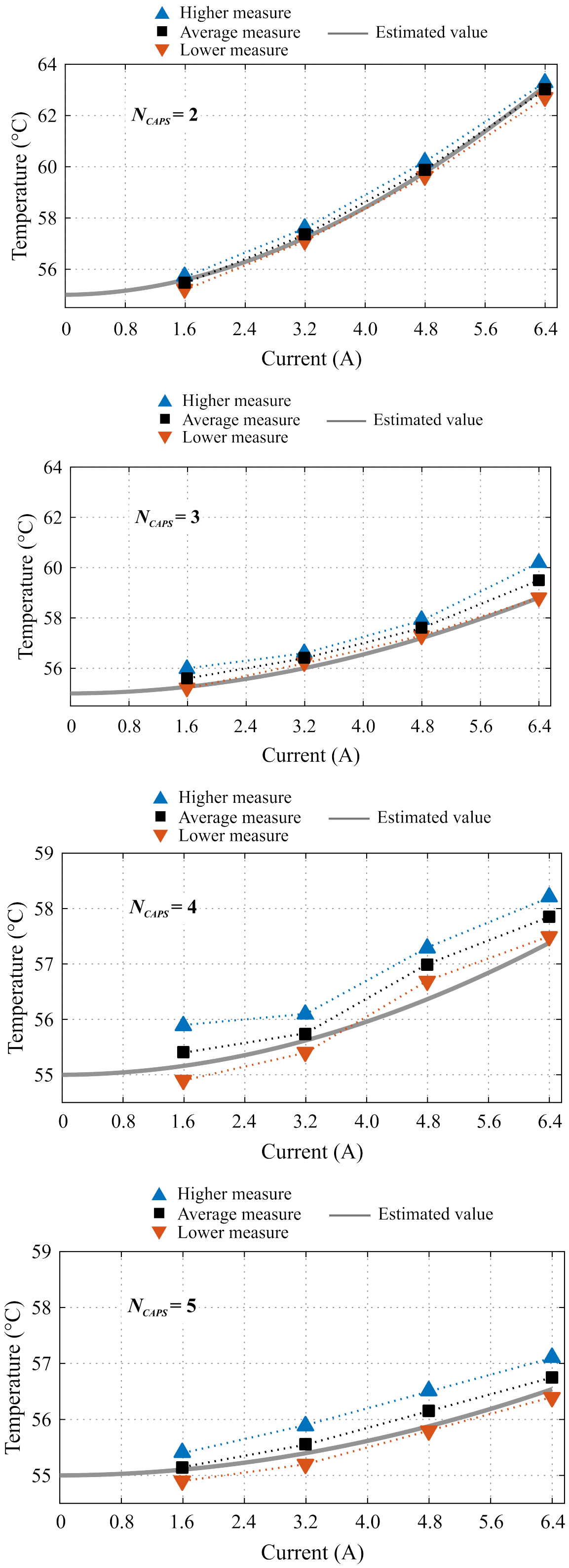

Source: personal archive

Figure 34 – Comparison between experimental and modeled steady-state temperature for capacitor banks in different power loss condition and at 65 °C of ambient temperature.

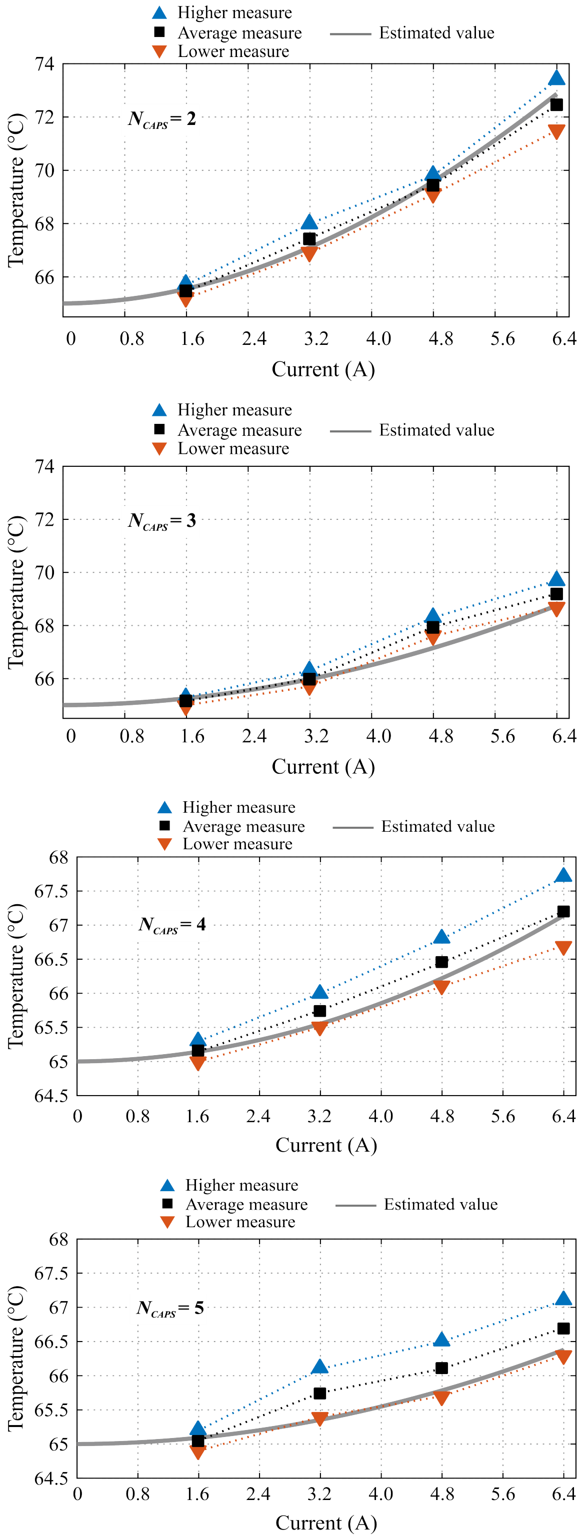

Source: personal archive

In Figures 35-37, a 3D-view is composed of the individual capacitor steady-state temperature in function to the capacitor bank size and total current. Similar to the results of the thermal response of a single capacitor, the increase in capacitor temperature (ΔT_{CAP}) for the same ripple current is higher at lower ambient temperature; this is caused due to the higher *ESR*. In low current levels, the power losses are so small that there is no significant heating; on the other hand, increasing the number of capacitors in parallel significantly decreased T_{CAP} as expected.

Figure 35 – Experimental look-up table for capacitor core temperature in relationship to capacitor bank size and power losses, at 40 °C of ambient temperature.

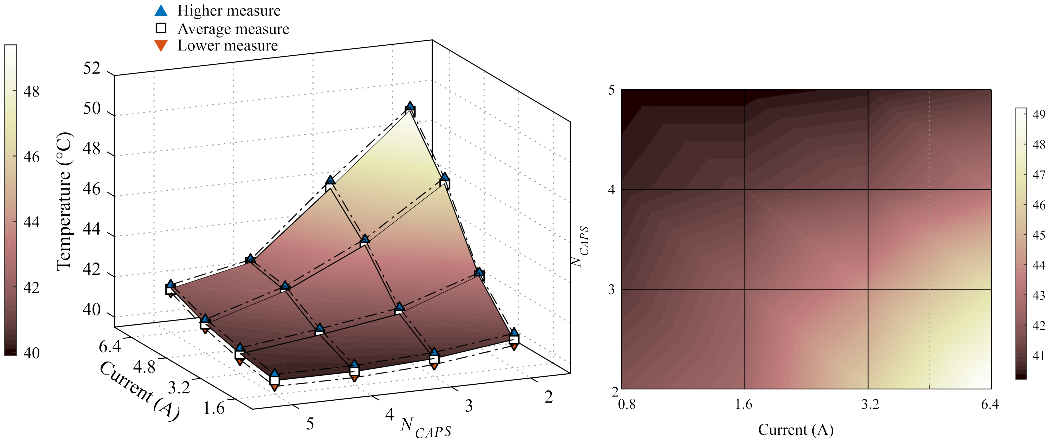

Source: personal archive

Figure 36 – Experimental look-up table for capacitor core temperature in relationship to capacitor bank size and power losses, at 55 °C of ambient temperature.

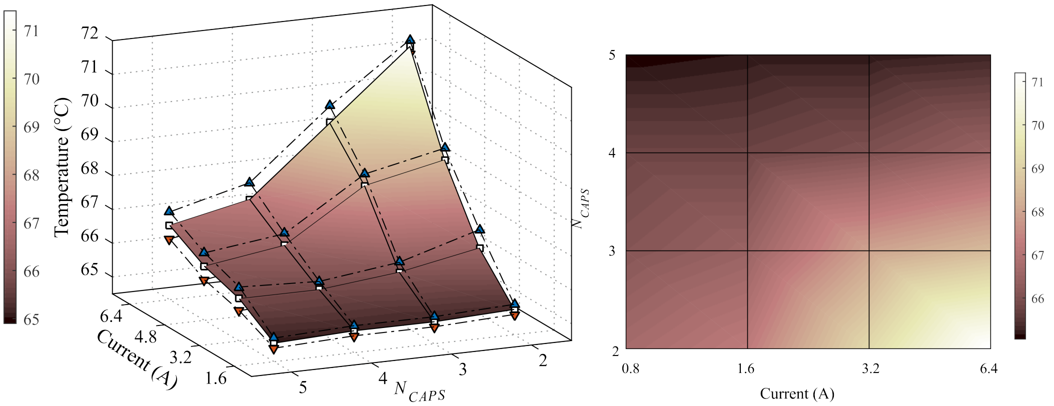

Source: personal archive

Figure 37 – Experimental look-up table for capacitor core temperature in relationship to capacitor bank size and power losses, at 65 °C of ambient temperature.

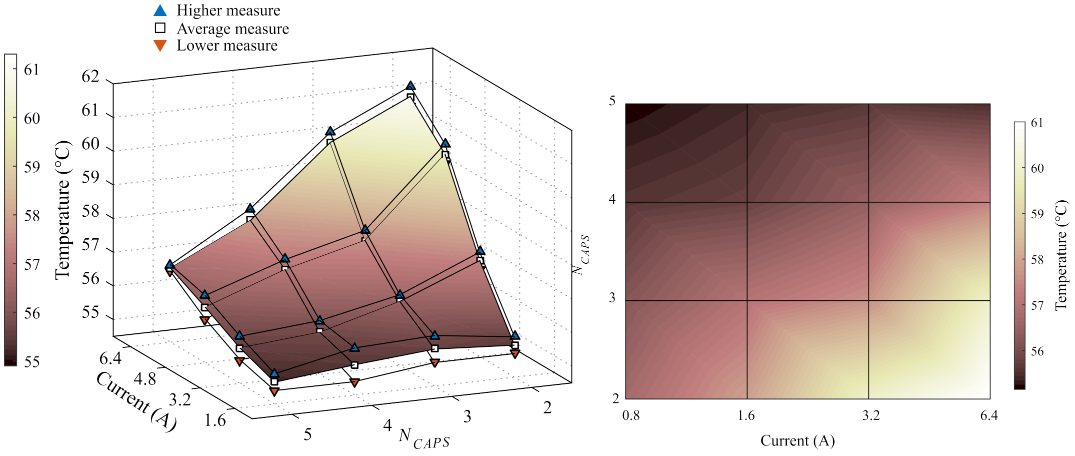

Source: personal archive

3.3.1.2 Thermal response for the dynamic current profile

To further validate the capacitor bank thermal modeling, a test is conducted using two different energy profiles. Using the controllable ripple current source previously described, these two profiles were defined to emulate a realistic energy profile expected to be processed by a PV power converter. In the first scenario, the current through the capacitor bank increases monotonically in intervals of 5 minutes until it reaches a maximum, afterward it decreases until zero; this represents the solar energy profile in a clear-sky day. Conversely, in the second scenario, the current through the capacitor bank increases and decreases irregularly during the whole test period, emulating a cloudy condition where the PV power changes abruptly throughout the day. The values of ripple current are chosen arbitrarily and respect the capacitors' limits.

Three different capacitor bank sizes (N_{CAPS} equal to 2, 3, and 4) are tested at a controlled ambient temperature of 55 °C. Once more, the T_{CAP} of the samples specially manufactures are measured and their values in time are compared to the ones estimated by the model using the forced cooling thermal impedance. In Figures 38-39 it is shown the current through the capacitor bank, the measured and estimated capacitor core temperature, and the absolute error obtained, for both tested current profiles.

Figure 38 – Capacitor electro-thermal validation in time considering different capacitor bank sizes and current variation.

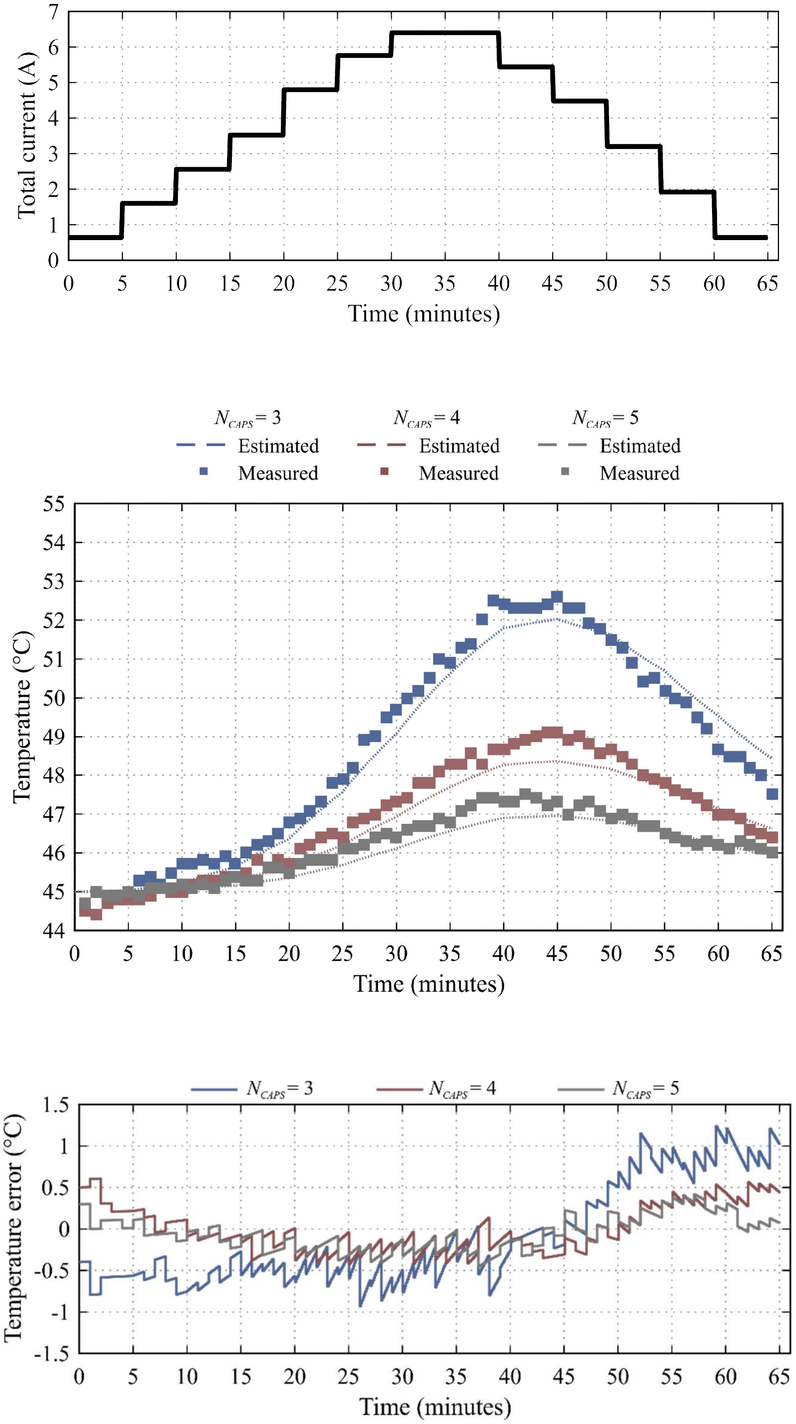

Source: personal archive

Figure 39 – Capacitor electro-thermal validation in time considering different capacitor bank sizes and current variation.

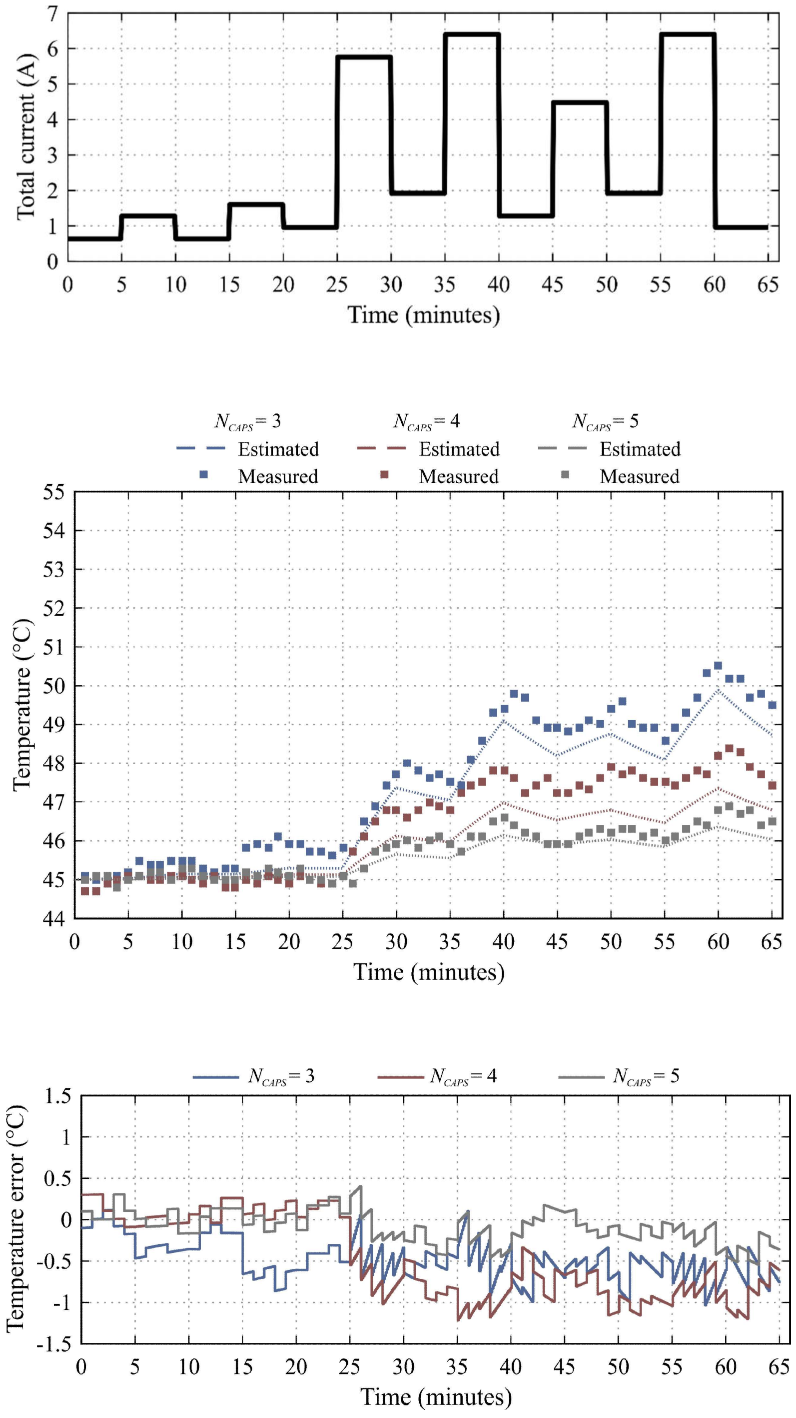

Source: personal archive

Although there are errors between measured and estimated T_{CAP} both in magnitude and in time shift, the model results are considered satisfactory to represent the thermal behavior of capacitors for a given condition of current and ambient temperature.

3.4 DISCUSSION

A thorough electrolytic capacitor modeling was presented considering both electrical and thermal domains. Experimental results were obtained to validate this modeling, using samples of a specific part number which was specially prepared by the manufacturer so the capacitor's core temperature could be measured. The model and results were obtained for two different heat transfer mechanisms (free convection and forced cooling), for different numbers of capacitors in connection, and for different ripple current profiles.

Knowing the electro-thermal characteristics of a capacitor is essential in order to make long-term forecasting of their power losses and operating temperature. The more accurate is this modeling, the better will be the forecasting and the reliability prediction. Although the experimental results were obtained for a specific part number, the methodology can easily be expanded for different capacitors or manufacturers.

4 CAPACITOR RELIABILITY

Power electronics have become one of the most essential equipment in energy conversion systems (ECS), not only due to the need of regulation of voltage and current levels but also for its role in ensuring that the maximum available power is processed at all moments. The latter reason is especially true in RES, where energy profiles are usually intermittent – *e.g.* solar and wind - and dependent on non-controllable factors. ECS are also a major economic asset for three main reasons: a) power converter and ancillary unit overall costs (installation and O&M) weight heavily in any design or feasibility analysis; b) their efficiency in processing energy directly affects the produced net power locally consumed and/or injected into the grid; *3)* ECS is an obligatory pathway between the energy source and consumer, there is no energy transfer without it. A failure of any hardware or component-level unit in an ECS is likely to cause a full interruption and require replacement.

Ensuring high reliability of power electronics components in power converters and/or its ancillary units is, therefore, desirable under the economical and operational point of view; *time is money* as one might say. A power converter with a high failure rate in a grid-tied RES will drastically increase O&M costs, decrease energy savings, and decrease revenues of selling electricity – especially in utility-scale power plants. Each of these factors has a different impact when calculating the cost of energy and return of investment (ROI). Thus, power converters' reliability may shorten or push forward the payback time of RES power plants.

4.1 RELIABILITY AS A FIGURE OF MERIT

To be reliable is arguably one of the most important characteristics of any engineered product since it will have no market future if its failure rate surpasses its usefulness. In electronics, the best design could be defined as the best compromise between the product reliability requirements, cost-effectiveness, and time-to-market for a particular application (SUHIR, 2013). However, this balance is not achieved effortlessly: if a product is superfluously robust for its intended application, it means that the manufacturer spent more than necessary in production; if it is not robust enough, it may cost money and reputation. Each industry and/or application have its own reliability goal, as shown in Table 6, and electronic systems should be designed aiming accordingly.

Table 6 – Typical lifetime target for electronics in different industries (CHUNG et al., 2015).

Applications	Typical design target of lifetime
Aircraft	24 years (100,000 hours flight operation)
Automotive	15 years (10,000 operating hours, 300,000 km)
Industry motor drives	5-20 years (60,000 hours in at full load)
Railway	20-30 years (73,000-110,000 hours)
Wind turbines	20 years (120,000 hours)
Photovoltaic plants	30 years (90,000-130,000 hours)

For decades, the automotive, aerospace, and military industries have used reliability analysis of electronic components due to their intrinsic safety requirements. The most common methodologies employed in the 20th century – and still used by some authors (ADINOLFI et al., 2015; JIMÉNEZ et al., 2010; RAHMANI et al., 2012)) – were based in Mean-Time-To-Failure (MTTF) and Mean-Time-Between-Failure (MTBF) calculation, using the popular Reliability Prediction of Electronic Equipment (US DoD, 1991) – a Military Handbook (MIL-HDBK-217), initially published by the U.S. Department of Defense in 1961. The purpose of MIL-HDBK-217 was "*to establish and maintain consistent and uniform methods for estimating inherent reliability of military electronic equipment and systems*". It consisted of two methods of reliability prediction that were built upon an extensive dataset of failed electronic components under various operating conditions.

The MIL-HDB-217 relied on the assumption of a constant failure rate for a specific component technology under a specific load, as depicted in Figure 40. Although this assumption is approximately consistent in some cases, it disregards the effects of time-varying stress and wear-out. Therefore, the handbook's main limitation lied in simply giving a statistical correlation from collected failed components data, rather than understanding how and why a failure occurs. Even though data from the MIL-HDBK-217 suffered continuous revisions since its first publication, in 1995 the handbook was officially discontinued.

Handbook and bathtub-based methods are now considered inadequate to predict failures in power electronic systems (CHUNG et al., 2015) for not considering significant aspects such as temperature cycling, failure rate change with the material, combined environment conditions, quality and technology variations, among others (WANG et al., 2012). Modern reliability research is undergoing a paradigm shift away from pure empirical-based approaches and towards a methodology that focuses on identifying and modeling the physical phenomena that cause failure. The physics of failure (PoF) approach is based on root cause failure mechanisms analysis and the impact of materials, defects, and stresses on product reliability (PECHT and DAGUSHA, 1995).

Figure 40 – Failure rates on a bathtub curve during three distinct periods.

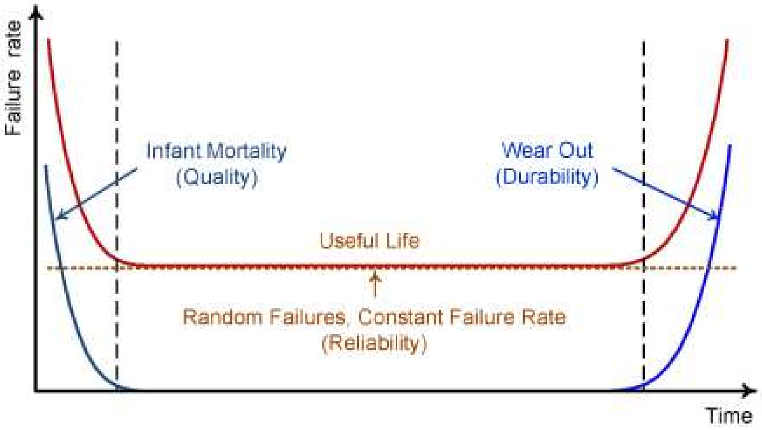

Source: (WANG et al., 2012)

Reliability and lifetime cannot, however, be assured; uncertainty and variability are a dominant background when predicting failure. The mechanisms that lead to a component's degradation are functions dependent on time and operating condition, and statistics is a necessary basis to analyze reliability data. Nevertheless, quantifying lifetime provides a powerful set of information even without certainty; lifetime estimations may be used as a figure of merit that enables the designer to make a decision based on known conditions in which a system will operate.

4.2 DESIGN FOR RELIABILITY

There exists an intrinsic trade-off between a system's desired reliability and the necessary financial cost for such. Economics is a major player in any engineering application and, in RES, it is also a determining factor for the execution or not of a new power plant. Ensuring the highest possible power electronics reliability in a PV system, for instance, may also increase its complexity and will certainly increase its cost. On the other hand, neglecting this kind of analysis may lead to an inadmissible failure rate and long-term financial losses.

The optimal reliability level may be described as the investment which achieves the best balance between long-term and investment costs. In order to achieve this optimum point, the designer must make adequate choices of topology, components, and operating conditions so that the system under analysis is not over-engineered nor under-reliable. The investment and effort needed to increase a system's reliability are dependent on its specific dynamics and complexity, so a customized analysis is required in order to evaluate which are the weakest elements and possible solutions to increase robustness.

In order to overcome inadequate failure rates and reduce maintenance and replacement costs, reliability analysis should be considered before a specific product reaches the production phase and market. The costs associated with different manufacturing phases tend to grow exponentially, as depicted in Figure 41, and not predicting potential defects may be the difference between a product's success or failure.

Figure 41 – Cost of unreliability relative to the manufacturing phases.

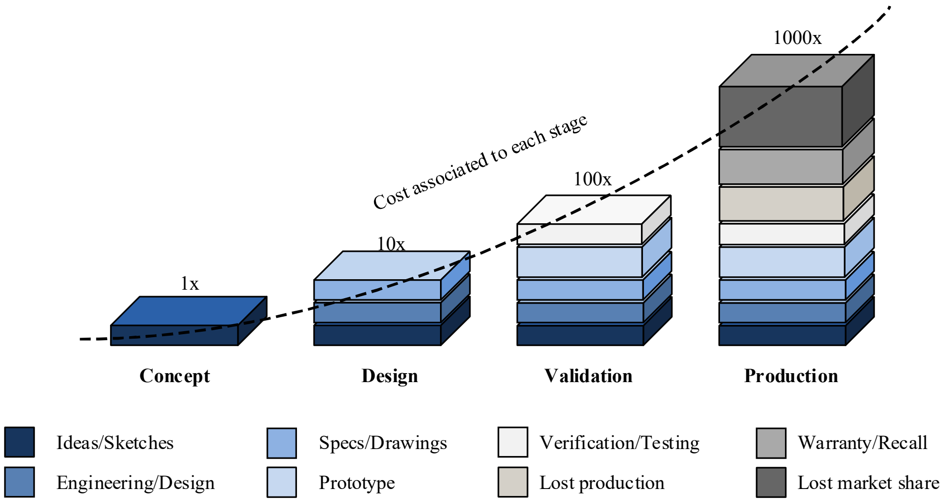

Source: Personal archive adapted from DfR Solutions.

As previously discussed, power electronics are one of the core elements in BOS of renewable energy systems. The overall reliability of a power plant is hence directly linked to the failure rate of the power converters used for energy processing and voltage and current regulation. Thus, it is clear that there exists a relationship between converter reliability, a power plant O&M costs, and the LCOE in renewables. A modern solution to avoid an unexpected and unreliable performance is the Design For Reliability (DFR) approach, where an assessment of potential failure risks is made in the design phase.

4.2.1 DFR in PV Power Electronics

Case studies frequently show that power converters are the element most prone to failure in PV systems and, therefore, the design of more reliable power converters is a necessity (RISTOW et al., 2008; ZHANG et al., 2012). A five-year report of a 3.51 MW PV power plant operated by Tucson Electric Power Company, USA, highlighted that the inverters were the cause of 37% from all unscheduled maintenance occurrences and 59% of the associated cost (MOORE and POST, 2008). Specialized magazines and professionals in the PV industry also point to the inverter as the most common cause of failure in power plants (SOLARPRO, 2010, PV-MAGAZINE, 2016) – especially microinverters (SOLARPRO, 2015). Some even claim that inverter failures have been responsible for approximately 80% of all PV downtime (UTILITY PRODUCTS, 2011).

Traditional design of power converters and inverters tend to disregard long-term lifetime analysis and failure prediction, especially due to the complexity of these subjects and the lack of available tools for such. As a result, lifetime expectancy and warranty tend to be smaller; in photovoltaic systems, this issue is evident when analyzing the mismatch between the inverter's typical warranty (~ 7 to 10 years) and the PV modules typical life expectancy (~25 to 30 years).

If a comprehensive reliability analysis of a power converter is included in the design phase and the weakest elements are identified, a better performance and lifetime may be achieved after production and market entry. By introducing a lifetime analysis tool in pre-design and design of power electronics, a more promising approach for improving reliability is enabled where flaws and/or weaknesses may be quickly identified and corrected before a project is put into production and/or market (YANG et al., 2015).

4.2.2 Where to start?

One of the foundations of the PoF approach is to understand the different mechanisms that can cause a failure – and not only to quantify them. Different failure mechanisms are characterized by different physical phenomena and different activation energies (Suhir, 2013), thus identifying the relevant phenomena that allows the designer to prioritize what should be avoided.

Capacitors are widely known to be one of the weakest elements in power electronic systems (FURUKAWA et al., 2014; KIRISKEN and UGURDAG, 2014), especially when used as energy buffer in bus banks. Mainly, the three capacitive technologies employed in DC-links are Aluminum electrolytic (Al-Cap), Metallized Polypropylene Film (MPPF), and Multi-Layer Ceramic (MLC), where each type has its own advantages and weaknesses. Although ceramic or polypropylene film capacitors are a trend in PV applications, electrolyte capacitors are still studied (WANG et al., 2013) and used due to its low cost and superior energy density (WANG and BLAABJERG, 2014).

Failure of a capacitor may be either catastrophic – resulting in a short- or open-circuit - or caused by a variation of its parameters (capacitance and/or *ESR*) above a specific operational threshold. In both cases, however, it is very likely that the complete degradation of a capacitor will lead to failure or interruption of the whole system since they are a vital part of power electronics.

For these reasons, in the preliminary analyses presented in this work, only the lifetime of Al-Caps was considered. The electro-thermal and lifetime modeling of these capacitors in PV applications was studied in order to develop a figure of merit for designing power converters. Further developments will aim for the reliability analysis of other capacitor technologies and of semiconductors, in order to create a more comprehensive design methodology.

4.3 CAPACITOR LIFETIME ESTIMATION

To estimate the lifetime of a capacitor in a given application, it is necessary to evaluate its energy processing and operating levels in function of time.

4.3.1 Lifetime models

Failures in e-caps may occur due to external and/or random factors, such as manufacturing defect, improper design, environmental overstress, abnormal operation condition, among others. However, they usually occur non-predictably and catastrophically – where a single event leads to failure. Thus, they are difficult to model or foresee and are usually deemed as random events.

The electrolyte vaporization and wear-out of electrical parameters is one of the dominant mechanisms that may lead to the failure of either the capacitor itself or of the circuit/control scheme in which the capacitor is inserted. A typical and widely used approach for estimating the useful life of e-caps the simplification of the Arrhenius law (WANG and BLAAJBERG, 2014, ZHOU et al., 2016), which yields in lifetime (L) as a function of the capacitor operating temperature and voltage (V_{CAP}) as

$$L\left(T_{CAP},V_{CAP}\right)=L_0 2^{\frac{T_0-T_{CAP}}{n_1}}\left(\frac{V_{CAP}}{V_0}\right)^{-n_2} \tag{17}$$

where L_0, T_0, and V_0 are the capacitor rated lifetime, temperature, and voltage, respectively, which are usually specified by the manufacturer. This equation gives a good representation of the expected lifetime according to several manufacturers, and in this work $n_1 = 10$ and $n_2 = 4$ are adopted, which are within the typical range for e-caps (WANG and BLAAJBERG, 2014).

To quantify how time-variant stress impacts on the overall lifetime, a linear damage accumulation is used by calculating the ratio of operating hours in a given stress level, t_{Li}, and the estimated lifetime (15) at that given condition (ZHOU et al., 2018), as in

$$AD=\sum\frac{t_{Li}}{L_i\left(T_{cap},V_{cap}\right)} \tag{18}$$

where AD is the accumulated damage over the period analyzed; the failure is assumed to happen when AD is equal to unity. Although a capacitor degradation is typically non-linear (WANG et al., 2018) and (18) considers that all stress levels cause the same impact on lifetime, the Miner's rule is used part numbers and capacitor bank designs can be used as a figure of merit for design choices.

4.3.2 Monte-Carlo Simulation and *Bx* Lifetime

Since not all capacitors are identical and even their degradation may occur differently for the same stress level, a statistical approach is combined with a parametric variation in order to calculate the B_x lifetime – which is the time when x% of the samples would fail (AGHDAM and ABAPOUR, 2016). This is done by including a stochastic process between the capacitor thermal modeling and the lifetime estimation through one or more variables.

To do this, the electrical and thermal parameters of interest are assumed to follow a normal distribution confined in a 3 standard deviation region (3σ, 99.7% confidence interval) and centered at their rated or specified value. The parameter standard deviation is defined by the designer and can also be considered as a design variable since it will affect the confidence of the reliability analysis.

Then, a Monte Carlo simulation is performed considering all the specified parameter distributions and a population of 10,000 samples. The stochastic parameters T_{CAP} and V_{CAP} are initially converted into static values T'_{CAP} and V'_{CAP}, using (17) and (18) for the condition in which the AD is equal to one, based on the methodology proposed in (AGHDAM and ABAPOUR, 2016). Values of T'_{cap} and V'_{cap} are then fed to a Monte Carlo simulation – with 10,000 samples – using also the parametric normal variation. The output from the Monte Carlo simulation results is a random capacitor lifetime distribution, which is expected to follow a Weibull distribution given by

$$f(x) = \frac{\beta}{\eta^{\beta}} x^{\beta-1} \exp\left[-\left(\frac{x}{\eta}\right)^{\beta}\right] \tag{19}$$

where β is the shape parameter, η is the scale parameter, and x is the operation time. The wear-out failure probability curve $F(x)$ is then obtained through a cumulative density function (CDF), where

$$F(x) = \int_0^x f(x)\,dx\,. \tag{20}$$

The B_x lifetime – time when x % of the samples have failed – is then obtained from (20). B_x is used as the figure of merit for capacitor design in this proposed tool. A summarized description of the whole reliability analysis and methods is shown in Figure 42.

4.3.3 Component to system level reliability

The failure probability obtained through the method shown in Figure 42 is given for a single capacitor; therefore, this process must be repeated a number of times equal to the number of components being analyzed in an arbitrary capacitor bank. Thus, the whole capacitor bank reliability is determined considering the total number of capacitors (N_{CAPS}) versus the minimum required (N_{min}) for that specific design and criteria.

Figure 42 – Flowchart of the steps and models done for a capacitor reliability analysis.

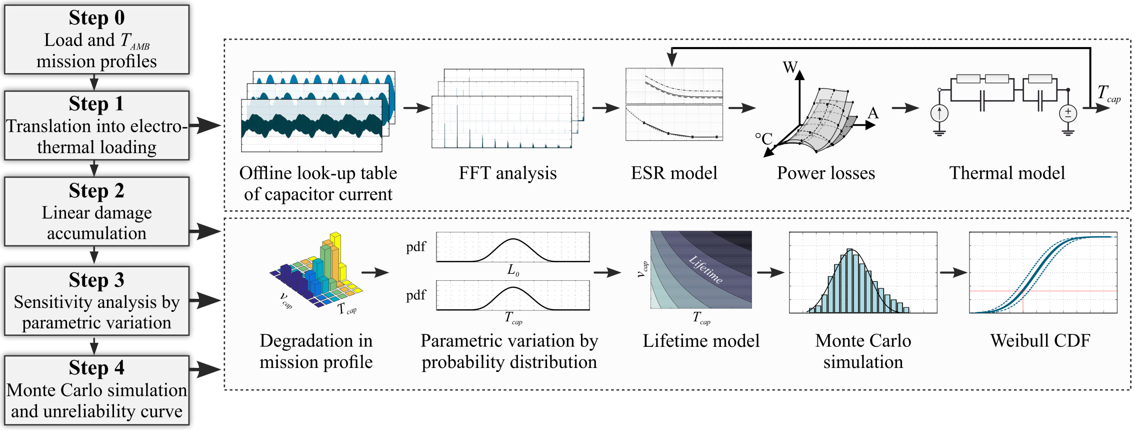

Source: personal archive

A reliability block diagram equivalent to the capacitor bank being analyzed is built, as shown in Figure 43. If the capacitor bank size is equal to the minimum required, then all capacitors are considered to be in series reliability-wise since the failure of one component will undermine the whole system's operation; the reliability of the system is then calculated through

$$P_S = \prod_{i=1}^{N_{\min}} (1 - F(C_i)) \tag{20}$$

where P_S is the reliability of the series system composed by N_{min} capacitors. Each extra capacitor in the bank is considered to be in parallel, reliability-wise, to one component from the minimum required group, thus

$$P_P = 1 - \prod_{i=1+N_{\min}+k}^{N_{CAPS}} F(C_i) \tag{21}$$

where P_P is the reliability between two capacitors in parallel reliability-wise.

Figure 43 – Reliability block diagram built for each capacitor bank design.

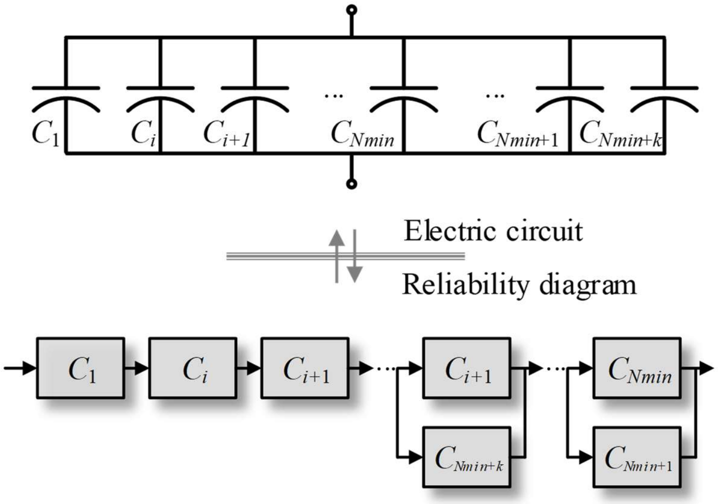

Source: personal archive

4.4 CHAPTER FINAL CONSIDERATIONS

Based on the previous discussion, one may conclude that the understanding of reliability physics is a key aspect of this type of analysis. Collected data from industry and real-field applications are essential due to their statistical significance, nevertheless, they lose some relevance without the understanding of how and why the failure occurred. This happens in reason that if only the number of failures is known, for a specific component on a specific application, there is no accurate way to make an assessment of what may be done to avoid future failures.

Although the DFR may be of substantial aid for the designer of power converters, it must be stated that this approach requires a certain amount of customization and constraints. Manufacturers usually prefer to limit their number of product variability and do not take local characteristics into account. The same PV inverter, for instance, is usually sold to operate in both arid or humid conditions, indoor or in open-rack, and so on.

However, through proper modeling of the operation profile of a capacitor – or any other electronic component, lifetime time analysis may be used as a figure of merit to make better decisions in the design stages of a power converter.

5 CASE STUDIES AND RESULTS

To investigate how the design parameter choices and the mission profile impact on the lifetime performance of capacitors, two case studies are designed, simulated, and analyzed using MATLAB, Simulink, and hardware-in-the-loop simulation, and combined with the experimental results of capacitor electro-thermal model. The case studies are defined as: 1) a single-phase single-stage (SSSP) inverter and 2) a double-conversion single-phase UPS.

5.1 SINGLE-STAGE SINGLE-PHASE PV INVERTER

Single-stage energy conversion systems are still a popular choice for PV systems due to their reduced cost and complexity when compared to double-stage configurations. One of the disadvantages of the grid-tied single-stage converter is the necessity of a single MPPT for multiple PV panels, due to the fact that a considerable number of modules, in series connection, is needed to build up a DC-link voltage for energy conversion. This configuration inevitably leads to a decreased efficiency of energy harvesting since a global MPP must be defined for the entire PV array, which is not ideal due to well-known issues such as shading and mismatch. Figure 44 shows an overview of the methodology and considerations presented so far.

Figure 44 – Diagram of the proposed methodology to analyze the lifetime of DC-link capacitors in SSSP PV converter.

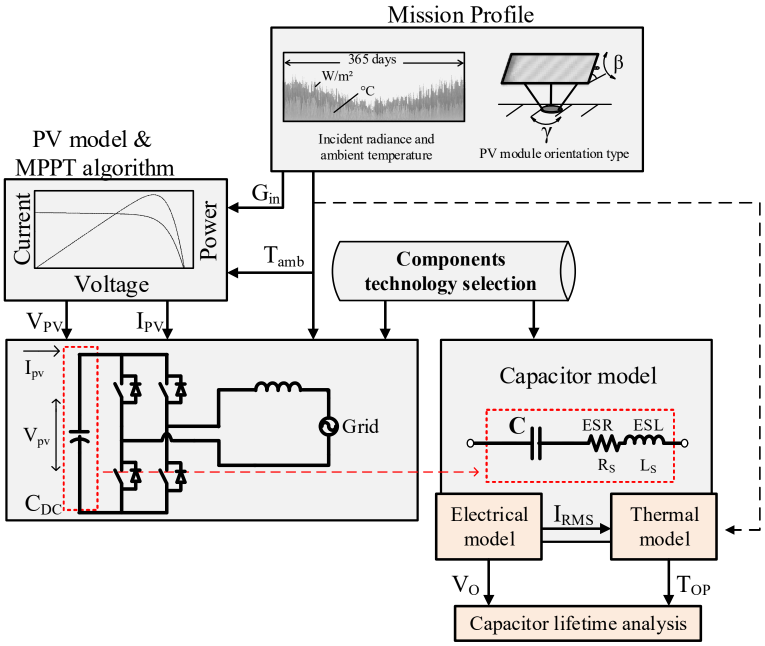

Source: personal archive

The three different PV mission profiles discussed in Chapter 2 are considered for the analysis of lifetime estimation for the DC-link capacitor bank of the SPSS, being *PTR-2x*, *LIN-Horiz*, and *IZA-fixed*. A PV array and inverter similar to the one described in Section 2.2 is used for this analysis, as described in Table 7. Since the analysis in focus in this design tool is the multi-objective performance of the DC-link capacitors, some considerations and simplifications are assumed as follows:

a) Only active power flow was considered, generated by the PV system and injected into the grid;

b) A perturb and observe maximum power point tracker algorithm was employed and considered having null error;

c) Inverter switching losses and dynamics were not considered;

d) PLL was used to provide unity power factor energy processing by synchronizing the SSSP output current with the grid voltage;

e) To ensure null error in steady-state, PI controller was designed and used to regulate the DC-link voltage in reference to the calculated MPP array voltage;

f) Maximum voltage ripple across the DC-link was defined as 14 V. This value was chosen in order to limit voltage fluctuation at 1 V per panel in the PV array, decreasing the MPP error;

Figure 45 – Overview of the analyzed single-stage PV inverter.

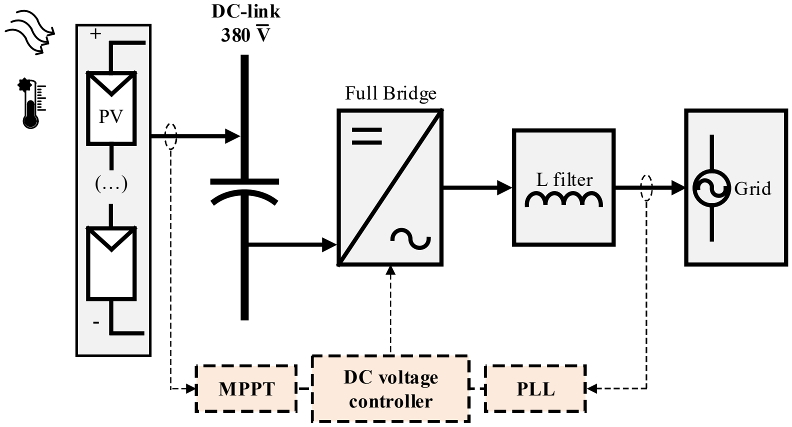

Source: personal archive

Table 7 – Design parameters used for the SSSP PV converter analyzed.

Parameter	Symbol	Value
PV array – 14 modules in series (SunEarth TPB 235 W)	-	3290 W @ STC
Rated power	P_R	3500 W
Rated DC-link voltage	V_{DC}	380 V
Maximum DC-voltage ripple	ΔV_{DC}	± 14 V
Switching frequency	f_{SW}	12 kHz
Switching modulation	-	Bipolar
L-filter	-	10 mH
Grid voltage	v_{AC}	220 V_{RMS}
Grid frequency	f_G	60 Hz

Source: personal archive

5.1.1 Capacitor design

Electrolytic capacitors with different constructive characteristics were considered and datasheet information for thermo-electrical modeling was used. The list of part numbers used in this section is described in Appendix A while Figure 46 shows a flowchart of the algorithm developed to automatically read datasheet information and built a component database.

Figure 46 –Algorithm flowchart for building a capacitor database.

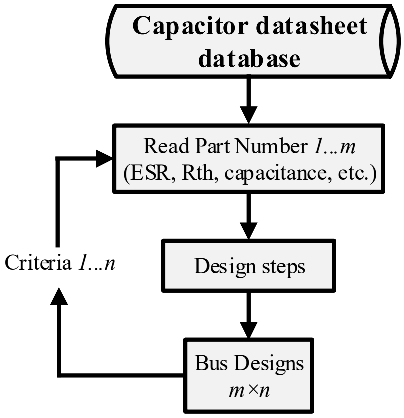

Source: personal archive

The part numbers used in this work are briefly described in the results section. In total, 18 capacitor bank designs are analyzed and their volume, cost, and lifetime performance studied. Different capacitors of the same part number are assumed as being all identical and their values equal to the provided in the manufacturer’s datasheet. In order to standardize the cost comparison among all part numbers, their cost per unit is collected from the same distributor. Since nonlinearities and mismatches are disregarded, it is assumed that the DC-link current is distributed equally in the capacitor bank.

In addition, two different design methods for the minimum DC-link capacitance are considered wherein criteria #1 is the traditional equation for minimum capacitance needed to ensure a desired voltage ripple; this work also proposes a second approach (criteria #2) to find the minimum number of capacitors in parallel in order to maintain their core temperature at a specified level, as follows:

1) **DC-link design criteria 1:** in this method, the DC-link capacitors are selected according to the minimum required capacitance and/or maximum supported ripple current using the single-stage inverter rated power, by means of

$$nCAPS^1 \times \min C^1{}_{DC,i} \geq \frac{P_R}{2\pi f_g V_{DC} \Delta v} \tag{22}$$

2) **DC-link design criteria 2:** after the minimum capacitance is guaranteed, a new criterion is proposed with the objective to limit the capacitor's core temperature elevation, based on the MP. A maximum threshold for temperature elevation ($max\Delta T_{CAP}$) in relation to the capacitor's local ambient temperature. The needed number of capacitors in parallel to respect $max\Delta T_{CAP}$ is calculated by

$$nCAPS_i^2 \times \geq \frac{i^{MP}_{CAP,RMS}}{\sqrt{\max \Delta T_{cap} \big/ ESR_{LF,i} R_{th,i}}} \tag{23}$$

where $nCAPS_i^2$ is the number of parallel capacitors needed, $i^{MP}_{CAP,RMS}$ is the maximum ripple current in the DC-link capacitor bank in that mission profile, and $ESR_{LF,i}$ and $R_{th,i}$ are the series equivalent resistance – at fundamental frequency – and thermal resistance, respectively, of the part number i. The temperature limit $_{max}\Delta T_{CAP}$ is obtained by rewriting the capacitor thermal model equations and solving with datasheet information. For the following analysis, $_{max}\Delta T_{CAP}$ is defined as 5 ºC.

5.1.2 Capacitor banks analyzed

The results of lifetime analysis of capacitors in a DC-link of an SSSP converter were obtained for all part numbers of Appendix A and using the two design methods discussed in the previous section and in Appendix C. Thus, a number of 18 capacitor bank designs were analyzed and their sizes are shown in Table 8. Additionally, the performance of these design sets was studied on three different mission profiles.

Table 8 – Number of capacitors in each designed capacitor bank, for each part number and design method.

Part number	$nCAPS^1$	$nCAPS^2$
	Design criteria #1	Design criteria #2
380LQ681M400A452	6	10
381LX102M450A102	5	7
383LX681M450N062	7	8
450C871M450BH8	3	5
383LX681M450B052V	6	7
382LX222M400B102V	2	4
550C102T400BJ2B	3	4
DCMC182T450BD2B	3	4
550C242T450DC2B	1	2

Source: personal archive

In order to standardize the cost comparison among all part numbers, their cost per unit was searched and collected in the same distributor and on the same day. Since nonlinearities and mismatches were disregarded, it was assumed that the DC-link current was equally distributed among each capacitor bank design.

5.1.3 Single-stage converter operation

As it has been discussed so far, to properly investigate the performance of a power converter and its components in different mission profiles, it is necessary to estimate the values of several variables not only on a single or few conditions but rather throughout a one-year operation. In order to reduce processing time and effort, a look-up table (LUT) approach was used by calculating and simulating the whole system's behavior considering the entire range of possible operation. Hence, LUTs of various variables on steady-state were built-in function of solar irradiance and ambient temperature by taking multiple steps of these environmental inputs.

This method reduces calculation time since it excludes the necessity of high-frequency dynamics simulation of the converter and its components in a one-year operation. With previously established look-up tables, the PV MP may be studied in a one-minute resolution through search and interpolation of the variables of interest. Although this approach disregards transitory and control dynamics, it is suitable for this work's objective since the main focus lies in long-term analysis.

5.1.4 Offline look-up table approach

Since solar irradiance on the PV modules and ambient temperature are the two factors that dictate PV power generation, these two variables were used as input for simulating the SSSP converter of Figure 45. The circuit and control presented in this section were simulated in Simulink® while all other analyses (mission profile, thermal, lifetime) were done in MATLAB®.

Alternately, irradiance was varied from 100 to 1200 W/m² while ambient temperature from -10 to 40 °C and measurements of PV array output, DC-link capacitor, and inverter were stored – the first two seconds of simulated data were discarded in order to allow the SSSP converter to reach steady state.

In Figure 47, the SSSP PV system behavior is shown with respect to solar irradiance variation and for an ambient temperature of 25 °C. Figure 47a shows the steps of irradiance with respect to time while Figure 32b shows the reference of PV power, calculated by the MPPT algorithm, and the power injected into the grid. In Figures 47c-d the DC-link voltage is also depicted in function of time and varying irradiance; although power increases and the ambient temperature is constant, the calculated reference voltage for the PV array considerably decreases in high radiances due to PV cell self-heating.

The DC-link current (i_{DC}) variation in function of solar irradiance steps is shown in detail in Figures 48a-c; in Figure 48c is important to note the double line frequency ripple superimposed to the inverter's switching frequency. Look-up tables of the i_{DC} were built using four full sample periods after steady state was reached; afterward, this stored data were later used to build two new sets of LUTs: one containing the sample's FFT from each step of G^{PV} and T_{amb}, the second with the RMS current value on the double-line frequency.

Figure 47 – SSSP power and DC-link voltage variation in respect to solar irradiance, for constant ambient temperature.

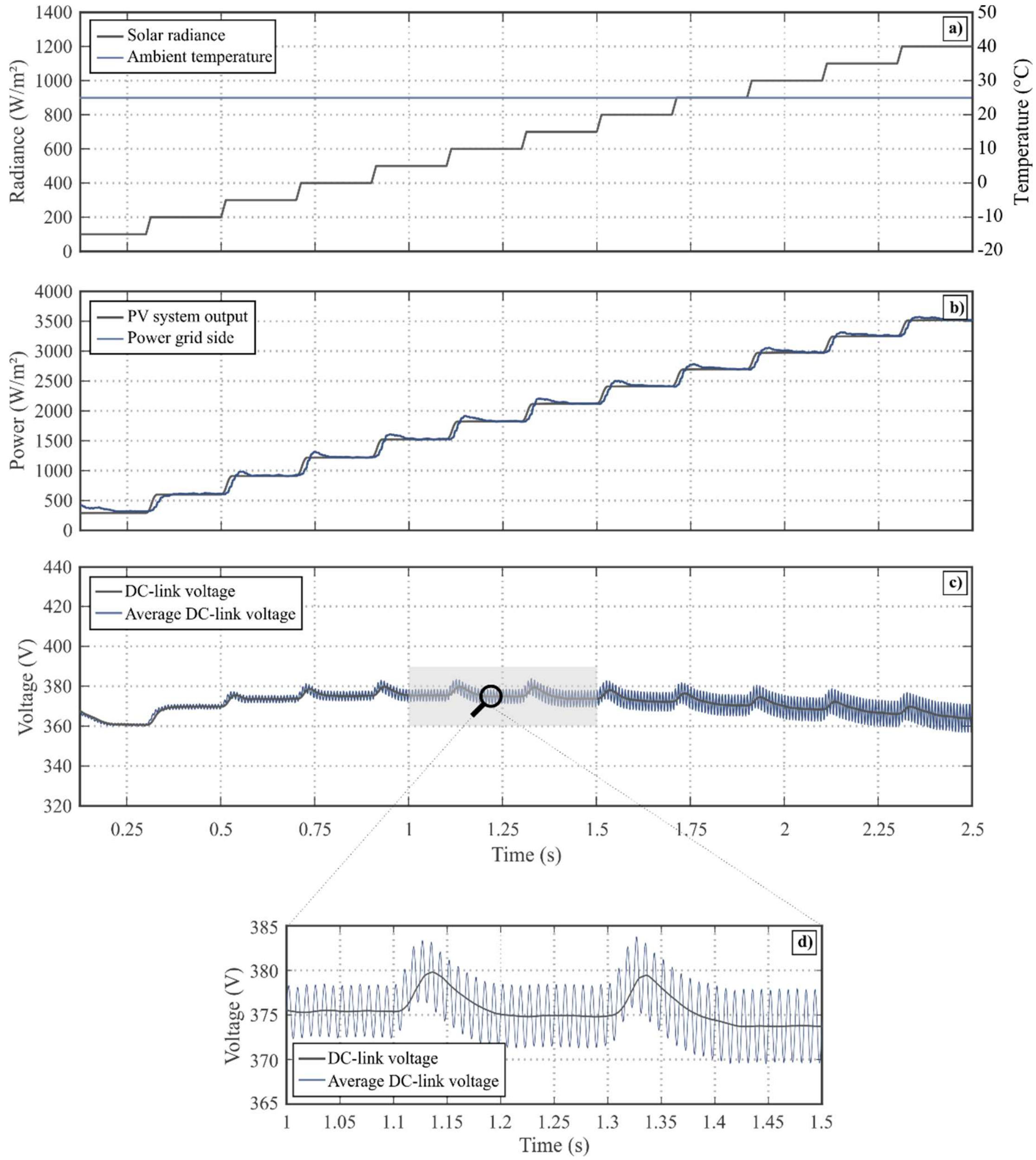

Source: personal archive

Figure 48 – Current through the SSSP DC-link with respect to solar irradiance, for constant ambient temperature.

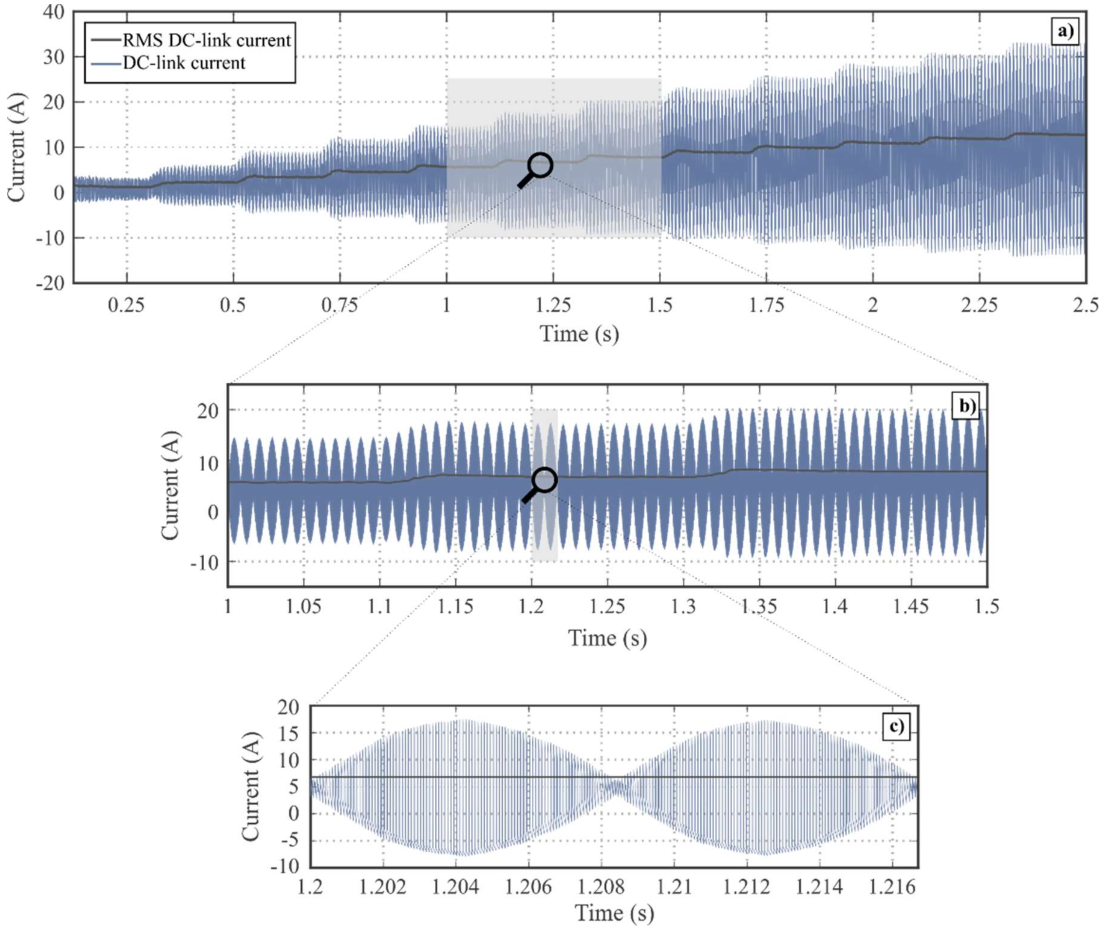

Source: personal archive

The same analyses are depicted in Figures 49-50 but for a constant solar irradiance, equal to 800 W/m^2, and varying steps of ambient temperature, from -10 to 40 °C. The amplitude of photovoltaic generation and power injected into the grid (Figure 47b) in this scenario is many times smaller compared to varying solar irradiance; power processed decreases in higher T_{amb} values in reason of the decrease of PV efficiency. In contrast with Figures 47.c and 48, Figures 49.c and 50 shows that the impact of the ambient temperature on v_{DC} and i_{DC} was inverse as to previous results. The DC-link voltage decreased with the increase of ambient temperature since the calculated MPP voltage reference was greatly affected; on the other hand, i_{DC} was not significantly altered.

Figure 49 – SSSP power and DC-link voltage variation in respect to ambient temperature, for constant solar irradiance.

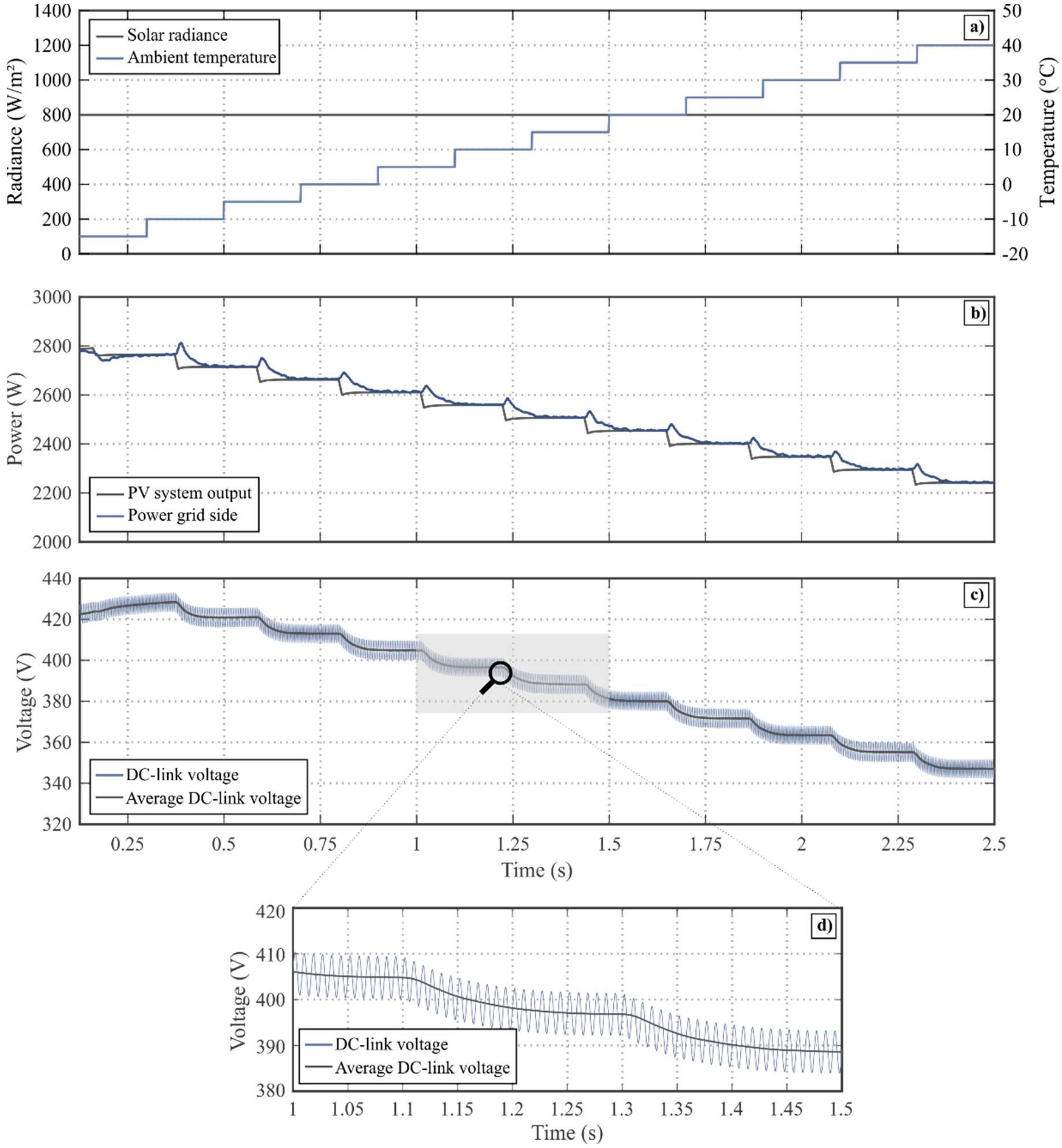

Source: personal archive

Accordingly, by simulating the energy processed by the SSSP converter in different levels of solar irradiance and ambient temperature, two 2-dimension LUTs were built – DC link voltages and currents – as shown respectively in Figures 51-52. Variables were stored only after all the SSSP converter reached steady-state.

Figure 50 – Current through the SSSP DC-link in respect to ambient temperature, for constant solar irradiance.

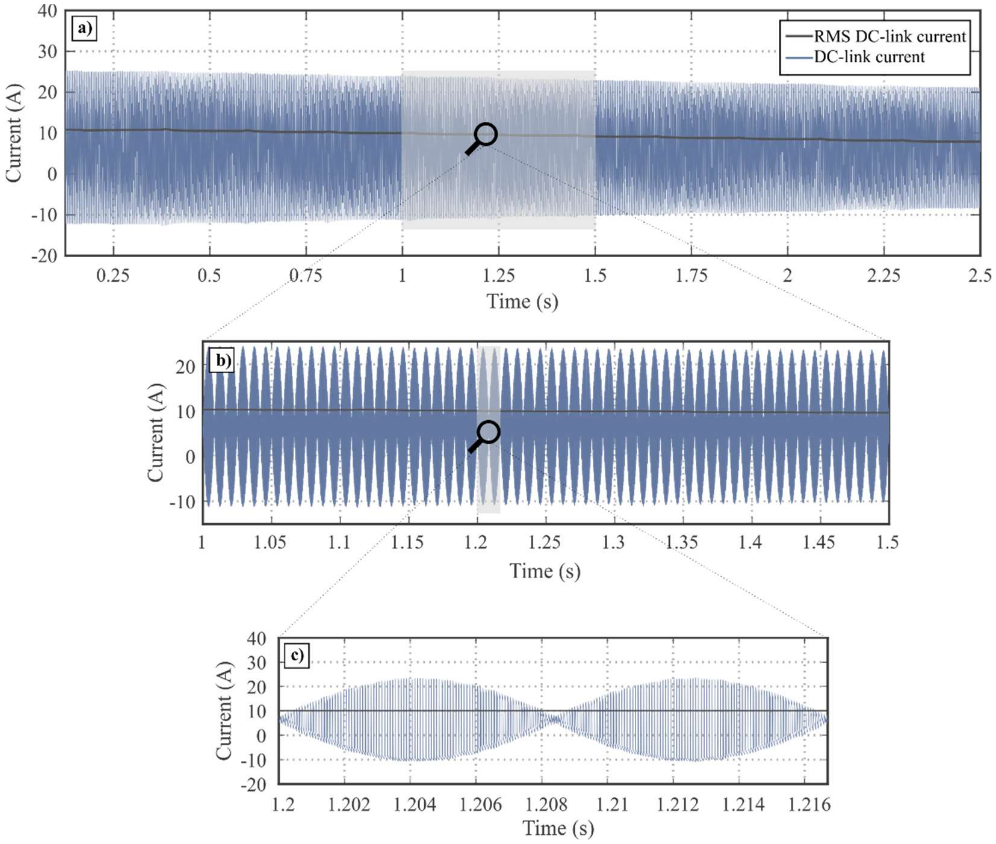

Source: personal archive

Figure 51 – Look-up table of average DC-link voltage in function of both G_{PV} and T_{amb}.

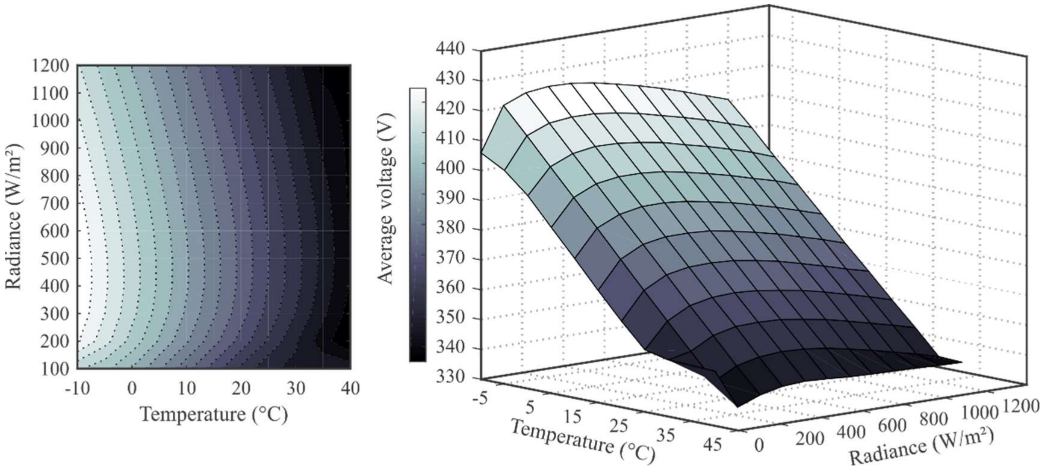

Source: personal archive

Figure 52 – Look-up table of RMS current through the DC-link in function of both G_{PV} and T_{amb}.

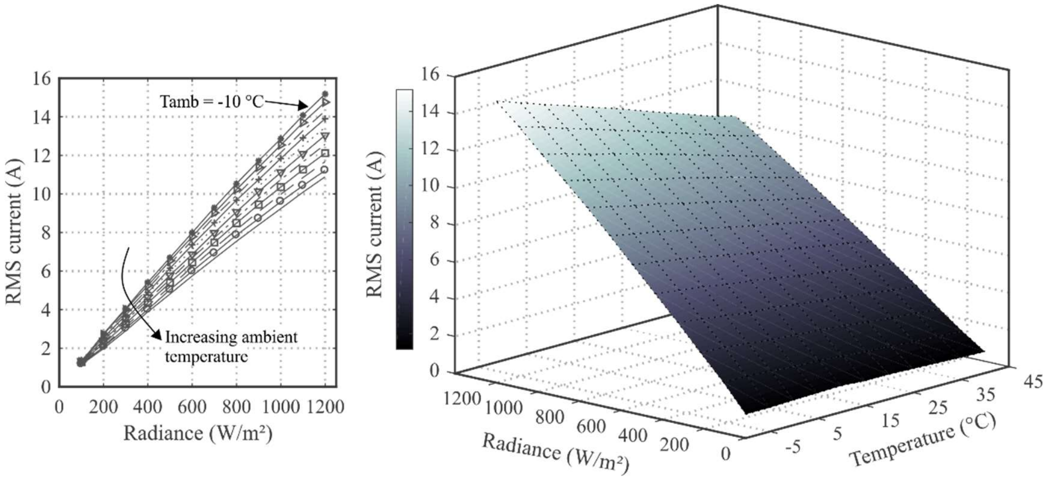

Source: personal archive

5.2.5 Ambience temperature

Operating temperature is a key factor for lifetime and reliability analysis of power electronics, not only because it may affect a component's characteristics but also for being a major stress factor. Thermal dynamics of electronics is a highly complex subject due to its dependency on several aspects, such as material properties, thermal dissipation, PCB layout and component positioning, cooling technique, and others. Thus, although electro-thermal modeling of power electronics has been widely discussed in the literature, authors usually focus on elements individually rather than on the entire system (CHIANG et al., 2013; DU et al., 2010).

One of the main consequences of this difficulty in thermo-electrical modeling is the definition of the ambient temperature, *i.e.* the temperature of the closed system which surrounds the component and/or system in respect. There two popular approaches for defining the ambient temperature: the first is to simply set the external air temperature as the same of the element in analysis (SINTAMAREAN et al., 2014); this choice, however, ignores the fact that a power converter will not operate in an open case and, hence, assumes its heat will be transferred entirely to the external environment without any thermal resistance. Additionally, external air temperature is usually lower than inside a converter's closed case which may lead to an underestimation of component temperature and lifetime.

The second usual choice is assuming the converter's internal temperature as constant in time (LI et al., 2017). This is a somewhat more realistic scenario than the former assumption since it considers higher operating temperatures; however, by doing this one disregards that factors such as the converter power level and the external air temperature have no impact on the internal thermal dynamics, which is also a problematic statement.

In order to avoid a simplistic approach on the thermal modeling of the DC-link capacitors, this work used the methodology proposed by (ZHANG et al., 2016) to estimate the internal SSSP converter temperature based on environmental variables (solar irradiance, ambient temperature, and wind speed) and on its operating levels (power, voltage, and current). An analysis of three commercial PV inverters in open-rack mounting with internal temperature modeling and measurements was performed by Zhang et al, 2016, during the period of one year; with the collected data, a correlation between the inverter head dissipation with environmental conditions was proposed. Following the methodology presented by the authors, the inverter heat sink temperature elevation may be obtained through

$$\Delta T_H = K_{ws} P_{CPR} \tag{27}$$

where K_{WS} is defined as the heat dissipation coefficient that is a function of wind speed, and P_{CPR} is the consumed power ratio (CPR) of the inverter, and be obtained by

$$P_{CPR} = \frac{P_{DC} - P_{AC}}{P_R} \tag{29}$$

where P_{DC}, P_{AC}, and P_R are the instantaneous input and output power and the rated power of the inverter, respectively. In this preliminary phase, wind speed has been considered null (inverter located on closed quarters); hence, according to (ZHANG et al., 2016) K_{WS} was defined as 550. In future work, however, the wind speed will be included in the MP in order to improve the thermal modeling of both the power converters as PV modules.

The injected power the grid (P_{AC}) in function of time was obtained by mapping the efficiency (η_{inv}) of a commercial single-stage PV inverter from SMA (SMA, 2016) in function of its input voltage, as shown in Figure 53. An efficiency look-up table was built in order to obtain η_{inv} for any input voltage and power level through 3-dimensional interpolation. By knowing the reference MPP voltage and the PV array power, an estimated power loss of the inverter was used to obtain the CPR.

Figure 53 – Mapped efficiency in function of power level and input voltage of the commercial PV inverter used as a basis for internal temperature estimation.

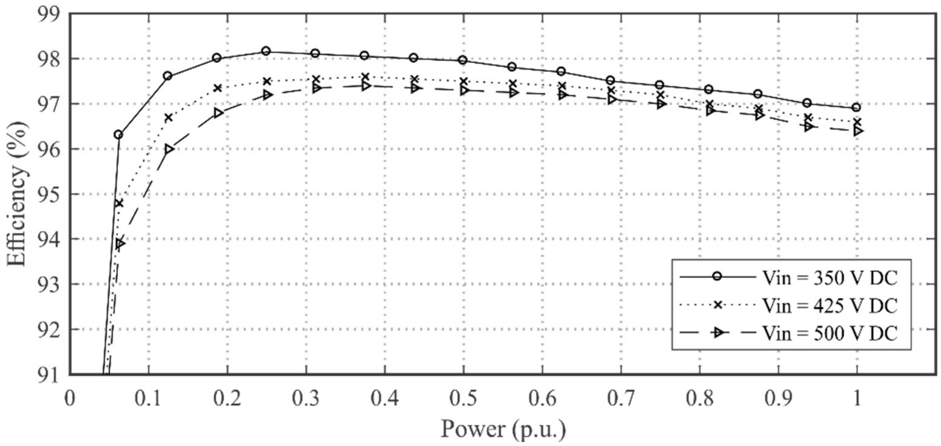

Source: personal archive

Thus, by combining the PV mission profile and SSSP converter with this inverter thermal model, a new variable was obtained as being the *ambiance* temperature (T_{abc}) according to

$$T_{abc} = T_{amb} + \Delta T_H + \Delta T_C \tag{30}$$

where ΔT_C is the component temperature elevation which, in this preliminary study, was considered as solely the capacitor temperature elevation.

This ambiance was defined as the surrounding temperature of the SSSP converter elements and used to estimate the core temperature of the DC-link capacitors. Figure 54 depicts a flowchart of the method used to determine T_{abc}.

Figure 54 – Block flowchart of the methodology used to estimate the inverter internal temperature.

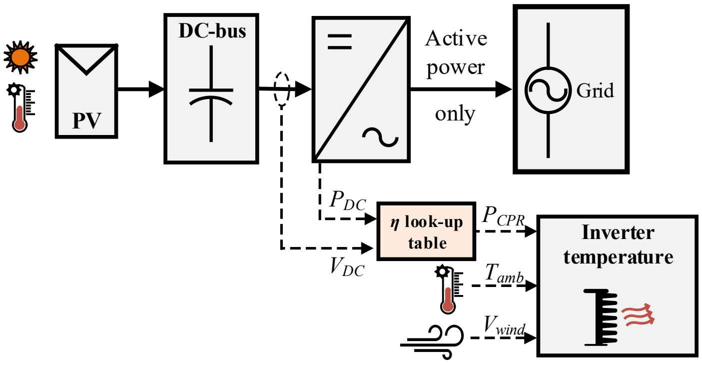

Source: personal archive

Although this approach is still not ideal and some simplifying assumptions were made, it may grant a better estimation of component-level thermal behavior than from the constant or ambient temperature methods. In addition, a thermal lag of T_{abc} was included by taking the weighted average of the calculated ambiance temperature in the last 5 minutes.

5.1.6 Mission profile impact on operating condition

So far, several modeling steps were discussed and presented, as follows:

a) PV mission profile: methodology to estimate photovoltaic power generation accurately and in detail, in order to understand the relevant conditions in which a power converter will operate;

b) SSSP PV converter: the operating conditions of a single-stage full-bridge inverter were mapped in function of the PV mission profile. Thru this step, the entire range of steady-state DC-link current and voltage was estimated and stored in look-up tables;

c) Ambiance temperature: a methodology to estimate the temperature inside the closed case of an SSSP converter was introduced to improve the calculation of the capacitor core temperature, in function of both the external environment and the inverter power level;

d) Capacitor electro-thermal modeling considering the influence of heat transfer mechanisms, parameters dependency on frequency and temperature, and total number of connected capacitors in a DC-link.

All these steps are necessary in order to be able to estimate and understand the thermo-electrical behavior of each capacitor not only on a fixed operating point but rather in function of time and through different energy and environmental conditions. Hence, the lifetime models described in Section 4.3.1 were used to investigate the impact of the different mission profiles on the performance of the capacitor banks of Table 8, according to the flowchart of Figure 55.

Figure 55 – Detailed diagram of the combined methodologies for determining long-term operation behavior of the DC-link capacitors.

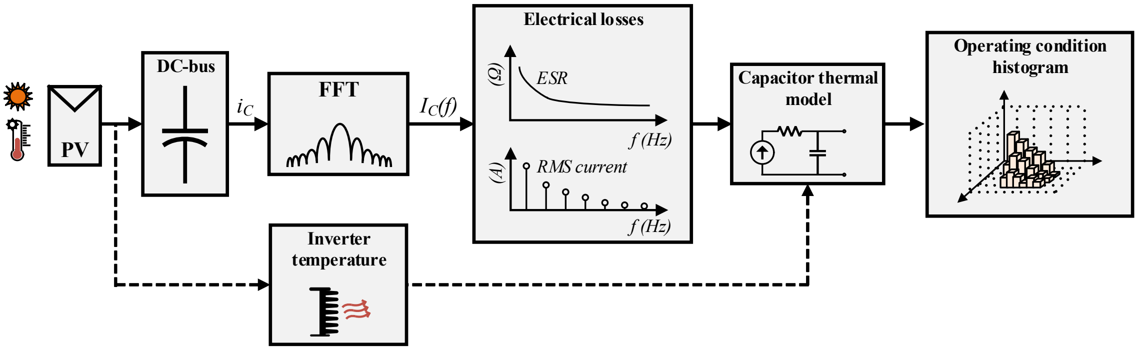

Source: personal archive

Petrolina has a very low climate variability and its TAY is composed mainly of hot temperatures, this significantly reduced the value of DC-link voltage and made the region of operation thinner, as shown in Figure 56. Also, the higher ambient temperatures affected the capacitor core temperature in two different ways: by one side, it decreased the PV power generation and, consequently, the energy processed by them; by the other, it elevates the ambiance temperature. This resulted in a somewhat even distribution for this mission profile and favors the capacitor's lifetime due to the few occurrences of high temperature and high voltage.

The MP of Izaña is also unique due to its high energy availability with moderate ambient temperatures, which explains the larger concentration of capacitor operation at high temperatures. In addition, the distribution of voltage across the capacitors is also usually higher

Figure 56 – Distribution of minute occurrences of capacitor voltage and core temperature after 1-year operation in *PTR-2x*.

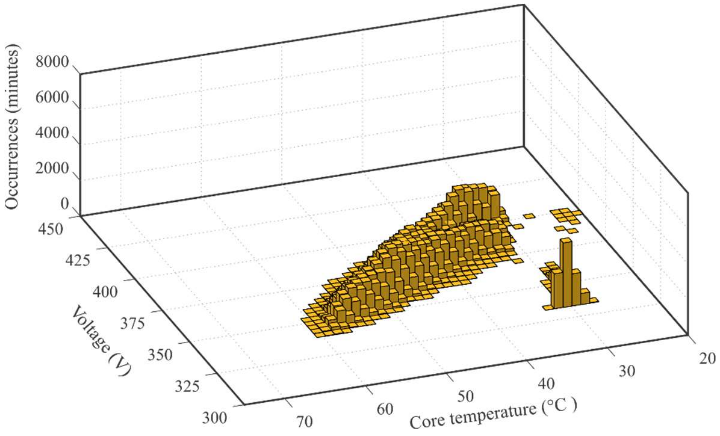

Source: personal archive

In accordance to the MP analysis of Chapter 2, Figure 58 shows that the DC-link capacitors in the Lindenberg MP operated in a wider range of voltages, with a predominance of higher values due to the very low ambient temperatures in that location; this also explains a larger concentration of lower core temperature operation. Nevertheless, Lindenberg has higher climate variability and amplitude in both solar irradiance and ambient temperature (Figure 12), this was reflected with occurrences also in high values of core temperature. This greater count of elevated V_{CAP} and T_{CAP} is prejudicial to the capacitor's lifetime.

Figure 57 – Distribution of minute occurrences of capacitor voltage and core temperature after 1-year operation in *IZA-fixed*.

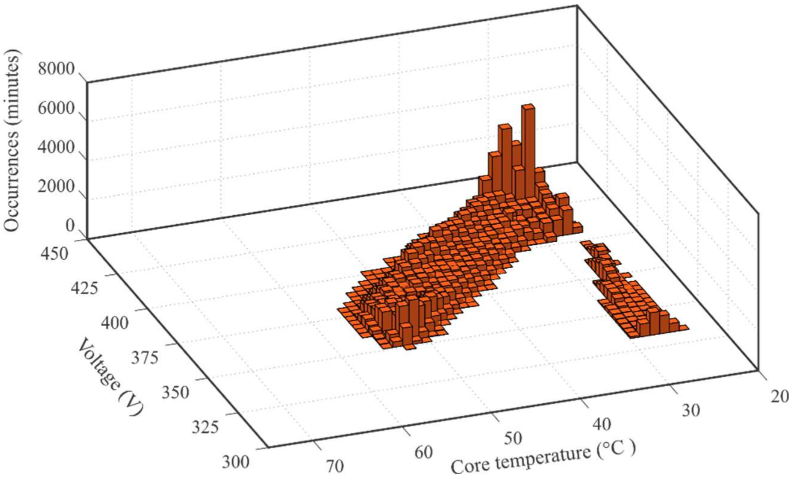

Source: personal archive

Figure 58 – Distribution of minute occurrences of capacitor voltage and core temperature after 1-year operation in *LIN-horiz*.

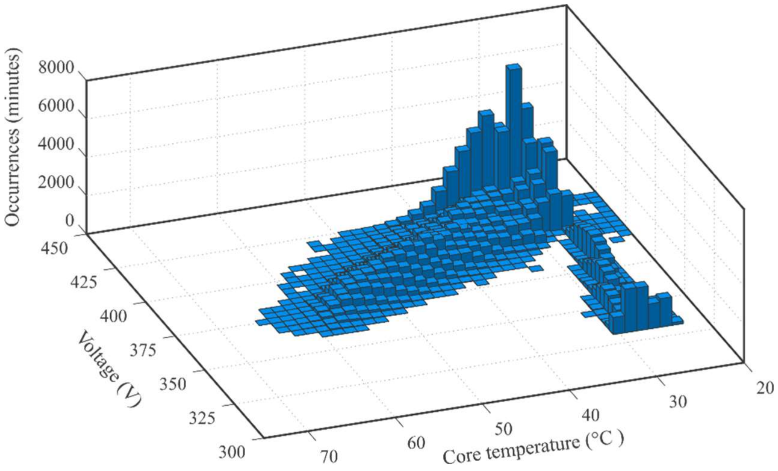

Source: personal archive

It is important to highlight that a populated region of occurrences at low core temperatures and a wide range of v_{DC} was present in all three scenarios. This region may be explained as the occurrences in low power conditions such as early mornings, where the inverter is still cold and DC-link voltage increases together with the rising sun.

5.1.7 DC-link capacitor bank choice through design tool

In this section, the proposed design tool is further analyzed for the PTR-2x mission profile using the part numbers and design criteria described previously. Figure 59 shows a flowchart of the main steps done in order to make a multi-objective performance analyze of multiple designs.

Figure 59 – Main steps of the proposed design tool to optimize DC-link capacitors in PV inverters.

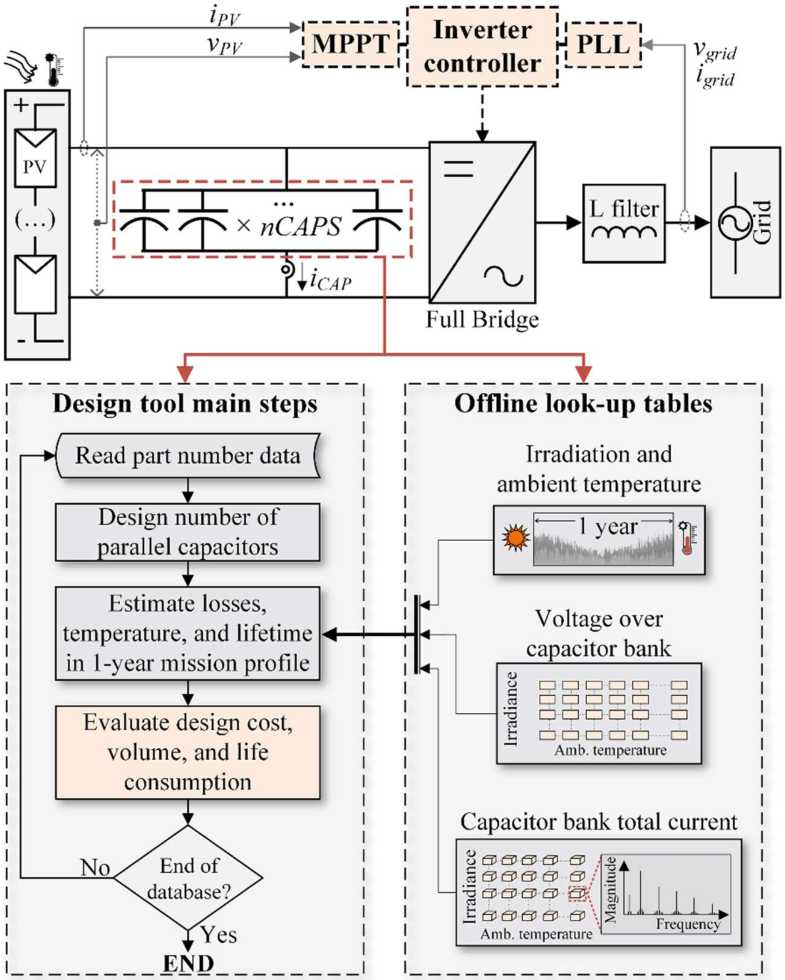

Source: personal archive

It is highlighted that due to a large number of capacitors in parallel yielding small equivalent *ESR*, the differences in voltage ripple of each design are not considered. Thus, the overall voltage across the capacitors in function of time is assumed to be equal for all analyzed designs. Figure 60 shows the hourly histogram distribution of v_{CAP} for the 1-year operation in the mission profile previously described.

In reason of the low annual variability and medium-to-high values of ambient temperature in the used MP (Figure 12b) and that the DC-link voltage decreases in high temperatures (Figure 51), the distribution of v_{CAP} is majorly below the nominal DC-link voltage of 400 V.

Figure 60 – Hourly histogram of DC-link voltage in one year of operation in the considered mission profile.

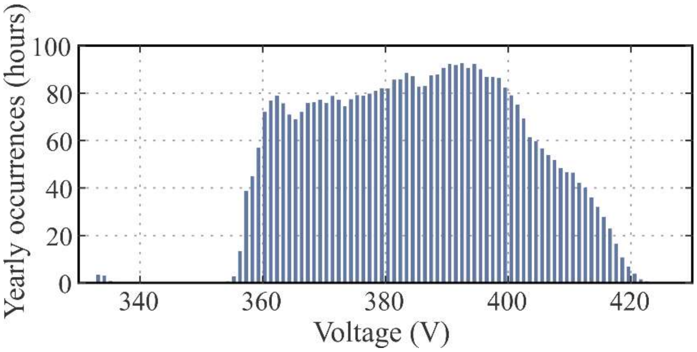

Source: personal archive

Through the method shown in Figure 55, a histogram of the capacitor temperature in each design is built; Figure 61 shows this annual distribution, in hours of operation, for the capacitors in designs #7 and #17, along with the mission profile typical average ambient temperature distribution.

It becomes evident from Figure 61 that not only the overall processed power in the inverter and the ambient temperature affect the capacitor's core temperature, but also design choices such as technology, part number, and total number of capacitors.

In design #17, the current through the DC-link is divided equally among all 4 capacitors, while it goes through only 3 capacitors in Design #7. Also, e-caps of design #7 have an ESR 24% higher and thermal resistance 18% higher than those in Design #17, which also significantly contributes to the higher temperature distribution of the former.

Figure 61 – DC-link operating conditions look-up table of average voltage in function of solar energy and ambient temperature.

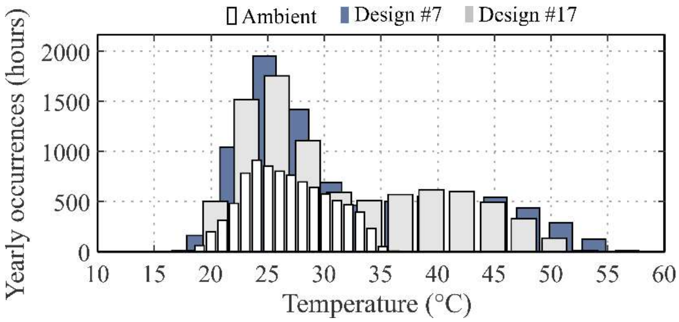

Source: personal archive

The difference between operating capacitor temperature and local ambient temperature, ΔT_{CAP}, in the 1-year mission profile, is shown in Figure 62 for capacitor bank designs using the same part number and Methods #1 and #2 (Designs #9 and #18, respectively).

Although using the proposed Method #2 may ensure lower operating temperatures, the cost-benefit of this approach should still be analyzed in view of other aspects such as the increase in cost. In addition, different MPs will have different impacts on this matter, i.e. if the power converter has a mission profile of high-load operation more frequently, than following (23) may be more cost-effective in long term.

Figure 62 – Temperature difference ($\Delta T_{CAP,i}$) between capacitor core ($T_{CAP,i}$) and capacitor local ambient (T_{abc}), in the 1-year MP, for the same part number and using different design criteria.

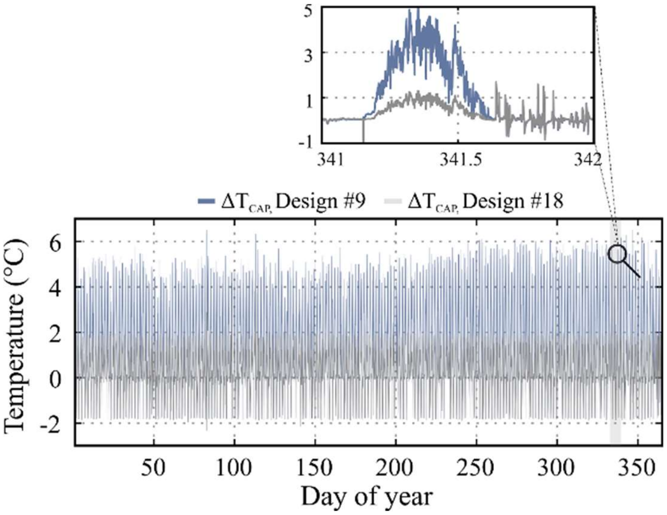

Source: personal archive

Through the proposed design tool, a multi-objective analysis is obtained for all capacitor banks in Table 8 operating in the considered PV inverter and mission profile. Figures 63a and 63b show the total volume and cost of each capacitor bank, while Figure 63c shows the B_{10} of all designs after 1-year of operation in the used MP.

Figure 63 – Results provided by the proposed design tool, for each considered design, in function of a) overall volume, b) cost, and c) B_{10} lifetime.

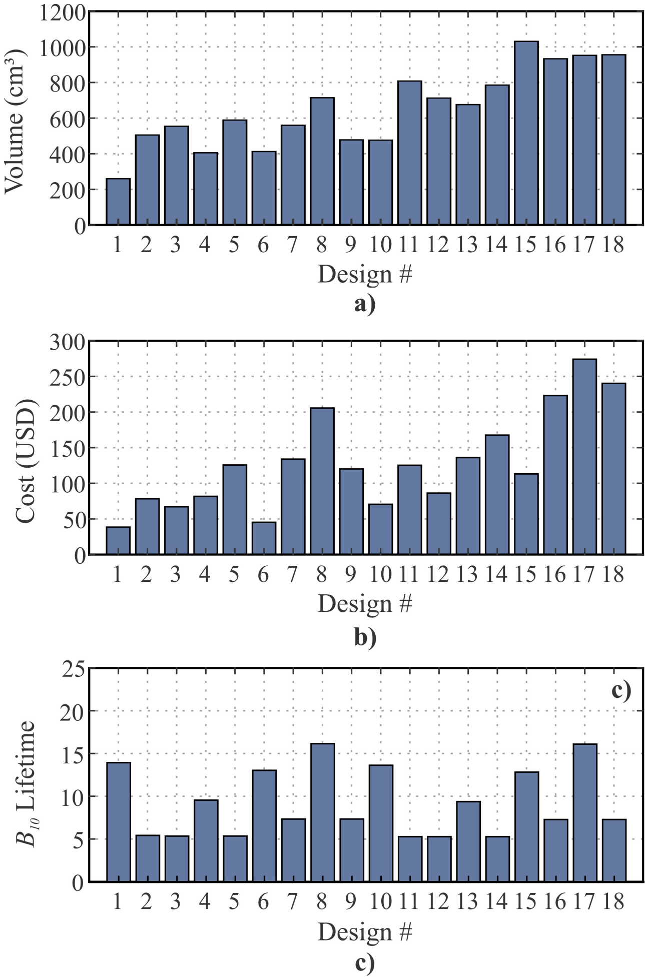

Source: personal archive

5.2 DOUBLE-CONVERSION UNINTERRUPTABLE POWER SUPPLY

A second case study is considered by making a multi-objective design analysis of DC-link capacitors in a double-conversion UPS. In UPS application, the DC-link is designed to ensure the hold-up time – period of time in which the inverter is able to supply energy to the load after a fault in its main feeder – (SONG and WANG, 2013, MURDOCK et al., 2006). A hold-up time longer than 17 ms is usually adopted for UPSs connected in 60 Hz grids, which results in the necessity of expensive and bulky DC-links (ANDERSEN et al., 2018). Considering the importance of capacitive components in double-conversion UPSs, there is a relationship between the system's overall reliability and the DC-link capacitors' lifetime.

The topology of the single-phase double-conversion UPS used in this work is composed by an input stage with the double functionality proposed by (VENTURINI et al., 2018) and a half-bridge inverter with an LC filter, as shown in Figure 64; more details on the topology and its parameters are found in (VENTURINI et al., 2018).

Figure 64 – Single-phase double-conversion UPS topology used.

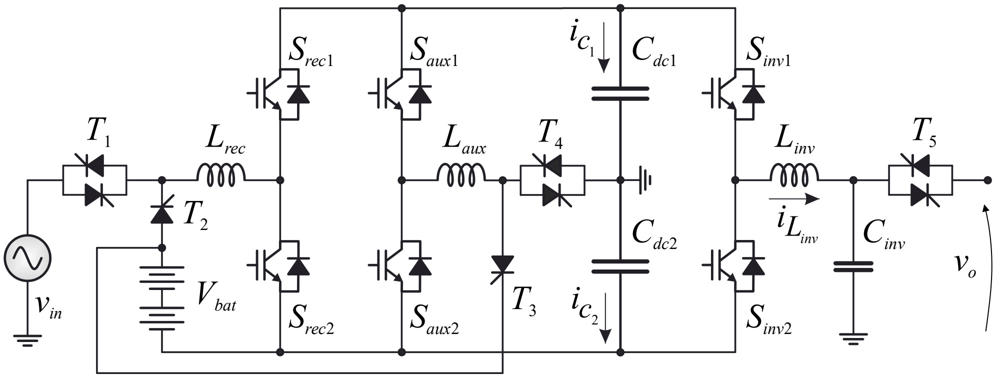

Source: (VENTURINI et al., 2018)

The design tool is used to analyze the long-term electro-thermal behavior of each side of the divided DC-link, as shown in Figure 65. Using the hold-up time of (VENTURINI et al., 2015) to assure the minimum required capacitance, and part numbers of Appendix B three design criteria are analyzed:

- N_{CAPS} that ensures the minimum capacitance ($C_{DC,min}$) of hold-up time requirement;
- N_{CAPS} that yields in extra 30% of safety margin for $C_{DC,min}$;

- N_{CAPS} that yields in extra 50% of safety margin for $C_{DC,min}$;

Safety margins as the latter two criteria are common practice in general electronics design, however, the compromise in cost is usually not studied in detail.

Figure 65 – Divided capacitor bank structure of the UPS.

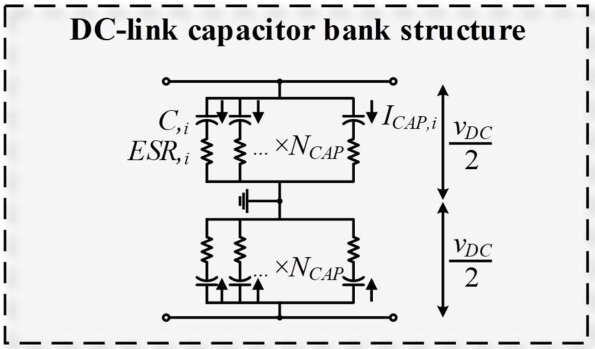

Source: personal archive

5.2.1 UPS mission profile

To make a more realistic analysis of long-term operation as a study case, it assumed that the UPS unit must feed a set of resistive loads which follow a 1-day 3-level cycle as described in Table 9. The loads are assumed to always be resistive and of the same values, in addition, small transients and random faults in the grid are not considered since they are out of the scope of this work. Also, the UPS is considered to be operating outdoors and subject to the ambient temperature profile of PTR (Figure 12). Thus, assuming that the load profile is unaltered, a 1-year mission profile of power level and ambient temperature is built as shown in Figure 66.

Table 9 – Daily load profile considered for the UPS case study.

Time of day	Load (p.u.)	Load (W)
01:00 – 07:59	0.3	3,000
08:00 – 17:59	0.65	5,800
18:00 – 00:59	0.8	8,000

Figure 66 – Overview of the annual mission profile built for the UPS case study.

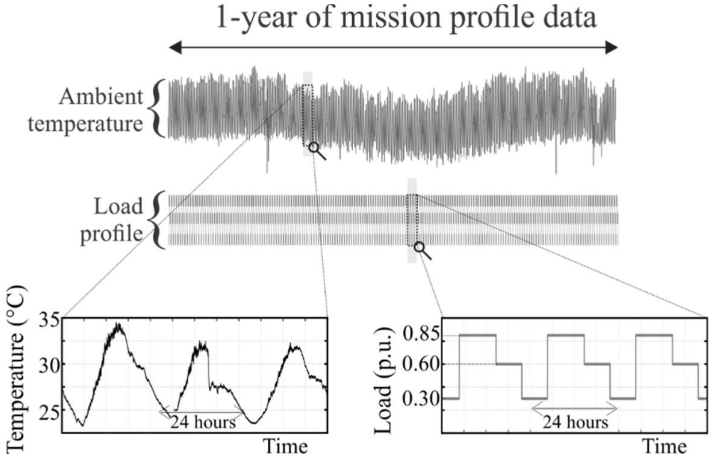

Source: personal archive

5.2.2 UPS offline look-up tables

The DC-link voltage is tightly controlled to ensure high-quality voltage and current waveforms at the load, where a voltage ripple of $\Delta v_{DC} < 1$ V is obtained. For this reason, the voltage across the capacitors is assumed to be constant and equal to its nominal value; disturbances and changes in the UPS operation mode are disregarded and will be investigated in future works.

In collaboration with this current work, a fully operational 10 kVA UPS unit is implemented in the Typhoon HIL 402 platform by (VENTURINI et al., 2018); the control system is implemented in a Texas Instruments TMS320F28355 DSP. Through hardware-in-the-loop simulation, the total current going through the capacitor bank in the DC-link is evaluated for different power levels and stored offline. Similar to the previous study case, these offline LUTs are then used to determine the capacitor power losses in time and in function of the load being supplied by the UPS. Figures 67 show the instantaneous and RMS current through each side of the DC-link for the power levels described in Table 9.

5.2.3 Long-term electro-thermal behavior

Using the mission profile given by Figure 66, the capacitors' power losses and operating temperature in time for each capacitor bank designed through the proposed method is evaluated. Yearly histograms of the operating temperature are built and used to calculate the damage accumulation and lifetime estimation. As previously shown, the choice of part number and capacitor bank size have a great influence on thermal behavior.

Figure 67 – Total current going through each side of the UPS divided DC-link, for loads of (a) 3 kW, (b) 5.8 kW, and (c) 8 kW.

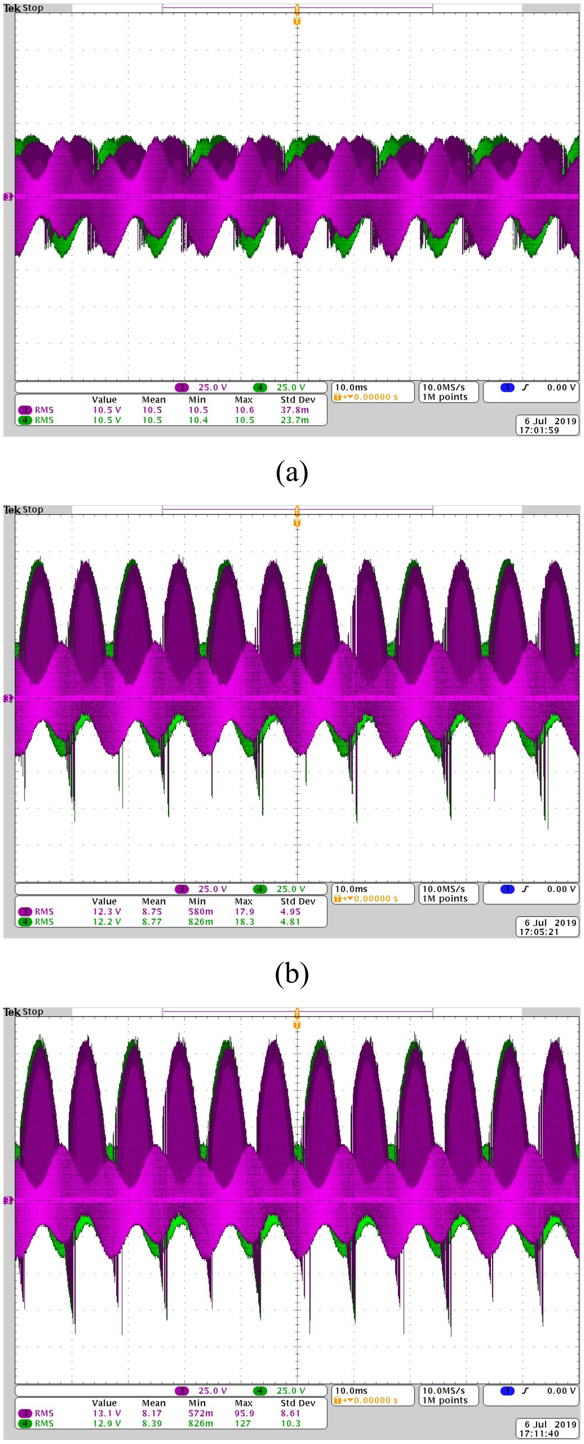

(a)

(b)

(c)

Source: personal archive

To illustrate, T_{CAP} of two different designs are shown in Figure 68 for a two-days interval, along with the ambient temperature and load profile. Due to the smaller size and higher thermal resistances, the temperatures in Design #9 reach values more than 10 °C higher compared to those in Design #4 during high load. This is again evident in Figure 69, where a yearly histogram of T_{CAP} is for these two designs are compared; not only the capacitors in Design #9 operate in higher temperatures, but they also do so more frequently throughout the year.

Figure 68 – Close look of Designs #4 and #9 T_{CAP} in time, along with T_{amb} and the UPS load level.

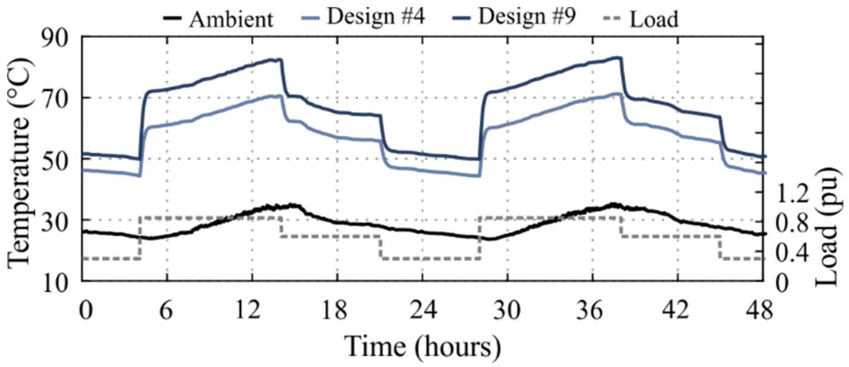

Source: personal archive

Figure 69 – Yearly histogram of operating hours versus temperature for Designs #4 and #9, along with T_{amb}.

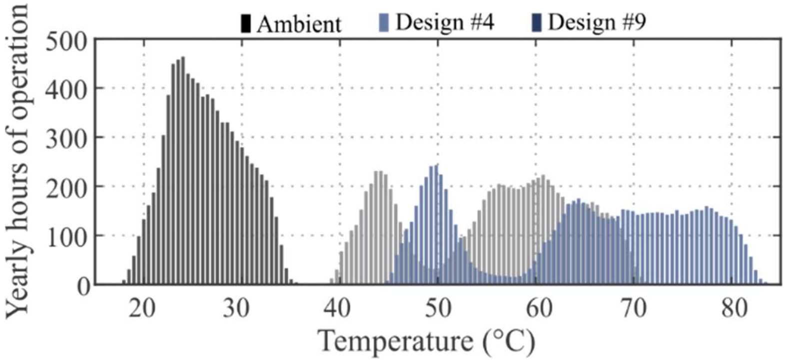

Source: personal archive

5.2.4 Mission profile oriented design

Finally, to demonstrate the proposed tool performance analyses, a project requirement of price (40 USD), volume (400 cm³), and lifetime (8 years) is defined for the UPS DC-link capacitor bank. In Figure 70 it is shown a performance comparison of all the designs obtained in function of cost, volume, and the reliability that each design will fulfill the lifetime requirement.

Figure 70 – Multi-objective evaluation results of several capacitor bank designs for the UPS case study.

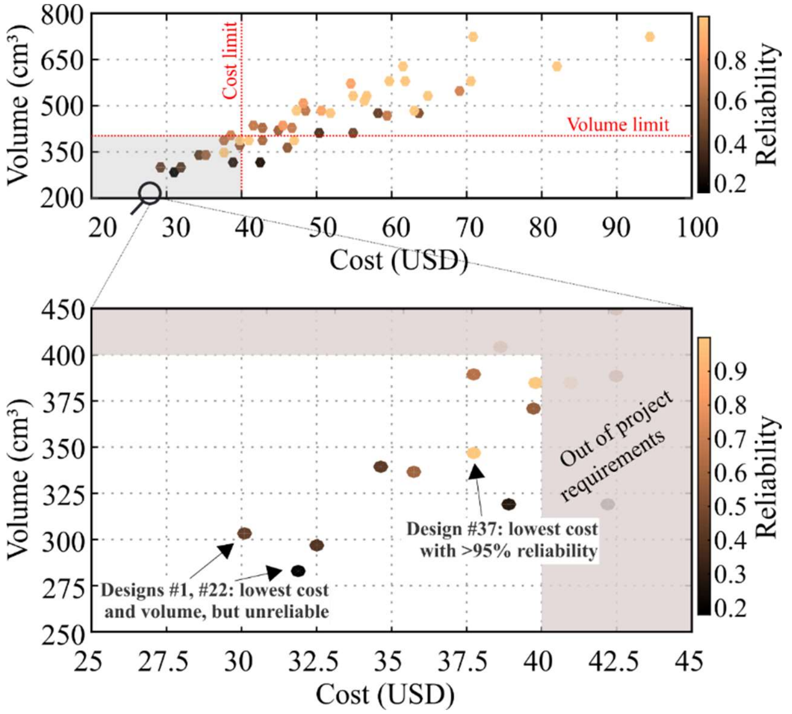

Source: personal archive

5.3 PROPOSED TOOL AS AN AID FOR RELIABILITY ANALYSES

Aside from its design purpose, the proposed methodology can also be used as an auxiliary tool for electro-thermal and reliability analysis. To better illustrate this, a final study case is done to evaluate the impact of a proposed thermal management control loop in the lifetime of the DC-link capacitors in parallel UPSs. To achieve this, a hierarchical control loop with the objective to equalize the capacitor temperatures in parallel units operating under different ambient conditions is used.

The modeling and analysis of this control structure are out of the scope of this work, so it will be only briefly described as follows. Two UPS units are assumed to be connected in the same microgrid but placed separately and subject to different ambient temperatures, as shown in Figure 71. Traditionally, a hierarchical control is applied with droop technique (MENG et al., 2017) in order to compensate the discrepancies in line impedances, provide adequate voltage levels to the load, and balance the power-sharing among the parallel units.

Figure 71 – Parallel operation of *N* UPS units under different ambient temperature conditions and connected to a point of common coupling.

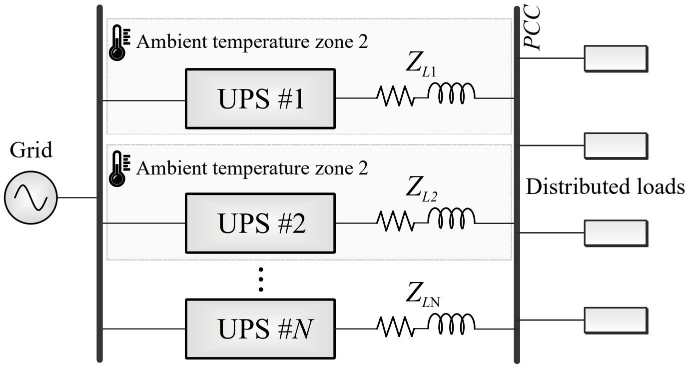

Source: personal archive

However, inverters in parallel operation are subject to different temperature dynamics – even if an adequate power-sharing is employed – in reason of distinct location and ambient conditions, discrepancy among technologies and component values, or even by parametrical degradation that different hours of operation can cause. Thus, the proposed control structure acts in unbalancing the power reference among the inverters in other to equalize the capacitors' operating temperatures, using T_{CAP} as a control variable.

The aim of this case study is to use the proposed tool to help the designer in evaluating thermal and lifetime performance of this control structure.

5.3.1 Thermal behavior

Using the same electro-thermal modeling and same load profile of Figure 66, the temperature in time of DC-link capacitors in both UPS units is obtained. Figure 72 shows T_{CAP} for operation with and without the thermal balance loop – in all further results the use or not of this structure level 3 are analyzed independently. Figure 72 shows the proposed control loop being enabled at a specific time only for a clear presentation of its effect in temperature management.

Assuming the UPSs' mission profile is not altered and the temperature values of Figure 72 being continuously cyclic, the daily values of T_{CAP} are translated into a 1-year of hours of operation histogram. The DC-link is controlled in a low margin of voltage ripple so that V_{CAP}

is considered constant and equal to its rated value of 225 V. Thus, the Al e-caps accumulated damage after 1-year can be found through (17) and (18), yielding in 0.1245 and 0.0615 for UPS #1 and #2, respectively, without use of the additional loop, and 0.0863 for both units with the proposed thermal balance loop.

Figure 72 – Estimated DC-link capacitors temperatures in both UPSs during typical daily operation in the defined load profile.

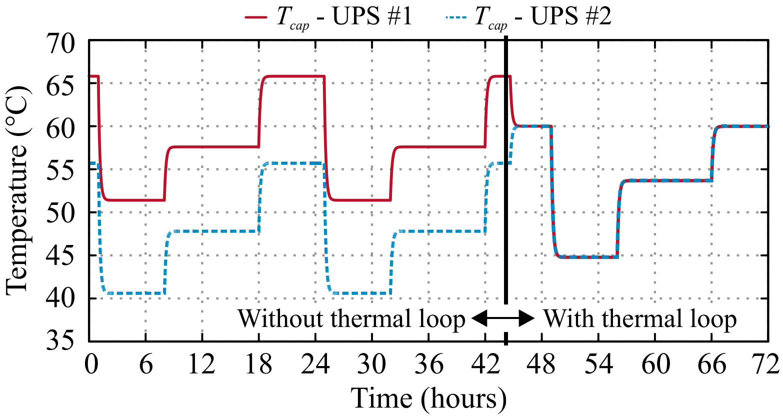

Source: personal archive

The *AD* values of each condition are used to obtain an equivalent temperature and voltage stress which are then used in a stochastic analysis through Monte Carlo simulation, as described in Section 4. The lifetime distribution of 10,000 samples is obtained for Al e-caps in UPS #1 and #2 with and without the thermal balance loop, as shown in Figure 73, alongside with the scale and shape coefficients of their fitted Weibull distribution. As expected, without the proposed control structure, an equal power-sharing caused the DC-link capacitors in UPS #1 to have a significantly lower life expectancy than those in UPS #2 due to their operating temperatures being on average 10 °C higher.

Finally, a cumulative distribution function is obtained from the Weibull results of Figure 73 and the *B10* lifetime for each scenario analyzed so far is calculated, as shown in Figure 74. Using the classical hierarchical control structure for inverters in parallel, the *B10* lifetime of DC-link capacitors in UPS #1 ($B10_{UPS\#1}$ = 4.9 years) is ~55% smaller than those in UPS #2 ($B10_{UPS\#2}$ = 10.8 years), mainly due to their different ambient temperature conditions.

The thermal balance loop proposed here equalized the *B10* of e-caps in both units to 7.4 years. With the compromise of reducing the lifetime of capacitors in UPS #2, the unit in a harsher environment had an increase in ~51% years of operation. Considering that warranty period and lifetime design targets are directly related to long-term financial revenues, this additional control loop could minimize costs of unscheduled maintenances and replacement of the capacitors. Also, it improves the reliability of double-conversion UPSs which are usually employed in mission-critical loads.

Figure 73 – Lifetime distribution resulted from the Monte Carlo simulation with parametric variation and their respective fitted Weibull distribution.

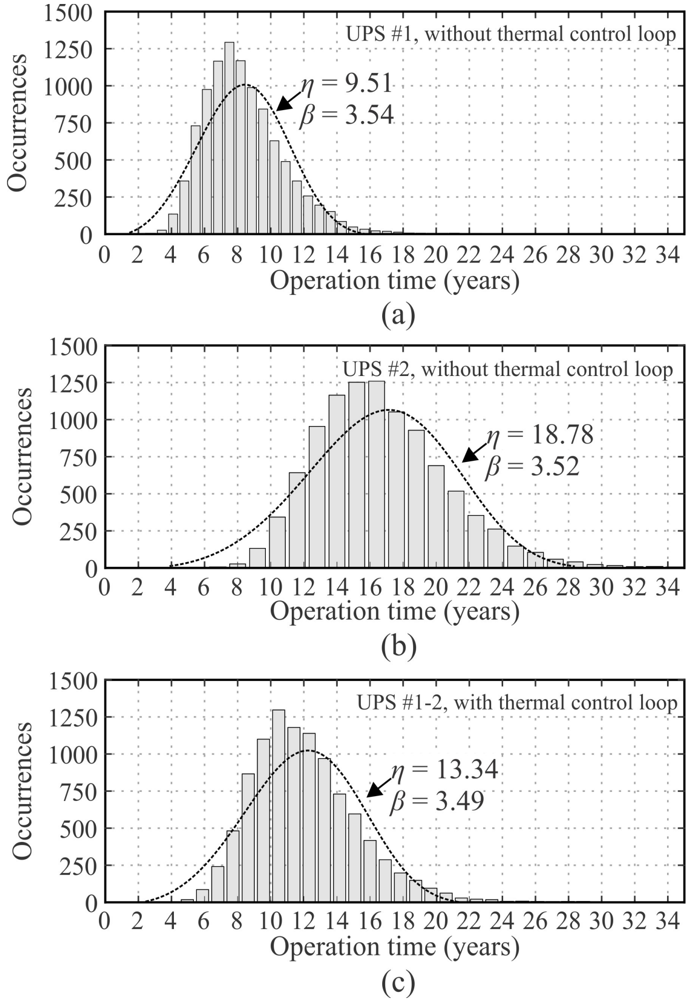

Source: personal archive

Results show that the hierarchical structure implemented not only provided adequate voltage and power supply to the load but was also able to reduce the thermal stresses of DC-link capacitors in the unit placed in a room with higher ambient temperature. By understanding that equal power-sharing may not be ideal if the operating conditions are not the same, a daily average reduction of 5.48 °C in capacitor temperature was achieved for the load profile analyzed. On average, the power reference was altered by +1.58 kW and -1.58 kW for the units in lower and higher ambient temperatures, respectively.

Figure 74 – Cumulative distribution of failure probability for DC-link capacitors of UPS #1 and #2 with and without the proposed control loop. (a) 30 year operation time. (b) Zoom-in of the same results in the B_{10} region.

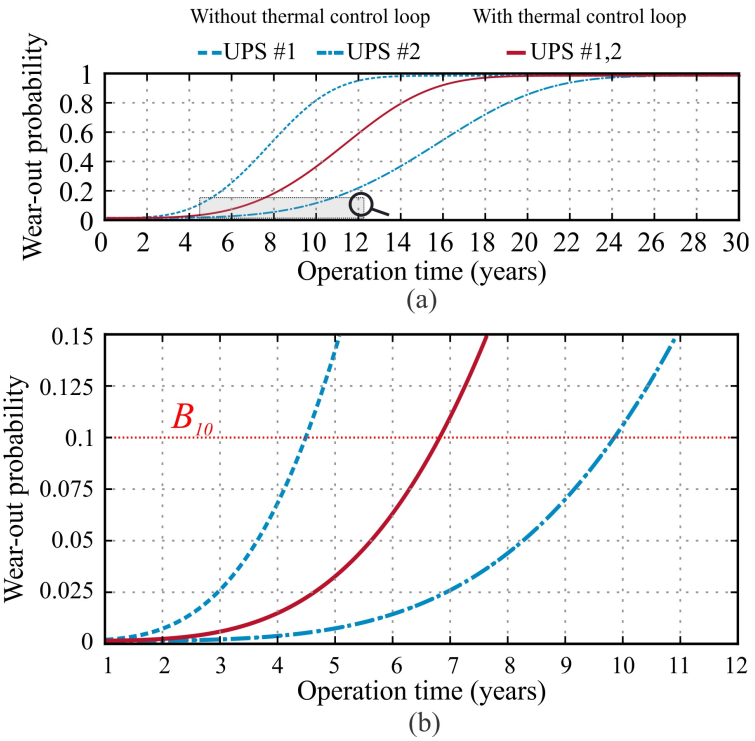

Source: personal archive

5.4 DISCUSSION

This chapter presented a comprehensive analysis of two distinct case studies of power electronics systems and showed how the use of the methodology proposed in this dissertation can give the designer insightful information on the long-term electro-thermal behavior of capacitors. With proper knowledge of the converter mission profile, this proposed design tool simplifies the decision process and enables to find more balanced solutions which yields good lifetime performance without much compromise of volume and cost.

However, thermal management and lifetime are not the only factors to consider when designing a power converter. The increase of power density is also a modern demand which significantly affects layout design, component count, technology choice, among other factors. Thus, the volume of the design is also a major deciding factor. Ultimately, the cost is an imperative aspect of any engineering project and all choices should be pondered over it.

6 FINAL CONSIDERATIONS

The next big step needed in energy conversion systems – such as photovoltaics – is the improvement of power converters on a long-term basis. In order to achieve this goal, design methodologies must also take this long-term view into account and not only the basic knowledge of rated and maximum values for a fixed operating level. The designer choices on the early conception stages of a power converter will determine its performance and, consequently, may also influence its financial success.

The energy profile estimation of a PV power plant is a key requirement in pre-design phase and it provides essential information of the minimum, typical, and critical levels of PV operation, and, thus, the levels in which the power converter and its elements will operate. The methodology and analysis presented to obtain a PV MP was applied as a tool to obtain useful information for the design of high performance and reliable PV power converters. Characterizing the mission profile of a photovoltaic power plant accurately allows the forecasting of critical and relevant operating conditions, hence, providing data that enables the improvement of power converter efficiency and reliability.

The results presented in this dissertation showed that capacitors' electro-thermal behavior in long-term is affected differently according to the mission profile in which they are submitted. Varying the location and energy processing profile led to different voltage and core temperature behavior of the capacitors throughout a 1-year operation, which in turn also affected their life estimation. It was also able to find capacitor bank designs with higher reliability and that still suited the cost and volume constraints in a UPS case study.

6.1 MAIN CONTRIBUTIONS

The main contributions achieved by this dissertation may be summarized as follows:

- ✓ A methodology to characterize the PV mission profile through long-term weather data for any location, PV technology, and mounting configuration. Providing a comprehensive set of information regarding the PV system current and voltage levels, relevant operating regions;
- ✓ A comprehensive methodology to evaluate power converter capacitors in function of time-variant load and ambient conditions. This tool also includes a reliability analysis to estimate lifetime and parameter degradation;

- ✓ A multi-domain multi-timescale design tool that provides to the user a large number of possible capacitor bank designs according to their input of topology, mission profile, and design requirements. From these, a multi-objective optimization is possible considering the total cost, volume, and lifetime estimation.

6.2 FUTURE WORKS

The following objectives are cited as future work:

- Develop and include in the current design tool a platform to analyze the electro-thermal behavior and evaluate the reliability of power devices;
- Integrate the power device reliability analysis with the capacitors in order to obtain a system-level reliability figure of metric;
- Develop simulations in finite element methods on component- and system-levels and integrate with the proposed design tool, in order to better evaluate thermal management and its impact in reliability and design choices.

6.3 PUBLICATIONS RELATED TO THIS WORK

The list of scientific papers presented and published during the development of this dissertation are described in Appendix D.

REFERENCES

ACCETTA, G., PIRODDI, L., FERRARINI, L., Energy Production Estimation Of A Photovoltaic System With Temperature-Dependent Coefficients. **IEEE Int. Conf. Sustain. Energy Technol. ICSET**, pp. 189–195. 2012.

ADINOLFI, G., GRADITI, G., SIANO, P., PICCOLO, A., Multiobjective Optimal Design Of Photovoltaic Synchronous Boost Converters Assessing Efficiency, Reliability, And Cost Savings. **IEEE Trans. Ind. Informatics** , v. 11, pp. 1038–1048. 2015.

AGDHAM, F., ABAPOUR, M., Reliability And Cost Analysis Of Multistage Boost Converters Connected To PV Panels, **IEEE Journal Of Photovoltaics**, Vol. 6, No. 4., Pp 981-989. 2016.

ANDRESEN, M., KUPRAT, J., RAVEENDRAN, V., FALCK, J., LISERRE, M., Active Thermal Control For Delaying Maintenance Of Power Electronics Converters, **Chinese J. Electr. Eng.**, Vol. 4, No. 3, Pp. 13–20, Sep. 2018.

BELTRAME, F., DUPONT, F.H., SARTORI, H.C., CANCIAN, E.C., RECH, C., PINHEIRO, J.R., Efficiency Optimization Of DC/DC Boost Converter Applied To The Photovoltaic System. **IECON Proc. Industrial Electron. Conf.** 706–711. 2013.

BELTRAME, F., DUPONT, F.H., SARTORI, H.C., PINHEIRO, J.R., Design Methodology To Improve The Converters ' Efficiency Applied To Photovoltaic Systems. **Proceedings, IECON 2014 - 40th Annu. Conf. IEEE Ind. Electron. Soc.** 1397–1403. 2014.

BOWER, W.N.L., WHITAKER, C. ENDECON E., ERDMAN, W.E.I., BEHNKE, M. BEW E.I., FITZGERALD, M. **Institute For S.T.**, Performance Test Protocol For Evaluating Inverters Used In Grid-Connected Photovoltaic Systems 41. 2004.

CDE. Aluminum Electrolytic Capacitor Application Guide 1–22. 2019.

CHANG, Y.P., YANG, L.D., Optimal Tilt Angle For PV Modules Considering The Uncertainty Of Temperature And Solar Radiation. **Int. Conf. Renew. Energy Res. Appl. ICRERA** 2012.

Channegowda, P., John, V., Filter Optimization For Grid Interactive Voltage Source Inverters. **IEEE Trans. Ind. Electron.** 57, 4106–4114. 2010.

CHAVES, E.N., REIS, J.H., COELHO, E.A.A., FREITAS, L.C.G., JÚNIOR, J.B. V, FREITAS, L.C.G., Simulated Annealing – MPPT In Partially Shaded PV Systems. **IEEE Lat. Am. Trans.** 14, 235–241. 2016.

CHIANG, C.-J., YANG, J.-L., CHENG, W., Dynamic Modeling Of The Electrical And Thermal Behavior Of Ultracapacitors. 10th **IEEE Int. Conf. Control Autom.** 1839–1844. 2013.

CHUNG, H.S., WANG, H., BLAABJERG, F., PECHT, M., Reliability Of Power Electronic Converter Systems. **Institution Of Engineering And Technology**. 2015.

CIOBOTARU, M., TEODORESCU, R., BLAABJERG, F., Control Of Single-Stage Single-Phase PV Inverter, **European Power Electronics & EPE ECCE**. Pp. 20–26. 2005.

CLAVIJO, G., SP1000 Single-Axis Solar Tracker. Technical Guide. 2012

COELHO, R.F., CONCER, F., MARTINS, D.C., A Proposed Photovoltaic Module And Array Mathematical Modeling Destined To Simulation. **IEEE Int. Symp. Ind. Electron.** 1624–1629. 2009.

DEB, J., YOHANIS, Y.G., NORTON, B., The Impact Of Array Inclination And Orientation On The Performance Of A Grid-Connected Photovoltaic System, **Renewable Energy**, 32, 118–140. 2007.

DU, B., HUDGINS, J.L., SANTI, E., BRYANT, A.T., PALMER, P.R., MANTOOTH, H.A., Transient Electrothermal Simulation Of Power Semiconductor Devices. **IEEE Trans. Power Electron.** 25, 237–248. 2010.

ELSAHARTY, M.A., ASHOUR, H.A., Passive L And LCL Filter Design Method For Grid-Connected Inverters. **2014 IEEE Innov. Smart Grid Technol. - Asia, ISGT ASIA** 13–18. 2014.

EPCOS AG, Film Capacitors. **General Technical Information**. Tech. Data 1–42. 2015.

FREIBURGER, P., Transient Thermal Modeling Of Aluminum Electrolytic Capacitors Under Varying Mounting Boundary Conditions, **21st International Workshop On Thermal Investigations Of Ics And Systems**. Pp. 1–5. 2015.

FREITAS, S., SERRA, F., BRITO, M.C., PV Layout Optimization : String Tiling Using A Multi-Objective Genetic Algorithm, **Solar Energy**, 118, 562–574. 2015.

FURUKAWA, T., SENZAI, D., YOSHIDA, T., Electrolytic Capacitor Thermal Model And Life Study For Forklift Motor Drive Application. **World Electr. Veh. Symp. Exhib. EVS 2014**, 1–6. 2014.

GRUPO.CLAVIJO, SR10 Dual-Axis Solar Tracker - Technical Information. 2012.

HUNG, C.H., GILMORE, J., HUANG, C.P., DAI, P.G., ZHU, W., Bos Cost Savings And LCOE Reduction For A 10 MW PV System With The 500 Kw Transformerless Inverter, **2nd International Symposium On Power Electronics For Distributed Generation Systems, PEDG 2010**. Pp. 924–928. 2010.

INTERNATIONAL ENERGY AGENCY, World Energy Outlook 2016 (Executive Summary). IEA-WEO. 2016.

IRENA, Renewable Power Generation Costs In 2014 : An Overview. 2015.

IRENA, Solar Photovoltaics. 2013.

JIMÉNEZ, H., CALLEJA, H., CLAUDIO, A., The Lifetime / Volume Ratio As An Index To Assess The Reliability Of Power Converters. **2010 IEEE Energy Conversion Congress And Exposition** Pp. 963–969. 2010.

KIRISKEN, B., UGURDAG, H.F., Cost-Benefit Approach To Degradation Of Electrolytic Capacitors. **2014 Reliab. Maintainab. Symp.** 1–6. 2014.

LEWIS, G., Optimum Tilt Of Solar Collectors, Solar And Wind Technology. **Solar & Wind Technology**, V. 4, Pp 407-410 1987.

LI, H., LIAO, X., ZENG, Z., HU, Y., LI, Y., LIU, S., RAN, L., Thermal Coupling Analysis In A Multichip Paralleled IGBT Module For A DFIG Wind Turbine Power Converter. **IEEE Trans. Energy Convers.** 32, 80–90. 2017.

MECA.SOLAR, High Tech Solar Trackers 1-Horizontal Axis - Technical Datasheet. 2014a.

MECA.SOLAR, High Tech Solar Trackers 1-Axis Polar Technical Datasheet. 2014b.

MENG, L., SHAFIEE, Q., TRECATE, G.F., KARIMI, H., FULWANI, D., LU, X., GUERRERO, J.M., Review On Control Of DC Microgrids And Multiple Microgrid Clusters.

IEEE J. Emerg. Sel. Top. Power Electron. 5, 928–948. 2017.

MOORE, L.M., POST, H.N., Five Years Of Operating Experience At A Large , Utility-Scale Photovoltaic Generating Plant, **Prog. Photovolt: Res. Appl.**, V. 16 Pp 249–259. 2008.

MURDOCK, D.A., TORRES, J.E R., CONNORS, J.J., LORENZ, R.D., Active Thermal Control Of Power Electronic Modules, **IEEE Trans. Ind. Appl.**, Vol. 42, No. 2, Pp. 552–558, 2006.

OECD/IEA, IRENA, Perspectives For The Energy Transition – Investment Needs For A Low-Carbon Energy System. 2017.

PAIRAN Gmbh, Tracking System CPV40 - Technical Information. 2015.

PESOS, Sunflex SD Tracking Systems Technical Information For Control Systems SF20-60SD. 2015.

PV-MAGAZINE, Issue 01-2016, 2016.

RAHMAN, S.A., VANDERHEIDE, T., VARMA, R.K., Generalised Model Of A Photovoltaic Panel. **IET Renew. Power Gener.** V. 8, Pp. 217–229. 2014.

RAHMANI, A., ABDI, B., YAZDANPARAST, L., The Effect Of Topology On Life Time Of SMPS, I**nternational Conference And Exposition On Electrical And Power Engineering**. Pp. 25–27. 2012.

REDA, I., ANDREAS, A., Solar Position Algorithm For Solar Radiation Applications. 2008.

REINDL, D.T., BECKMAN, W.A., DUFFIE, J.A., Evaluation Of Hourly Tilted Surface Radiation Models. **Sol. Energy** 45, 9–17. 1990.

REN21, Renewables 2016: Global Status Report. 2016.

RISTOW, A., BEGOVIĆ, M., PREGELJ, A., ROHATGI, A., Development Of A Methodology For Improving Photovoltaic Inverter Reliability. **IEEE Trans. Ind. Electron.** 55, 2581–2592. 2008.

RODRIGO, P.M., VELÁZQUEZ, R., FERNÁNDEZ, E.F., DC / AC Conversion Efficiency Of Grid-Connected Photovoltaic Inverters In Central Mexico. **Sol. Energy** 139, 650–665. 2016.

SARIDAKIS, S., KOUTROULIS, E., BLAABJERG, F., Optimal Design Of Modern Transformerless PV Inverter Topologies. **IEEE Trans. Energy Convers.** 28, 394–404. 2013.

SINTAMAREAN, N.C., BLAABJERG, F., WANG, H., YANG, Y., Real Field Mission Profile Oriented Design Of A Sic-Based PV-Inverter Application. **IEEE Trans. Ind. Appl.** 50, 4082–4089. 2014.

SINTAMAREAN, N C, WANG, H., BLAABJERG, F., RIMMEN, P. De P., A Design Tool To Study The Impact Of Mission-Profile On The Reliability Of Sic-Based PV-Inverter Devices. **Microelectron. Reliab.** 54, 1655–1660. 2014.

SIRAKI, A.G., PILLAY, P., Study Of Optimum Tilt Angles For Solar Panels In Different Latitudes For Urban Applications. **Sol. Energy** 86, 1920–1928. 2012.

SKOPLAKI, E., PALYVOS, J. A. On The Temperature Dependence Of Photovoltaic Module Electrical Performance: A Review Of Efficiency/Power Correlations. **Sol. Energy** 83, 614–624. 2009a

SKOPLAKI, E., PALYVOS, J.A., Operating Temperature Of Photovoltaic Modules: A Survey Of Pertinent Correlations. **Renew. Energy** 34, 23–29. 2009b.

SMA, Sunny Mini Central 6000TL / 7000TL / 8000TL Technical Data. 2016.

SOLAR POWER EUROPE, Global Market Outlook For Solar Power 2017-2021. 2017.

SOLARPRO, Issue 3.4, Jun/Jul, 2010.

SOLARPRO, Issue 8.3, Jul/Aug, 2015.

SONG Y., WANG, B., Survey On Reliability Of Power Electronic Systems, **IEEE Trans. Power Electron.**, Vol. 28, No. 1, Pp. 591–604, 2013.

SUHIR, E., Could Electronics Reliability Be Predicted , Quantified And Assured? **Microelectron. Reliab.** 53, 925–936. 2013.

U. S. ENERGY INFORMATION AGENCY, Levelized Cost And Levelized Avoided Cost Of New Generation Resources In The Annual Energy Outlook. 1–12. 2017.

US, Dod., Military Handbook (MIL-HDBK-217F) - Reliability Prediction Of Electronic Equipment. 1991.

VENTURINI, W.A., JANK, H., MARTINS, M.L.S., BISOGNO, F.E., PINHEIRO, H., RECH, C., PINHEIRO, J.R., BUENO, A.G., A Low Cost Three-Phase Transformerless Online UPS. **2015 IEEE 13th Brazilian Power Electron. Conf. 1st South. Power Electron. Conf. COBEP/SPEC** 2015.

VENTURINI, W.A., JANK, H., BISOGNO, F.E., MARTINS, M.L.S., PINHEIRO, H., Input Stage With Double Functionality Applied To A High Performance Three-Phase UPS, **Eletrônica De Potência**, Vol. 23, No. 2, Pp. 244–255, Apr. 2018a.

VENTURINI, W.A., LENZ, J.M., JANK, H., BISOGNO, F.E., PINHEIRO, J.R., Hierarchical Control Structure For Parallelism Of Double Conversion UPS With Equalization Of The DC-Link Capacitors Temperatures. **Eletrônica De Potência** 23, 442–453. 2018b.

VILLALVA, M.G.G., GAZOLI, J.R.R., FILHO, E.R.R., Comprehensive Approach To Modeling And Simulation Of Photovoltaic Arrays. **IEEE Trans. Power Electron.** 24, 1198–1208. 2009.

WANG, H., BLAABJERG, F., Reliability Of Capacitors For DC-Link Applications In Power Electronic Converters—An Overview. **IEEE Trans. Ind. Appl.** 50, 3569–3578. 2014.

WANG, H., MA, K., BLAABJERG, F., Design For Reliability Of Power Electronic Systems. **IECON 2012 - 38th Annu. Conf. IEEE Ind. Electron. Soc.** 33–44. 2012.

WANG, H., YANG, Y., BLAABJERG, F., Reliability-Oriented Design And Analysis Of Input Capacitors In Single-Phase Transformer-Less Photovoltaic Inverters. **IEEE Appl. Power Electron. Conf. Expo. - APEC** 2929–2933. 2013.

WANG, H., POOYA, D., WANG, H., DINESH, K., FIRUZ, Z., BLAABJERG, F., Lifetime Estimation Of DC-Link Capacitors In Adjustable Speed Drives Under Grid Voltage Unbalances, **IEEE Trans. Power Electron.**, Vol. 34, No. 5, Pp. 4064-4078, 2019.

YADAV, A.K., MALIK, H., Optimization Of Tilt Angle For Installation Of Solar Photovoltaic System For Six Sites In India, **International Conference On Energy Economics And Environment**. 2015.

YANG, Y., **Advanced Control Strategies To Enable A More Wide-Scale Adoption Of Single-Phase Photovoltaic Systems**. Phd. Dissertation - Aalborg University, Aalborg, Denmark. 2014.

YANG, Y., MA, K., WANG, H., BLAABJERG, F., Instantaneous Thermal Modeling Of The DC-Link Capacitor In Photovoltaic Systems, **IEEE Applied Power Electronics Conference And Exposition (APEC)**. IEEE, Pp. 2733–2739. 2015a.

YANG, Y., SULAREA, V., BLAABJERG, F., Advanced Design Tools For The Reliability Of Power Electronics. **IECON 2015 - Annu. Conf. IEEE Ind. Electron. Soc.**, 2828-2833. 2015b.

ZHANG, P., WANG, Y., XIAO, W., LI, W., Reliability Evaluation Of Grid-Connected Photovoltaic Power Systems. **IEEE Trans. Sustain. Energy** 3, 379–389. 2012.

ZHANG, Z., WANG, L., KURTZ, S., WU, J., QUAN, P., SORENSEN, R., LIU, S., BAI, J.B., ZHU, Z.W., Operating Temperatures Of Open-Rack Installed Photovoltaic Inverters. **Sol. Energy** 137, 344–351. 2016.

ZHAO, J., ZHOU, X., MA, Y., LIU, W., A Novel Maximum Power Point Tracking Strategy Based On Optimal Voltage Control For Photovoltaic Systems Under Variable Environmental Conditions. **Sol. Energy** 122, 640–649. 2015.

ZHOU, D., WANG, H., BLAABJERG, F., Mission Profile Based System-Level Reliability Analysis Of DC/DC Converters For A Backup Power Application. **IEEE Trans. Power Electron.** 33, 8030–8039. 2018.

ZINE, S., MAZARI, B., BOUZID, M.A., MIHOUB, Y., Sliding Mode Control Of Wind Turbine Emulator. **Int. Renew. Sustain. Energy Conf. (IRSEC)**, 2014, Pp 822–826. 2014.

ZVEI, Handbook For Robustness Validation Of Automotive Electrical / Electronic Modules. 2008.

APPENDIX A

CDE capacitors dabatase. (only part numbers highlighted in green were used)

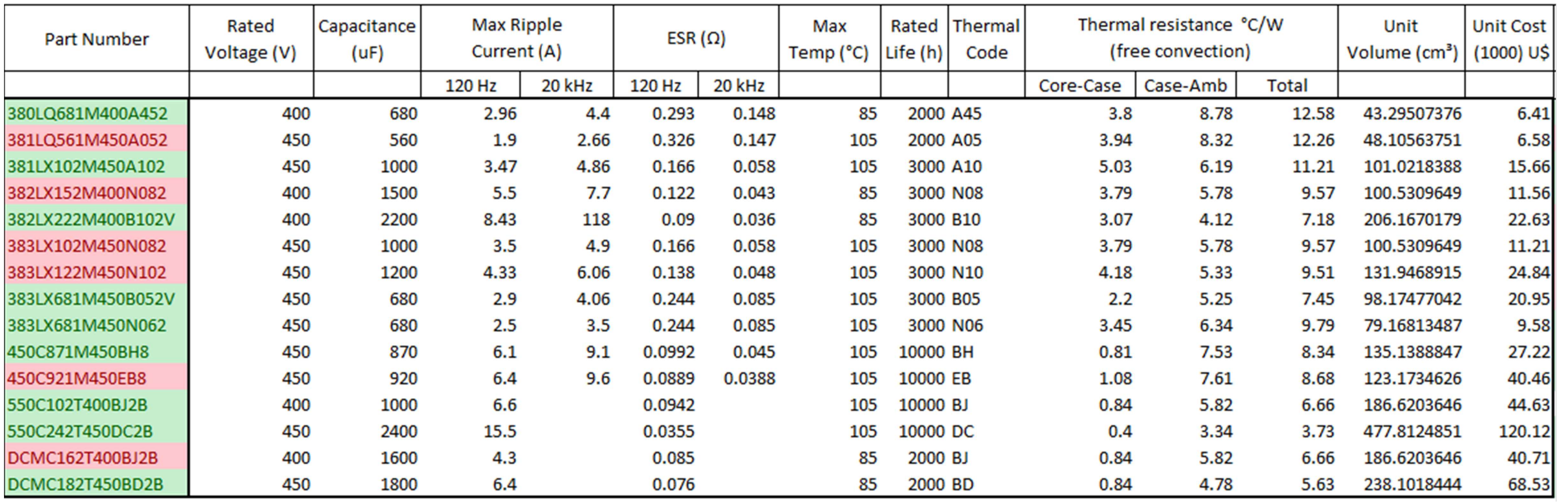

Part Number	Rated Voltage (V)	Capacitance (uF)	Max Ripple Current (A)		ESR (Ω)		Max Temp (°C)	Rated Life (h)	Thermal Code	Thermal resistance °C/W (free convection)			Unit Volume (cm³)	Unit Cost (1000) U$
			120 Hz	20 kHz	120 Hz	20 kHz				Core-Case	Case-Amb	Total		
380LQ681M400A452	400	680	2.96	4.4	0.293	0.148	85	2000	A45	3.8	8.78	12.58	43.29507376	6.41
381LQ561M450A052	450	560	1.9	2.66	0.326	0.147	105	2000	A05	3.94	8.32	12.26	48.10563751	6.58
381LX102M450A102	450	1000	3.47	4.86	0.166	0.058	105	3000	A10	5.03	6.19	11.21	101.0218388	15.66
382LX152M400N082	400	1500	5.5	7.7	0.122	0.043	85	3000	N08	3.79	5.78	9.57	100.5309649	11.56
382LX222M400B102V	400	2200	8.43	118	0.09	0.036	85	3000	B10	3.07	4.12	7.18	206.1670179	22.63
383LX102M450N082	450	1000	3.5	4.9	0.166	0.058	105	3000	N08	3.79	5.78	9.57	100.5309649	11.21
383LX122M450N102	450	1200	4.33	6.06	0.138	0.048	105	3000	N10	4.18	5.33	9.51	131.9468915	24.84
383LX681M450B052V	450	680	2.9	4.06	0.244	0.085	105	3000	B05	2.2	5.25	7.45	98.17477042	20.95
383LX681M450N062	450	680	2.5	3.5	0.244	0.085	105	3000	N06	3.45	6.34	9.79	79.16813487	9.58
450C871M450BH8	450	870	6.1	9.1	0.0992	0.045	105	10000	BH	0.81	7.53	8.34	135.1388847	27.22
450C921M450EB8	450	920	6.4	9.6	0.0889	0.0388	105	10000	EB	1.08	7.61	8.68	123.1734626	40.46
550C102T400BJ2B	400	1000	6.6		0.0942		105	10000	BJ	0.84	5.82	6.66	186.6203646	44.63
550C242T450DC2B	450	2400	15.5		0.0355		105	10000	DC	0.4	3.34	3.73	477.8124851	120.12
DCMC162T400BJ2B	400	1600	4.3		0.085		85	2000	BJ	0.84	5.82	6.66	186.6203646	40.71
DCMC182T450BD2B	450	1800	6.4		0.076		85	2000	BD	0.84	4.78	5.63	238.1018444	68.53

APPENDIX B

NCC capacitors database.

Part Number	Rated voltage (V)	Rated lifetime (hours)	Maximum temperature (°C)	Rated capacitance (uF)	ESR @ 120 Hz, 25°C (Ohms)	Max ripple current @ 120 Hz, rated temp. (A)	Cost (USD)	Rth	Volume (cm³)	Thermal time constant (s)
ESMR451VSN821MA50S	450	2000	85	820	0.1617	3.6	5.05	12.26	48104.2	1080.0
ESMR451VSN471MA35S	450	2000	85	470	0.2822	2.54	3.21	11.21	33673.0	748.3
ESMR451VSN221MP40S	450	2000	85	220	0.6029	1.67	1.92	9.79	15204.9	337.9
ESMR421VSN681MR50S	420	2000	85	680	0.1950	3.28	3.89	8.34	35341.9	785.4
ESMR421VSN471MR40S	420	2000	85	470	0.2822	2.61	2.85	7.45	28273.5	628.3
ESMR421VSN221MP35S	420	2000	85	220	0.6029	1.68	1.77	7.18	13304.3	295.7
ESMR401VSN821MA45S	400	2000	85	820	0.1213	3.25	4.17	12.26	43293.8	962.1
ESMR401VSN471MR35S	400	2000	85	470	0.2116	2.6	2.65	11.21	24739.3	549.8
ESMR401VSN221MP35S	400	2000	85	220	0.4522	1.69	1.62	9.79	13304.3	295.7
ESMM401VSN681MA50S	400	3000	85	680	0.1463	3.1	5.14	7.18	48104.2	1069.0
ESMM421VSN681MA50S	420	3000	85	680	0.1950	3.15	5.88	7.18	48104.2	1069.0
ESMM451VSN561MA50S	450	3000	85	560	0.2368	2.88	6.3	7.18	48104.2	1069.0
EKMQ401VSN681MA45S	400	2000	105	680	0.1463	2.12	4.7	12.26	43293.8	962.1
EKMQ421VSN681MA50S	420	2000	105	680	0.1950	2.2	4.98	8.34	48104.2	1069.0
EKMQ451VSN561MA50S	450	2000	105	560	0.2368	1.9	4.73	9.79	48104.2	1068.0

APPENDIX C

This appendix brings further detailing on the three different design methods used to calculate the minimum DC-link capacitance in the SSSP PV converter.

DC-link design criteria 1: in this method, the DC-link capacitors were selected according to the minimum required capacitance and/or maximum supported ripple current using the SSSP rated power. The following steps were used:

Step 1: Ignoring the losses of the inverter and *L* filter, the minimum bus capacitance ($minC_{DC}$) was obtained through

$$\min C_{DC} = \frac{P_R}{2\pi f_g V_{DC} \Delta v} \tag{C.1}$$

Step 2: The minimum number of capacitors needed – for each part number – to reach the $minC_{DC}$ was calculated;

$$nCAPS \times \left(C_{design,i}(\mu F) \right) \ \geq \ \min C_{DC} \tag{C.2}$$

Step 3: Using datasheet information and *nCAPS*, each part number was verified if the critical RMS current through

$$I_{RMS}^{critic} \approx \frac{P_{in}}{\sqrt{2} V_{DC}} \tag{C.3}$$

$$\frac{I_{RMS}^{MAX}}{nCAPS} \ \leq \ \mathrm{C_i} \ \text{max current} \tag{C.4}$$

Step 4: For each part number, the DC-link is defined as the number of parallel capacitors that satisfies both Step 2 and 3

Step 5: The additional voltage ripple caused by the ESR is included in order to verify if the desired Δv is ensured, through

$$\Delta v_{ESR} = \frac{P_R}{2\pi f_g (V_{DC} - I_{R,RMS} ESR_{LF,design,i}) C_{design,i}} \tag{C.5}$$

where $I_{R,RMS}$ is the rated RMS current of the SSSP converter.

If $\Delta v_{ESR} > \Delta v$, then $nCAPS^1{}_i$ is incremented until (B.5) is satisfied.

DC-link design criteria 2: a new criterion was proposed and analyzed where the objective was to limit the capacitor's core temperature elevation based on the MP. By first defining a maximum threshold for temperature elevation ($max\Delta T_{CAP}$), the needed number of capacitors in parallel to respect $max\Delta T_{CAP}$ was calculated by

$$nCAPS^3 \geq \frac{I_{PV,RMS}^{MP}}{\sqrt{\max \Delta T_{cap} \Big/ ESR_{LF,i} R_{th,i}}} \tag{C.6}$$

where the temperature limit $maxT_{CAP}$ was obtained by rewriting (14) and solving with datasheet information and the mission profile MOR, as in

$$\max \Delta T_{cap} \leq \left(\frac{I_{PV,RMS}^{MP}}{nCAPS} \right)^2 ESR_{LF,i} \left(R_{th\_cc,i} + R_{th\_ca,i} \right) \tag{C.7}$$

$$\begin{cases} \mathrm{ESR}_{\mathrm{LF}}, \mathrm{R}_{\mathrm{th\_cc}}, \mathrm{R}_{\mathrm{th\_ca}} \text{: based on datasheet} \\ \max \mathrm{I}_{\mathrm{RMS}} \text{: based on Mission Profile} \end{cases}$$

APPENDIX D

Bellow follows the list of papers that were developed in relation to this Doctoral dissertation and in collaboration.

Journal papers:

P.I. **LENZ, JOÃO M.**; SARTORI, HAMILTOM C.; PINHEIRO, JOSÉ R., *Mission profile characterization of PV systems for the specification of power converter design requirements*. SOLAR ENERGY, v. 157, p. 263-276, 2017.

P.II **LENZ, J.M.**; Sartori, H.C.; PINHEIRO, J. R., *Defining Photovoltaic Mission Profile for the Pre-Design of Static Converters*. IEEE LAT. AM. TRANS., v. 16, no. 5, p. 1402-1409, 2018.

P.III. Venturini, W.A., **LENZ, J.M.**,.Jank, H. ; Bisogno, F., PINHEIRO, J. R., *Hierarchical Control Structure for Parallelism of Double Conversion UPS With Equalization of the DC-Link Capacitors Temperatures*. ELETRÔNICA DE POTÊNCIA, v. 23, no. 4, 2018.

P.IV. Cupertino, A.F.; **LENZ, JOÃO M.**; Brito, E.; Pereira, H.A.; Pinheiro, J.R.; Seleme, I.S. *Impact of the Mission Profile Length on Lifetime Prediction of PV Inverters*. MICROELECTRONICS RELIABILITY, v. 100-101, 2019.

P.V. **LENZ, JOÃO M.**; Cupertino, A.F.; Pereira, H.A.; Zhou, D.; Wang, H.; Pinheiro, J.R. *Benchmarking of Capacitor Power Loss Calculation Methods for Wear-Out Failure Prediction in PV Inverters*. MICROELECTRONICS RELIABILITY, v. 100-101, 2019.

Conference papers:

P.VI. **LENZ, J. M.** ; Zhou, D. ; Wang, H. ; Pinheiro, J.R. . *Optimization Tool for Dc-Link Capacitor Bank Design in PV Inverters*. In: 10th International Conference on Power Electronics-ECCE Asia, 2019, Busan. 10th International Conference on Power Electronics-ECCE Asia, 2019.

P.VII **LENZ Joao M.**; PINHEIRO, JOSE R., 2018, Paris. 2018 7th International Conference on Renewable Energy Research and Applications (ICRERA), 2018. p. 976.

P.VIII. VENTURINI, W. A.**; LENZ, JOÃO M.**; JANK, H.; BISOGNO, F. E.; PINHEIRO, J. R., 2018, João Pessoa. Congresso Brasileiro de Automática, 2018, 2018.

P.IX. **LENZ, J.M.**; PINHEIRO, J. R. *Análise da Vida Útil de Capacitor Eletrolítico em Conversor Boost Fotovoltaico*. In: 10th Seminar on Power Electronics and Control, Santa Maria. SEPOC 2017 Proceedings, 2017.

P.X. **LENZ, J.M.**; SARTORI, H.C.; PINHEIRO, J. R. *DC-link Electrolyte Capacitor Lifetime Analysis for a PV Boost Converter*. In: 8th International Symposium on Power Electronics for Distributed Generation Systems, Florianópolis. PEDG 2017 Proceedings, 2017.

P.XI **LENZ, J.M.**; SARTORI, H.C.; Pinheiro, J.R. *Cálculo Customizado da Eficiência Média Ponderada em Conversores Fotovoltaicos*. In: 12th IEEE/IAS International Conference on Industry Applications - INDUSCON, Curitiba. INDUSCON Proceedings, 2016.

P.XII **LENZ, J.M.**; PINHEIRO, J. R. *Modelagem da Eficiência Média Ponderada Customizada à Aplicação Fotovoltaca*. In: CBA2016 "Congresso Brasileiro de Automática, Vitória. CBA Proceedings 2016.